

# 1 Dissolved iron in the North Atlantic Ocean and Labrador Sea along 2 the GEOVIDE section (GEOTRACES section GA01)

3 Manon Tonnard<sup>1,2,3</sup>, H el ene Planquette<sup>1</sup>, Andrew R. Bowie<sup>2,3</sup>, Pier van der Merwe<sup>2</sup>, Morgane Gallinari<sup>1</sup>,  
4 Floriane Desprez de G esincourt<sup>1</sup>, Yoan Germain<sup>4</sup>, Arthur Gourain<sup>5</sup>, Marion Benetti<sup>6,7</sup>, Gilles Reverdin<sup>7</sup>,  
5 Paul Tr eguer<sup>1</sup>, Julia Boutorh<sup>1</sup>, Marie Cheize<sup>1</sup>, [Fran ois Lacan](#)<sup>8</sup>, Jan-Lukas Menzel Barraqueta<sup>9</sup>, Leonardo  
6 Pereira-Contreira<sup>10</sup>, Rachel Shelley<sup>1,11,12</sup>, [Pascale Lherminier](#)<sup>13</sup>, G eraldine Sarthou<sup>1</sup>

7 <sup>1</sup>Laboratoire des sciences de l'Environnement MARin – CNRS UMR 6539 – Institut Universitaire Europ een de la Mer,  
8 [Universit  de Bretagne Occidentale](#), Plouzan , 29280, France

9 <sup>2</sup>Antarctic Climate and Ecosystems – Cooperative Research Centre, [University of Tasmania](#), Hobart, TAS 7001, Australia

10 <sup>3</sup>Institute for Marine and Antarctic Studies, University of Tasmania, Hobart, TAS 7001, Australia

11 <sup>4</sup>Laboratoire Cycles G eochimiques et ressources – Ifremer, Plouzan , 29280, France

12 <sup>5</sup>Ocean Sciences Department, School of Environmental Sciences, University of Liverpool, L69 3GP, UK

13 <sup>6</sup>Institute of Earth Sciences, University of Iceland, Reykjavik, Iceland

14 <sup>7</sup>LOCEAN, Sorbonne Universit s, UPMC/CNRS/IRD/MNHN, Paris, [France](#)

15 <sup>8</sup>LEGOS, [Universit  de Toulouse - CNRS/IRD/CNES/UPS – Observatoire Midi-Pyr n es, Toulouse, France](#)

16 <sup>9</sup>GEOMAR Helmholtz-Zentrum f r Ozeanforschung Kiel Wischhofstra e 1-3, Geb. 12 D-24148 Kiel, Germany

17 <sup>10</sup>Funda o Universidade Federal do Rio Grande (FURG), R. Luis Lor a, Rio Grande –RS, 96200-350, Brazil

18 <sup>11</sup>Dept. Earth, Ocean and Atmospheric Science, Florida State University, 117 N Woodward Ave, Tallahassee, Florida, 32301,  
19 USA

20 <sup>12</sup>School of Geography, Earth and Environmental Sciences, University of Plymouth, Drake Circus, Plymouth, PL4 8AA, UK

21 <sup>13</sup>Ifremer, Universit  de Bretagne Occidentale (UBO), CNRS, IRD, Laboratoire d'Oc anographie Physique et Spatiale  
22 (LOPS), IUEM, F-29280, Plouzan , France

23

24 *Correspondence to:* Manon Tonnard (Manon.Tonnard@utas.edu.au)

25

26 **Abstract.** Dissolved Fe (DFe) samples from the GEOVIDE voyage (GEOTRACES GA01, May-June 2014) in the North  
27 Atlantic Ocean were analysed using a SeaFAST-pico<sup>TM</sup> coupled to an Element XR [SF<sub>6</sub>-ICP-MS](#) and provided interesting  
28 insights on the Fe sources in this area. Overall, DFe concentrations ranged from  $0.09 \pm 0.01$  nmol L<sup>-1</sup> to  $7.8 \pm 0.5$  nmol L<sup>-1</sup>.  
29 Elevated DFe concentrations were observed above the Iberian, Greenland and Newfoundland Margins likely due to riverine  
30 inputs from the Tagus River, meteoric water inputs and sedimentary inputs. [Enhanced air-sea](#) interactions were suspected to  
31 be responsible for the increase in DFe concentrations within subsurface waters of the Irminger Sea due to deep convection  
32 occurring the previous [winter, which](#) provided iron-to-nitrate ratios sufficient to sustain phytoplankton growth. Increasing DFe  
33 concentrations along the flow path of the Labrador Sea Water were attributed to sedimentary inputs from the Newfoundland  
34 Margin. Bottom waters from the Irminger Sea displayed high DFe concentrations likely due to the dissolution of Fe-rich  
35 particles [in the Denmark Strait Overflow Water](#) and the Polar Intermediate Water. Finally, the nepheloid layers [located in the](#)  
36 [different basins and at the Iberian Margin](#) were found to act as either a source or a sink of DFe depending on the nature of  
37 particles [with organic particles likely releasing DFe and Mn-particles scavenging DFe](#).

Formatted

Formatted: Superscript

Deleted: <sup>8</sup>

Deleted: <sup>9</sup>

Deleted: <sup>0</sup>

Deleted: <sup>1</sup>

Deleted: <sup>2</sup>

Deleted: France

Formatted: Superscript

Deleted: <sup>8</sup>

Deleted: <sup>9</sup>

Deleted: <sup>0</sup>

Deleted: <sup>1</sup>

Deleted: <sup>2</sup>

Deleted: HR

Deleted: A

Deleted: winter, that

Deleted: from

Deleted: .

## 1 Introduction

The North Atlantic Ocean is known for its pronounced spring phytoplankton blooms (Henson et al., 2009; Longhurst, 2007). Phytoplankton blooms induce the capture of aqueous carbon dioxide through photosynthesis, and conversion into particulate organic carbon (POC). This POC is then exported into deeper waters through the production of sinking biogenic particles and ocean currents. Via these processes, and in conjunction with the physical carbon pump, the North Atlantic Ocean is the largest oceanic sink of anthropogenic CO<sub>2</sub> (Pérez et al., 2013), despite covering only 15% of global ocean area (Humphreys et al., 2016; Sabine et al., 2004) and is therefore crucial for Earth's climate.

Indeed, phytoplankton must obtain, besides light and inorganic carbon, chemical forms of essential elements, termed nutrients to be able of photosynthesis. Indeed, Fe is a key element for a number of metabolic processes (e.g. Morel et al., 2008). The availability of these nutrients in the upper ocean frequently limits the activity and abundance of these organisms together with light conditions (Moore et al., 2013). In particular, winter nutrient reserves in surface waters set an upper limit for biomass accumulation during the annual spring-to-summer bloom and will influence the duration of the bloom (Follows and Dutkiewicz, 2001; Henson et al., 2009; Moore et al., 2013; 2008). Hence, nutrient depletion due to biological consumption is considered as a major factor in the decline of blooms (Harrison et al., 2013).

The extensive studies conducted in the North Atlantic Ocean through the Continuous Plankton Recorder (CPR) have highlighted the relationship between the strength of the westerlies and the displacement of the subarctic front (SAF), (which corresponds to the North Atlantic Oscillation (NAO) index (Bersch et al., 2007)), and the phytoplankton dynamics of the central North Atlantic Ocean (Barton et al., 2003). Therefore, the SAF not only delineates the subtropical gyre from the subpolar gyre but also two distinct systems in which phytoplankton limitations are controlled by different factors. In the North Atlantic Ocean, spring phytoplankton growth is largely light-limited within the subpolar gyre. Light levels are primarily set by freeze-thaw cycles of sea ice and the high-latitude extremes in the solar cycle (Longhurst, 2007). Simultaneously, intense winter mixing supplies surface waters with high concentrations of nutrients. In contrast, within the subtropical gyre, the spring phytoplankton growth is less impacted by the light regime and has been shown to be N and P-co-limited (e.g. Harrison et al., 2013; Moore et al., 2008). This is principally driven by Ekman downwelling with an associated export of nutrients out of the euphotic zone (Oschlies, 2002). Thus, depending on the location of the SAF, phytoplankton communities from the central North Atlantic Ocean will be primarily light or nutrient limited.

However, once the water column stratifies and phytoplankton are released from light limitation, seasonal high-nutrient, low chlorophyll (HNLC) conditions were reported at the transition zone between the gyres, especially in the Irminger Sea and Iceland Basin (Sanders et al., 2005). In these HNLC zones, trace metals are most likely limiting the biological carbon pump. Among all the trace metals, Fe has been recognized as the prime limiting element of North Atlantic primary productivity (e.g.

Moved (insertion) [7]

Deleted: also

Deleted: ,

Deleted: a region of high phytoplankton production

Deleted: that

Deleted: , a key driver of the biological carbon pump through photosynthesis and transfer of energy to higher trophic levels

Deleted: atmospheric

Deleted: which allows its

Deleted: (Henson et al., 2009)

Deleted: ()

Deleted: and through the Atlantic Meridional Overturning Circulation (AMOC), The North Atlantic Ocean is a crucial area for Earth's climate as a result of deep water formation. The formation of the North Atlantic Deep Water (NADW) is essential to the Atlantic Meridional Overturning Circulation (AMOC), which is responsible for transporting large amounts of water, heat, salt, carbon, nutrient( ...

Moved up [7]: The North Atlantic Ocean is also a region of high

Deleted: The North Atlantic Ocean is also a region of high

Deleted: shows

Deleted: storagestores huge amounts rate

Deleted: through both the physical and biological carbon pumps

Deleted: the

Moved down [11]: However, the rapid attenuation of light with

Deleted: The extensive studies conducted in the North Atlantic

Moved (insertion) [11]

Deleted: However, the rapid attenuation of light with depth

Deleted: a lower

Deleted: More specifically, i

Deleted: the

Moved (insertion) [8]

Deleted: , which is

Deleted: at its northern boundaries (i.e. the Arctic Ocean, margi( ...

Deleted: , as the

Deleted: fuels the

Deleted: as it undergoes an

Deleted: more or less prompt to

Deleted: ations

Deleted: in the subpolar gyre and

Deleted: , thus suggesting that

Deleted: were potentially

Deleted: the

1 [Boyd et al., 2000](#); [Martin et al., 1994](#); [1988](#); [1990](#). However, the phytoplankton community has been shown to become N  
2 and/or Fe-(co)-limited in the Iceland Basin and the Irminger Sea (e.g. [Nielsdóttir et al., 2009](#); [Painter et al., 2014](#); [Sanders et](#)  
3 [al., 2005](#)).

4  
5 In the North Atlantic Ocean, dissolved Fe (DFe) is delivered through multiple pathways such as ice-melting (e.g. [Klunder et](#)  
6 [al., 2012](#); [Tovar-Sanchez et al., 2010](#)), atmospheric inputs ([Achterberg et al., 2018](#); [Baker et al., 2013](#); [Shelley et al., 2015](#);  
7 [2017](#)), coastal runoff ([Rijkenberg et al., 2014](#)), sediment inputs ([Hatta et al., 2015](#)), hydrothermal inputs ([Achterberg et al.,](#)  
8 [2018](#); [Conway and John, 2014](#)) and by water mass circulation (vertical and lateral advections, e.g. [Laes et al., 2003](#)). Dissolved  
9 Fe can be regenerated through biological recycling (microbial loop, zooplankton grazing, e.g. [Boyd et al., 2010](#); [Sarhou et al.,](#)  
10 [2008](#)). Iron is removed from the dissolved phase by biological uptake, export and scavenging along the water column and  
11 precipitation (itself a function of salinity, pH of seawater and ligand concentrations).

12  
13 Although many studies investigated the distribution of DFe in the North Atlantic Ocean, much of this work was restricted to  
14 the upper layers (< 1000 m depth) or to one basin. Therefore, uncertainties remain on the large-scale distribution of DFe in the  
15 North Atlantic Ocean and more specifically within the subpolar gyre where few studies have been undertaken, and even fewer  
16 in the Labrador Sea. In this biogeochemically important area, high-resolution studies are still lacking for understanding the  
17 processes influencing the cycle of DFe.

18  
19 The aim of this paper is to elucidate the sources and sinks of DFe, its distribution regarding water masses and assesses the  
20 links with biological activity along the GEOVIDE (GEOTRACES-GA01) transect. This transect spanned several  
21 biogeochemical provinces including the West European Basin, the Iceland Basin, the Irminger and the Labrador Seas (Fig. 1).  
22 In doing so we hope to constrain the potential long-range transport of DFe through the Deep Western Boundary Current  
23 (DWBC) via the investigation of the local processes effecting the DFe concentrations within the three main water masses that  
24 constitute it, Iceland Scotland Overflow Water (ISOW), Denmark Strait Overflow Water (DSOW) and Labrador Sea Water  
25 (LSW).

## 26 2 Material and methods

### 27 2.1 Study area and sampling activities

28 Samples were collected during the GEOVIDE (GEOTRACES-GA01 section, Fig. 1) oceanographic voyage from 15 May 2014  
29 (Lisbon, Portugal) to 30 June 2014 (St. John's, Newfoundland, Canada) aboard *N/O Pourquoi Pas?*. The study was carried  
30 out along the OVIDE line (<http://www.umr-lops.fr/Projets/Projets-actifs/OVIDE>, previously referred to as the WOCE A25  
31 Greenland to Portugal section), and in the Labrador Sea (corresponding to the WOCE A01 leg 3 Greenland to Newfoundland  
32 section). The OVIDE line has been sampled every two years since 2002 in the North Atlantic (e.g. [Mercier et al., 2015](#)), and

**Deleted:** and t...overherefore... it...he phytoplankton community has been shown to become N or (and...nd/or)

**Formatted**

**Deleted:** Recent observations showed a reduction of oceanic heat loss to the atmosphere due to the slowdown of the AMOC resulting to the reduction of carbon uptake ([Pérez et al., 2013](#)).  
In the North Atlantic Ocean, phytoplankton growth is largely light-limited at its northern boundaries (i.e. the Arctic Ocean, marginal ice zones, polynya areas and the Labrador Shelf) set primarily by freeze-thaw cycles of sea ice and the high-latitude extremes in the solar cycle ([Longhurst, 2007](#)). In contrast, at its more southerly boundaries (i.e. the subpolar and to a lesser extent the subtropical gyres), seasonal wind and thermal cycles that determine mixing patterns, have a greater influence on phytoplankton growth with the consequence that both light and nutrient inventories can limit productivity ([Harrison et al., 2013](#)). If light is thought to be the principal control on the timing of growth, nutrients play a significant role in the phytoplankton community structure. In particular, winter nutrient reserves in surface waters set a lower limit for biomass accumulation during the annual spring-to-summer bloom and will influence the duration of the bloom ([Follows and Dutkiewicz, 2001](#); [Henson et al., 2009](#); [Moore et al., 2013](#); [2008](#)). Hence, nutrient depletion due to biological consumption is considered as a major factor in the decline of blooms ([Harrison et al., 2013](#)). The North Atlantic Ocean is classically considered as a N-limited system ([Moore et al., 2013](#)). However, once the water column stratifies in

**Deleted:** Indeed, Fe is a key element for a number of metabolic processes (e.g. [Morel et al., 2008](#)) and within its physical speciation

**Formatted:** French (France)

**Formatted:** French (France)

**Formatted**

**Formatted**

**Moved up [8]:** phytoplankton growth is largely light-limited at its northern boundaries (i.e. the Arctic Ocean, marginal ice zones,

**Formatted**

**Deleted:** D

**Field Code Changed**

**Field Code Changed**

**Deleted:** and t

**Deleted:** Despite these studies,...uncertainties remain on the large-scale distribution of DFe in the North Atlantic Ocean and more

**Deleted:** In this context, t...he aim of this paper is to elucidates

**Deleted:**

**Deleted:** ,

**Deleted:**

**Deleted:** which...spanned several biogeochemical provinces including the West European Basin, the Iceland Basin, the Irminger

**Deleted:** the...N/O Pourquoi Pas?. The study was carried out along the OVIDE line ([\*\*Deleted:\*\* , which](http://www.umr-lops.fr/Projets/Projets-</a></p></div><div data-bbox=)

1 in the Labrador Sea (broadly corresponding to the WOCE A01 leg 3 Greenland to Newfoundland section). In total, 32 stations  
2 were occupied, and samples were usually collected at 22 depths, except at shallower stations close to the Iberian, Greenland  
3 and Canadian shelves (Fig. 1) where fewer samples (between 6 and 11) were collected. To avoid ship contamination of surface  
4 waters, the shallowest sampling depth was 15 m at all stations. Therefore, 'surface water samples' refers to 15m depth.

**Deleted:** These 15 m depth will be herein referred to as

5  
6 Samples were collected using a trace metal clean polyurethane powder-coated aluminium frame rosette (hereafter referred to  
7 as TMR) equipped with twenty-two 12L, externally closing, Teflon-lined, GO-FLO bottles (General Oceanics) and attached  
8 to a Kevlar® line. The cleaning protocols for sampling bottles and equipment followed the guidelines of the GEOTRACES  
9 Cookbook (www.geotraces.org, Cutter et al., 2017). After TMR recovery, GO-FLO bottles were transferred into a clean  
10 container equipped with a class 100 laminar flow hood. Samples were either taken from the filtrate of particulate samples  
11 (collected on polyethersulfone filters, 0.45 µm supor®, see Gourain et al., this issue) or after filtration using 0.2 µm filter  
12 cartridges (Sartorius SARTOBRAN® 300) due to water budget restriction (Table 1). No significant difference was observed  
13 between DFe values filtered through 0.2 µm and 0.45 µm filters (p-value > 0.2, Wilcoxon test) for most stations. Differences  
14 were only observed between profiles of stations 11 and 13 and, 13 and 15. Seawater was collected in acid-cleaned 60 mL

**Deleted:** the French-national ultra-clean sampling device. This consisted of

15 LDPE bottles, after rinsing 3 times with about 20 mL of seawater. Teflon® tubing used to connect the filter holders or cartridges  
16 to the GO-FLO bottles were washed in an acid-bath (10% v/v HCl, Suprapur®, Merck) for at least 12 h and rinsed three times  
17 with Ultra High Purity Water (UHPW > 18 MΩ.cm) prior to use. Samples were then acidified to ~ pH 1.7 with HCl (Ultrapur®  
18 Merck, 2 %o v/v) under a class 100 laminar flow hood inside the clean container. The sample bottles were then double bagged  
19 and stored at ambient temperature in the dark before shore-based analyses.

**Deleted:** , neither between stations (i.e. stations 17, 19, 21, 25, 26, 29, 32, 34, 42, 44, 49) while swapping between both filtration techniques (p-values > 0.05, Wilcoxon tests paired by depth and against the sign of the alternative hypothesis depending on the filtration technique used), except between station 11 and 13 and 13 and 15.

20 Large volumes of seawater sample (referred hereafter as the in-house standard seawater) were also collected using a towed  
21 fish at around 2-3 m deep and filtered in-line inside a clean container through a 0.2 µm pore size filter capsule (Sartorius  
22 SARTOBRAN® 300) and was stored unacidified in 20-30 L LDPE carboys (Nalgene™). All the carboys were cleaned  
23 following the guidelines of the GEOTRACES Cookbook (Cutter et al., 2017). This in-house standard seawater was used for  
24 calibration on the SeaFAST-pico™ - SF-ICP-MS (see Section 2.2) and was acidified to ~ pH 1.7 with HCl (Ultrapur® Merck,  
25 2 %o v/v) at least 24h prior to analysis.

**Deleted:** Samples were either taken from the filtrate of particulate samples (collected on polyethersulfone filters, 0.45 µm supor®, see Gourain et al., this issue) or after filtration on 0.2 µm filter cartridges (Sartorius SARTOBRAN® 300) (Table 1).

**Deleted:** 1.7 with

**Deleted:** 2 %o (v/v)

## 26 2.2 DFe analysis with SeaFAST-pico™

**Commented [MT1]:** I need information on how long before analysis was the calibration seawater acidified how many samples were run per day and how much samples were between each calibration curve  
Also need the way the errors were calculated: standard deviation of the calibration slopes or SD of the Element ?

**Deleted:** ¶

**Deleted:** to a

**Deleted:** via a SeaFAST-pico™ introduction system (Elemental Scientific Incorporated

**Deleted:** on a daily basis

**Formatted:** Font: 10 pt, Complex Script Font: 10 pt

**Formatted:** Font: 10 pt, Complex Script Font: 10 pt, Superscript

**Formatted:** Font: 10 pt, Complex Script Font: 10 pt

**Formatted:** Font: 10 pt, Complex Script Font: 10 pt, Superscript

**Formatted:** Font: 10 pt, Complex Script Font: 10 pt

27 Seawater samples were preconcentrated using a SeaFAST-pico™ (ESI, Elemental Scientific, USA) and the eluent was directly  
28 introduced via a PFA-ST nebulizer and a cyclonic spray chamber in an Element XR Sector Field Inductively Coupled Plasma  
29 Mass Spectrometry (Element XR SF-ICP-MS, Thermo Fisher Scientific Inc., Omaha, NE), following the protocol of  
30 Lagerström et al. (2013).

31 High-purity grade solutions and water (Milli-Q) were used to prepare the following reagents each day: the acetic acid-  
32 ammonium acetate buffer (CH<sub>3</sub>COO<sup>-</sup> and NH<sub>4</sub><sup>+</sup>) was made of 140 mL acetic acid (> 99% NORMATOM® - VWR chemicals)  
33 and ammonium hydroxide (25%, Merck Suprapur®) in 500 mL PTFE bottles and was adjusted to pH 6.0 ± 0.2 for the on-line

pH adjustment of the samples. The eluent was made of 1.4 M nitric acid (HNO<sub>3</sub>, Merck Ultrapur®) in Milli-Q water by a 10-fold dilution and spiked with 1 µg L<sup>-1</sup> <sup>115</sup>In (SCP Science calibration standards) to allow for drift correction. Autosampler and column rinsing solutions were made of HNO<sub>3</sub> 2.5% (v/v) (Merck Suprapur®) in Milli-Q water. The carrier solution driven by the syringe pumps to move the sample and buffer through the flow injection system was made in the same way.

All reagents, standards, samples, and blanks were prepared in acid cleaned low density polyethylene (LDPE) or Teflon fluorinated ethylene propylene (FEP) bottles. Bottles were cleaned following the GEOTRACES protocol (Cutter et al., 2017). Mixed element standard solution was prepared gravimetrically using high purity standards (Fe, Mn, Cd, Co, Zn, Cu, Pb; SCP Science calibration standards) in HNO<sub>3</sub> 3% (v/v) (Merck Ultrapur®). A six-point calibration curve was prepared by standard additions of the mixed element standard to our acidified in-house standard and ran at the beginning, the middle and the end of each analytical session. The distribution of the trace metals other than Fe will be reported elsewhere (Planquette et al., in prep.). Final concentrations of samples and procedural blanks were calculated from In-normalized data. Data were blank-corrected by subtracting an average acidified Milli-Q blank that were pre-concentrated on the SeaFAST-pico™ in the same way as the samples and seawater standards. Each analytical session consisted of about fifty samples and two calibrations, one at the beginning and another one at the end of each analytical session. The errors associated to each sample were calculated as the standard deviation for five measurements of low-Fe seawater samples. The mean Milli-Q blank was equal to 0.08 ± 0.09 nmol L<sup>-1</sup> (n = 17) all analytical session together. The detection limit, calculated for a given run as three times the standard deviation of the Milli-Q blanks, was on average 0.05 ± 0.05 nmol L<sup>-1</sup> (n = 17). Reproducibility was assessed through the standard deviation of replicate samples (every 10th sample was a replicate) and the average of the in-house standard seawater, and was equal to 17% (n = 84). Accuracy was determined from the analysis of consensus (SAFE S, GSP) and certified (NASS-7) seawater matrices (see Table 2) and in-house standard seawater (DFe = 0.42 ± 0.07 nmol L<sup>-1</sup>, n = 84). Note that all the DFe values were generated in nmol kg<sup>-1</sup> using the SeaFAST-pico™ coupled to an Element XR SF<sub>6</sub>-ICP-MS and were converted to nmol L<sup>-1</sup> (multiplied by a factor of 1.025 kg L<sup>-1</sup>) to be directly comparable with literature.

### 2.3 Meteoric water and sea ice fraction calculation

We separated the mass contributions to samples from stations 53, 61 and 78 in Sea-Ice Melt (SIM) Meteoric Water (MW) and saline seawater inputs using the procedure and mass balance calculations that are fully described in Benetti et al. (2016). Hereafter, we describe briefly the principle. We considered two types of seawater, namely the Atlantic Water (AW) and the Pacific Water (PW). After estimating the relative proportions of AW ( $f_{AW}$ ) and PW ( $f_{PW}$ ) and their respective salinity and  $\delta^{18}\text{O}$  affecting each samples, the contribution of SIM and MW can be determined using measured salinity ( $S_m$ ) and  $\delta^{18}\text{O}$  ( $\delta^{18}\text{O}_m^{18}$ ). The mass balance calculations are presented below:

$$f_{AW} + f_{PW} + f_{MW} + f_{SIM} = 1 \text{ (eq.1)}$$

$$f_{AW} \cdot S_{AW} + f_{PW} \cdot S_{PW} + f_{MW} \cdot S_{MW} + f_{SIM} \cdot S_{SIM} = S_m \text{ (eq.2)}$$

$$f_{AW} \cdot \delta^{18}\text{O}_{AW}^{18} + f_{PW} \cdot \delta^{18}\text{O}_{PW}^{18} + f_{MW} \cdot \delta^{18}\text{O}_{MW}^{18} + f_{SIM} \cdot \delta^{18}\text{O}_{SIM}^{18} = \delta^{18}\text{O}_m^{18} \text{ (eq.3)}$$

**Deleted:** was made of 0.5 M acetic acid (Merck ultrapur) and 0.6 M ammonium hydroxide (Merck ultrapur) and was adjusted to pH 8.3.

**Deleted:** tion acid

**Deleted:** 6

**Formatted:** Complex Script Font: 10 pt

**Deleted:** 1 µg mL<sup>-1</sup> Indium (In, PlasmaCAL calibration standards) to allow for drift correction.

**Formatted:** Font: 10 pt, Complex Script Font: 10 pt

**Formatted:** Font: 10 pt, Complex Script Font: 10 pt, Superscript

**Formatted:** Font: 10 pt, Complex Script Font: 10 pt

**Formatted:** Font: 10 pt, Complex Script Font: 10 pt, Superscript

**Formatted:** Font: 10 pt, Complex Script Font: 10 pt

**Deleted:** 0.012 M hydrochloric acid

**Formatted:** Subscript

**Deleted:** (HCl, Merck ultrapur) in

**Deleted:** PlasmaCAL

**Formatted:** Font: 10 pt, Complex Script Font: 10 pt

**Formatted:** Default, Justified, Line spacing: 1.5 lines

**Deleted:** calibration

**Deleted:** 0.8 M

**Formatted:** Font: 10 pt, Complex Script Font: 10 pt

**Deleted:** (GEOVIDE filtered seawater, collected at station 69, 40m depth)

**Deleted:** run

**Formatted:** Font: 10 pt, Complex Script Font: 10 pt

**Formatted:** Font: 10 pt, Superscript

**Formatted:** Font: 10 pt, Complex Script Font: 10 pt

**Deleted:**

**Formatted:** Font: 10 pt, Complex Script Font: 10 pt

**Formatted:** Font: 10 pt, Complex Script Font: 10 pt

**Formatted:** Font: 10 pt, Complex Script Font: 10 pt

**Formatted:** Font: 10 pt, Complex Script Font: 10 pt

**Formatted:** Font: 10 pt, Complex Script Font: 10 pt

**Deleted:** Precision was assessed through replicate samples (every 10th sample was a replicate) and accuracy was determined from ...

**Formatted:** Font: 10 pt, Complex Script Font: 10 pt

**Deleted:** HR

**Deleted:** in

**Formatted:** Font: 10 pt, Complex Script Font: 10 pt

1 where  $f_{AW}$ ,  $f_{PW}$ ,  $f_{MW}$ ,  $f_{SIM}$  are the relative fraction of AW, PW, MW, and SIM. To calculate the relative fractions of AW, PW,  
2 MW and SIM we used the following end-members:  $S_{AW} = 35.80_{AW}^{18} = +0.18\%$  (Benetti et al., 2016);  $S_{PW} = 32.5.80_{PW}^{18} = -$   
3  $1\%$  (Cooper et al., 1997; Woodgate and Aagaard, 2005);  $S_{MW} = 0.80_{MW}^{18} = -18.4\%$  (Cooper et al., 2008);  $S_{SIM} = 4.80_{SIM}^{18} =$   
4  $+0.5\%$  (Melling and Moore, 1995).  
5 Negative sea-ice fractions indicated a net brine release while positive sea-ice fractions indicated a net sea-ice melting. Note  
6 that for stations over the Greenland Shelf, we assumed that the Pacific Water (PW) contribution was negligible for the  
7 calculations, supported by the very low PW fractions found at Cape Farewell in May 2014 (see Figure B1 in Benetti et al.,  
8 2017), while for station 78, located on the Newfoundland shelf, we used nutrient measurements to calculate the PW fractions,  
9 following the approach from Jones et al. (1998) (the data are published in Benetti et al., 2017).

#### 10 2.4 Ancillary measurements and mixed layer depth determination

11 Potential temperature ( $\theta$ ), salinity (S), dissolved oxygen ( $O_2$ ) and beam attenuation data were retrieved from the CTD sensors  
12 (CTD SBE911 equipped with a SBE-43) that were deployed on a stainless steel rosette. Nutrient and pigment samples were  
13 obtained from the stainless steel rosette casts and analysed according to Aminot and Kerouel (2007) and Ras et al. (2008),  
14 respectively. We used the data from the stainless steel rosette casts that were deployed immediately before or after our TMR  
15 casts. All these data are available on the LEFE/CYBER database (<http://www.obs-vlfr.fr/proof/php/geovide/geovide.php>).  
16 The mixed layer depth ( $Z_m$ ) for each station was calculated using the function “calculate.mld” (part of the “realcofi” package,  
17 Ed Weber at NOAA SWFSC) created by Sam McClathie (NOAA Federal, 30<sup>th</sup> December 2013) for R software and where  $Z_m$   
18 is defined as an absolute change in the density of seawater at a given temperature ( $\Delta\sigma_t \geq 0.125 \text{ kg m}^{-3}$ ) with respect to an  
19 approximately uniform region of density just below the ocean surface (Kara et al., 2000). In addition to the density criterion,  
20 the temperature and salinity profiles were inspected at each station for uniformity within this layer. When they were not  
21 uniform, the depth of any perturbation in the profile was chosen as the base of the  $Z_m$  (Table 1).

#### 22 2.5 Statistical analysis

23 All statistical approaches, namely the comparison between the pore size used for filtration, correlations and Principal  
24 Component Analysis (PCA), were performed using the R statistical software (R development Core Team 2012). For all the  
25 results, p-values were calculated against the threshold value alpha ( $\alpha$ ), that we assigned at 0.05, corresponding to a 95% level  
26 of confidence. For all data sets, non-normal distributions were observed according to the Shapiro-Wilk test. Therefore, the  
27 significance level was determined with a Wilcoxon test.  
28 All sections and surface layer plots were prepared using Ocean Data View (Schlitzer, 2016).

Deleted:

Formatted: Font: (Asian) SimSun, Font color: Black, Complex Script Font: 10 pt, English (Australia)

Deleted: 3

Deleted: S

Deleted: CTD

Deleted: CTD casts

Deleted:

Deleted: /will be

Formatted: Subscript

Deleted: ,

Deleted: (

Deleted: 4

Deleted: measured

## 2.6 Water mass determination and associated DFe concentrations

The water mass structure in the North Atlantic Ocean from the GEOVIDE voyage was quantitatively assessed by means of an extended Optimum Multi-Parameter (eOMP) analysis with 14 water masses (for details see García-Ibáñez et al., 2015; this issue). Using this water mass determination, DFe concentrations were considered as representative of a specific water mass only when the contribution of this specific water mass was higher than 60% of the total water mass pool.

Deleted: 5

## 2.7 Database

The complete database of dissolved Fe is available in the electronic supplement [www.biogeosciences.net](http://www.biogeosciences.net). Overall, 540 data points of dissolved Fe are reported, among which 511 values are used in this manuscript. The remaining 29 values (5.7% of the total dataset) are flagged as (suspect) outliers. These 29 outliers were not used in figures and in the interpretation of this manuscript. The criteria for rejection were based on the comparison with other parameters measured from the same GO-FLO sampler, and curve fitting versus samples collected above and below the suspect sample. The complete data set will be available in national and international databases (LEFE-CYBER, <http://www.obs-vlfr.fr/proof/index2.php>, and GEOTRACES <http://www.bodc.ac.uk/geotraces/>).

Deleted: From this water mass determination, we considered only a contribution higher than 60% of a specific water mass to the total water mass pool and calculated the average DFe concentrations within each water mass and considered them as representative of the DFe concentrations within these water masses, as identifying representative end-members was not found to be possible due to the non-conservative behaviour of DFe in seawater.

Deleted: 6

Deleted: relational

Deleted: base

## 3 Results

### 3.1 Hydrography

The hydrology and circulation of the main water masses along the OVIDE section in the North Atlantic Subpolar Gyre and their contribution to the Atlantic Meridional Overturning Circulation (AMOC) have been described using an eOMP analysis by García-Ibáñez et al., (2015; this issue) and Zunino et al. (2017). For a schematic of water masses, currents and pathways, see Danialt et al. (2016). Hereafter we summarise the main features (Fig. 1 and 2).

Moved (insertion) [1]

Moved up [1]: For a schematic of water masses, currents and pathways, see Danialt et al. (2016).

*Upper waters (~ 0 – 800 m)* - The cyclonic circulation of the Eastern North Atlantic Central Water (ENACW) ( $12.3 < \theta < 16^{\circ}\text{C}$ ,  $35.66 < S < 36.2$ ,  $241 < O_2 < 251 \mu\text{mol kg}^{-1}$ ) occupied the water column from 0 to ~ 800 m depth from stations 1 to 25 contributing to 60% of the water mass pool. The sharp Subarctic Front (between stations 26 and 29), caused by the northern branch of the North Atlantic Current (NAC) separated the cyclonic subpolar from the anticyclonic subtropical gyre domains at  $50^{\circ}\text{N}$  and  $22.5^{\circ}\text{W}$ . The ENACW were also encountered to a lesser extent and only in surface waters (from 0 to ~ 100 m depth) between stations 29 and 34 (contributing to less than 40% of the water mass pool). West of the Subarctic Front, Iceland SubPolar Mode Waters (IcSPMW,  $7.07 < \theta < 8^{\circ}\text{C}$ ,  $35.16 < S < 35.23$ ,  $280 < O_2 < 289 \mu\text{mol kg}^{-1}$ ) was encountered from stations 34-40 (accounting for more than 45% of the water mass pool from 0 to ~ 800 m depth) and Irminger SubPolar Mode Waters (IrSPMW,  $\theta \approx 5^{\circ}\text{C}$ ,  $S \approx 35.014$ ) from stations 42-44 (contributing to 40% of the water mass pool from 0 to ~ 250 m

Deleted: se Central Waters

Deleted: were encountered

Deleted: stations 34-40 (accounting for more than 45% of the water mass pool from 0 to ~ 800 m depth) and

Deleted: 60

Deleted: contribution

1 depth) and stations 49 and 60 (accounting for 40% of the water mass pool down to 1300 m depth). The IcSPMW was also  
2 observed within the Subtropical gyre (stations 11-26), subducted below ENACW until ~ 1000 m depth. Stations 63 (> ~ 200  
3 m depth) and 64 (from surface down to ~ 500 m depth) exhibited a contribution of the IrSPMW higher than 45%. Stations 44,  
4 49 and 60, from the Irminger Sea, and 63 from the Labrador Sea were characterised by lower sea-surface salinity ranges ( $S =$   
5  $[34.636, 34.903]$ , stations 63 and 60, respectively). Subarctic Intermediate Water (SAIW,  $4.5 < \theta < 6.0^{\circ}\text{C}$ ,  $34.70 < S < 34.80$ )  
6 contributed to more than 40% of the water mass pool in the Iceland Basin between the surface and ~ 400 m depth at stations  
7 29 and 32 and throughout the water column of stations 53, 56 and 61 and from surface down to ~ 200 m depth at station 63.  
8 From stations 68 to 78 surface waters were characterized by a minimum of salinity and a maximum of oxygen ( $S = 34.91$ ,  $\text{O}_2$   
9  $= 285 \mu\text{mol kg}^{-1}$ ,  $\theta \approx 3^{\circ}\text{C}$ ) and corresponded to the newly formed Labrador Sea Water (LSW). The LSW was also observed in  
10 surface waters of station 44 with a similar contribution than IrSPMW (~ 40%).

11  
12 *Intermediate waters (~ 800 – 1400 m)* - The Mediterranean Outflow Water (MOW), distinguishable from surrounding Atlantic  
13 Water by its high salinity tongue (up to 36.2), a minimum of oxygen ( $\text{O}_2 = 210 \mu\text{mol kg}^{-1}$ ) and relatively high temperatures  
14 (up to  $11.7^{\circ}\text{C}$ ) was observed from station 1 to 21 between 800 and 1400 m depth at a neutral density ranging from 27.544 to  
15  $27.751 \text{ kg m}^{-3}$  with the maximum contribution to the whole water mass pool seen at station 1 ( $64 \pm 6\%$ ). Its main core was  
16 located at ~ 1200 m depth off the Iberian shelf from stations 1 to 11 and then gradually rising westward due to mixing with  
17 LSW within the North Atlantic subtropical gyre and a contribution of this water mass decreasing until station 21 down to 10-  
18 20%. The LSW ( $27.763 < \text{neutral density} < 27.724 \text{ kg m}^{-3}$ ) was sourced from the SPMW after intense heat loss and led to its  
19 deep convection. During GEOVIDE, LSW formed by deep convection the previous winter was found at several stations in the  
20 Labrador Sea (68, 69, 71 and 77). After convecting, LSW splits into three main branches with two main cores separated by the  
21 Reykjanes Ridge, (stations 1-32, West European and Iceland Basins; stations 40-60, Irminger Sea), and the last one, entering  
22 the West European Basin (Zunino et al., 2017).

23  
24 *Overflows and Deep waters (~ 1400 - 5500 m)* - North East Atlantic Deep Water (NEADW,  $1.98 < \theta < 2.50^{\circ}\text{C}$ ,  $34.895 < S <$   
25  $34.940$ ) was the dominant water mass in the West European Basin at stations 1-29 from 2000 m depth to the bottom and is  
26 characterized by high silicic acid ( $42 \pm 4 \mu\text{mol L}^{-1}$ ), nitrate ( $21.9 \pm 1.5 \mu\text{mol L}^{-1}$ ) concentrations and lower oxygen concentration  
27 ( $\text{O}_2 \approx 252 \mu\text{mol kg}^{-1}$ ) (see Sarthou et al., 2018). The core of the NEADW (stations 1-13) was located near the seafloor and  
28 gradually decreased westward. Polar Intermediate Water (PIW,  $\theta \approx 0^{\circ}\text{C}$ ,  $S \approx 34.65$ ) is a ventilated, dense, low-salinity water  
29 intrusion to the deep overflows within the Irminger and Labrador Seas that is formed at the Greenland shelf. PIW represents  
30 only a small contribution to the whole water mass pool (up to 27%) and was observed over the Greenland slope at stations 53  
31 and 61 as well as in surface waters from station 63 (from 0 to ~ 200 m depth), in intermediate waters of stations 49, 60 and 63  
32 (from ~ 500 to ~ 1500 m depth) and in bottom waters of stations 44, 68, 69, 71 and 77 with a contribution higher than 10%.  
33 Iceland Scotland Overflow Water (ISOW,  $\theta \approx 2.6^{\circ}\text{C}$ ,  $S \approx 34.98$ ) is partly formed within the Arctic Ocean by convection of the  
34 modified Atlantic water. ISOW comes from the Iceland-Scotland sills and flows southward towards the Charlie-Gibbs Fracture

Deleted: until

Deleted: for stations 49 and 60

Deleted: , respectively

Deleted: the Central Waters

Deleted: The

Deleted: The Mediterranean Water (MW) flows westward from the Mediterranean Sea and is then transported northward by the Azores counter current.

Deleted: GA01

Deleted: new

Deleted: formed by deep convection the previous winter

Deleted: from

Deleted: some the LSW flows north-eastward in the Iceland Basin and Irminger Sea and then back to the Labrador Sea, while some flows along the Canadian coast, more specifically above the Newfoundland Margin as confirmed by hydrographic station 76 ( $52.5^{\circ}\text{W}$ ,  $52.5^{\circ}\text{N}$ ) which exhibited the highest LSW fraction (up to 98% at the closest bottom sample, García-Ibáñez et al., this issue). On its way eastwards, the

Deleted: , that corresponds to its different pathways

Deleted: . One of the branches flows eastward at intermediate depth, following the circulation of the warm surface NAC and

Deleted: s

Deleted: and the Iceland Basin where it splits again into two branches (south-eastward and north-eastward flowing path, respectively).

Deleted: The

Formatted: Superscript

Deleted: Sarthou et al., 2018

Deleted: The

Deleted: shelf

Deleted: in

Deleted: PIW is in contact with the atmosphere once a year during the time of winter convection (Strass et al., 1993) and hence is ventilated ( $\text{O}_2 \approx 310 \mu\text{mol kg}^{-1}$ ) This water presented

Deleted: low

Deleted: entire

Deleted: . The PIW

Deleted: The

Deleted:



1 Zone (CGFZ) and Bight Fracture Zone (BFZ) (stations 34 and 36) after which it reverses its flowing path northward and enters  
2 the Irminger Sea (stations 40 and 42) to finally reach the Labrador Sea close to the Greenland coast (station 49, station 44  
3 being located in between this two opposite flow paths). Along the eastern (stations 26-36) and western (stations 40-44) flanks  
4 of the Reykjanes Ridge, ISOW had a contribution higher than 50% to the water mass pool. JSOW was observed from 1500 m  
5 depth to the bottom of the entire Iceland Basin (stations 29-38) and from 1800 to 3000 m depth within the Irminger Sea  
6 (stations 40-60). JSOW, despite having a fraction lower than 45% above the Reykjanes Ridge (station 38), was the main  
7 contributor to the water mass pool from 1300 m depth down to the bottom. JSOW was also observed within the Labrador Sea  
8 from stations 68 to 77. Finally, the deepest part of the Irminger (stations 42 and 44) and Labrador (stations 68-71) Seas were  
9 occupied by Denmark Strait Overflow Water (DSOW,  $\theta \approx 1.30^{\circ}\text{C}$ ,  $S \approx 34.905$ ).

## 10 3.2 Ancillary data

### 11 3.2.1 Nitrate

12 Surface nitrate ( $\text{NO}_3^-$ ) concentrations (García-Ibáñez et al., 2018; Pérez et al., 2018; Sarthou et al., 2018) ranged from 0.01 to  
13  $10.1 \mu\text{mol L}^{-1}$  (stations 53 and 63, respectively). There was considerable spatial variability in  $\text{NO}_3^-$  surface distributions with  
14 high concentrations found in the Iceland Basin and Irminger Sea (higher than  $6 \mu\text{mol L}^{-1}$ ), as well as at stations 63 ( $10.1 \mu\text{mol}$   
15  $\text{L}^{-1}$ ) and 64 ( $5.1 \mu\text{mol L}^{-1}$ ), and low concentrations observed in the West European Basin, in the Labrador Sea and above  
16 continental margins. The low surface concentrations in the West European Basin ranged from 0.02 (station 11) to  $3.9$  (station  
17  $25$ )  $\mu\text{mol L}^{-1}$ . Station 26 delineating the extreme western boundary of the West European Basin exhibited enhanced  $\text{NO}_3^-$   
18 concentrations as a result of mixing between ENACW and ICSPMW, although these surface waters were dominated by  
19 ENACW. In the Labrador Sea (stations 68-78) low surface concentrations were observed with values ranging from 0.04 (station  
20 68) to  $1.8$  (station 71)  $\mu\text{mol L}^{-1}$ . At depth, the lowest concentrations (lower than  $15.9 \mu\text{mol L}^{-1}$ ) were measured in ENACW (~  
21  $0 - 800 \text{ m depth}$ ) and DSOW ( $> 1400 \text{ m depth}$ ), while the highest concentrations were measured within NEADW (up to  $23.5$   
22  $\mu\text{mol L}^{-1}$ ), and in the mesopelagic zone of the West European and Iceland Basins (higher than  $18.4 \mu\text{mol L}^{-1}$ ).

### 23 3.2.2 Chlorophyll-*a*

24 Overall, most of the phytoplankton biomass was localised above 100 m depth with lower total chlorophyll-*a* (TChl-*a*)  
25 concentrations south of the Subarctic Front and higher at higher latitudes (see supplementary material Fig. S1). While  
26 comparing TChl-*a* maxima considering all stations, the lowest value ( $0.35 \text{ mg m}^{-3}$ ) was measured within the West European  
27 Basin (station 19, 50 m depth) while the highest values were measured at the Greenland (up to  $4.9 \text{ mg m}^{-3}$ , 30 m depth, station  
28 53 and up to  $6.6 \text{ mg m}^{-3}$ , 23 m depth, station 61) and Newfoundland (up to  $9.6 \text{ mg m}^{-3}$ , 30 m depth, station 78) margins.

**Deleted:** In this study, ISOW properties are defined after the mixing of the overflow with Atlantic Central Water and Labrador Water downstream the sills. ... along the eastern (stations 26-36) and western (stations 40-44) flanks of the Reykjanes Ridge, ISOW had a contribution higher than 50% to the water mass pool. The ...SOW was observed from 1500 m depth to the bottom of the entire Iceland Basin (stations 29-38) and from 1800 to 3000 m depth within the Irminger Sea (stations 40-60). The ...SOW, despite having a fraction lower than 45% above the Reykjanes Ridge (station 38), was the main contributor to the water mass pool from 1300 m depth down to the bottom. The ...SOW was also observed within the Labrador Sea from stations 68 to 77. Finally, the deepest part of the Irminger (stations 42 and 44) and Labrador (stations 68-71) Seas were occupied by the Denmark Strait Overflow Water (DSOW,  $\theta \approx 1.30^{\circ}\text{C}$ ,  $S \approx 34.905$ ), that spills over the Greenland-Scotland ridge system and overflows south-westward into the deep North Atlantic basins. This water mass is formed partly in the Arctic Ocean by convection of the branch of the NAC that flows northward between Greenland, Iceland and Scotland. DSOW is a young water mass with a 3 to 4-year residence time north of the sill after surface contact. ...

**Deleted:** Sarthou et al., in prep.) ... ranged from 0.01 to  $10.1 \mu\text{mol L}^{-1}$  (stations 53 and 63, respectively). There was considerable spatial variability in  $\text{NO}_3^-$  surface distributions with high  $\text{NO}_3^-$  concentrations found in the Iceland Basin and Irminger Sea (higher than  $6 \mu\text{mol L}^{-1}$ ), as well as at stations 63 ( $10.1 \mu\text{mol L}^{-1}$ ) and 64 ( $5.1 \mu\text{mol L}^{-1}$ ), and the lowest concentrations observed in the Western European Basin, in the Labrador Sea and above continental margins. The low surface  $\text{NO}_3^-$  concentrations in the Western European Basin extended from station 2 (closest station to continental land mass) to station 23 (most open ocean station) with concentrations ranging from 0.02 (station 11) to  $3.9$  (station 25)  $\mu\text{mol L}^{-1}$ . Station 26 delineating the extreme western boundary of the West European Basin exhibited enhanced  $\text{NO}_3^-$  concentrations as a result of mixing between ENACW and ICSPMW, although these surface waters were dominated by ENACW. The low nitrate concentrations in the Labrador Sea (stations 68-78) extended from station 68 to station 78 with low surface concentrations were observed with ranging from 0.04 (station 68) to  $1.8$  (station 71)  $\mu\text{mol L}^{-1}$ . At depth, the lowest  $\text{NO}_3^-$  concentrations (lower than  $15.9 \mu\text{mol L}^{-1}$ ) were measured in surface ENACW (~  $0 - 800 \text{ m depth}$ ) and deep DSOW ( $> 1400 \text{ m depth}$ ) ... while waters were found in the ...

**Deleted:** Overall, total chlorophyll-*a* (TChl-*a*) concentrations were significantly correlated with the more extensive dataset from the CTD mounted fluorometer ( $R^2 = 0.76$ ,  $n = 162$ ). TChl-*a* is the universal proxy for phytoplankton organisms. The maximum chlorophyll biomass ranged between  $0.35 \text{ mg m}^{-3}$  (Station 19, 50 m depth) and  $9.4 \text{ mg m}^{-3}$  (station 78, 30 m depth) highlighting the intense variability observed throughout this section (Fig. 3). Generally speaking, most of the phytoplankton biomass was localised above 100 m depth with lower total chlorophyll-*a* concentrations south of the Subarctic Front and higher at higher latitudes (see supplementary material Fig. S1). While comparing TChl-*a* maxima considering all stations, the lowest TChl-*a* value ( $< 0.75 \text{ mg m}^{-3}$ ) was measured within the West European Basin (station 19, 50 m depth) and Iceland (stations 34-38) Basins, while the highest concentrations values were measured at the Greenland (up to  $4.9 \text{ mg m}^{-3}$ , 30 m depth, stations 53 and up to  $6.6 \text{ mg m}^{-3}$ , 23 m depth, station 61) and Newfoundland (up to  $9.6 \text{ mg m}^{-3}$ , 30 m depth, station 78) margins (up to  $4.9$ ,  $6.6$  and  $9.6 \text{ mg m}^{-3}$ , respectively) ...

### 1 3.3 Dissolved Fe concentrations

2 Dissolved Fe concentrations (see supplementary material Table S1) ranged from  $0.09 \pm 0.01 \text{ nmol L}^{-1}$  (station 19, 20 m depth)  
3 to  $7.8 \pm 0.5 \text{ nmol L}^{-1}$  (station 78, 371 m depth) (see Fig. 3). Generally, vertical profiles of DFe for stations above the margins  
4 (2, 4, 53, 56, 61, and 78) showed an increase with depth, although sea-surface maxima were observed at stations 2, 4 and 56.  
5 For these margin stations, values ranged from  $0.7$  to  $1.0 \text{ nmol L}^{-1}$  in the surface waters. Concentrations increased towards the  
6 bottom, with more than  $7.8 \text{ nmol L}^{-1}$  measured at station 78, approximately  $1\text{-}3 \text{ nmol L}^{-1}$  for stations 2, 4, 53, and 61, and just  
7 above  $0.4 \text{ nmol L}^{-1}$  for station 56 (Fig. 4). Considering the four oceanic basins, mean vertical profiles (supplementary material  
8 Fig. S2) showed increasing DFe concentrations down to 3000 m depth followed by decreasing DFe concentrations down to  
9 the bottom. Among deep-water masses, the lowest DFe concentrations were measured in the West European Basin. The  
10 Irminger Sea displayed the highest DFe concentrations from 1000 m depth to the bottom relative to other basins at similar  
11 depths (Fig. 4 and supplementary material Fig. S2). In the Labrador Sea, DFe concentrations were low and relatively constant  
12 at about  $0.87 \pm 0.06 \text{ nmol L}^{-1}$  from 250 m to 3000 m depth (Fig. S2). Overall, surface DFe concentrations were higher ( $0.36 \pm$   
13  $0.18 \text{ nmol L}^{-1}$ ) in the North Atlantic Subpolar gyre (above  $52^\circ\text{N}$ ) than in the North Atlantic Subtropical gyre ( $0.17 \pm 0.05 \text{ nmol}$   
14  $\text{L}^{-1}$ ). The upper surface DFe concentrations were generally smaller than  $0.3 \text{ nmol L}^{-1}$ , except for few stations in the Iceland  
15 Basin (stations 32 and 38), Irminger (stations 40 and 42) and Labrador (station 63) Seas, where values ranged between  $0.4\text{-}0.5$   
16  $\text{nmol L}^{-1}$ .

### 18 3.4 Fingerprinting water masses

19 In the Labrador Sea, IrSPMW exhibited an average DFe concentration of  $0.61 \pm 0.21 \text{ nmol L}^{-1}$  ( $n=14$ ). DFe concentrations in  
20 the LSW were the lowest in this basin, with an average value of  $0.71 \pm 0.27 \text{ nmol L}^{-1}$  ( $n=53$ ) (see supplementary material Fig.  
21 S3). Deeper, ISOW displayed slightly higher average DFe concentrations ( $0.82 \pm 0.05 \text{ nmol L}^{-1}$ ,  $n=2$ ). Finally, DSOW had the  
22 lowest average ( $0.68 \pm 0.06 \text{ nmol L}^{-1}$ ,  $n=3$ , see supplementary material Fig. S3) and median ( $0.65 \text{ nmol L}^{-1}$ ) DFe values for  
23 intermediate and deep waters.  
24 In the Irminger Sea, surface waters were composed of SAIW ( $0.56 \pm 0.24 \text{ nmol L}^{-1}$ ,  $n=4$ ) and IrSPMW ( $0.72 \pm 0.32 \text{ nmol L}^{-1}$ ,  
25  $n=34$ ). The highest open-ocean DFe concentrations (up to  $2.5 \pm 0.3 \text{ nmol L}^{-1}$ , station 44, 2600 m depth) were measured within  
26 this basin. In the upper intermediate waters, LSW was identified only at stations 40 to 44, and had the highest DFe values with  
27 an average of  $1.2 \pm 0.3 \text{ nmol L}^{-1}$  ( $n=14$ ). ISOW showed higher DFe concentrations than in the Iceland Basin ( $1.3 \pm 0.2 \text{ nmol}$   
28  $\text{L}^{-1}$ ,  $n=4$ ). At the bottom, DSOW was mainly located at stations 42 and 44 and presented the highest average DFe values ( $1.4$   
29  $\pm 0.4 \text{ nmol L}^{-1}$ ,  $n=5$ ) as well as the highest variability from all the water masses presented in this section (see supplementary  
30 material Fig. S3).  
31 In the Iceland Basin, SAIW and IcSPMW displayed similar averaged DFe concentrations ( $0.67 \pm 0.30 \text{ nmol L}^{-1}$ ,  $n=7$ ) and  $0.55$   
32  $\pm 0.34 \text{ nmol L}^{-1}$ ,  $n=22$ , respectively). Averaged DFe concentrations were similar in both LSW and ISOW, and higher than in

Deleted: The dataset is well distributed between upper, intermediate and deep ocean samples with 36% of samples collected at depths shallower than 200 m, 27% of samples between 200 and 1000 m depth and 37% of samples from depths deeper than 1000 m, including 11% of samples below 2500 m depth. Samples are distributed as follows between basins: 38% of samples were collected within the West European Basin (stations 1 and 11-26), 17% with (...)

Deleted: 4

Deleted: ¶

Deleted: were around

Deleted: -

Deleted: 5

Deleted: ¶

Deleted: For all regions

Deleted: Fig. 6

Deleted: from the surface

Deleted: , with the

Deleted: deep values

Deleted: s

Deleted: 6

Deleted: 6

Formatted: Superscript

Deleted: 30

Deleted: Within the low-Fe West European Basin a few stations (...)

Deleted: 3.3.

Moved (insertion) [4]

Deleted: characterized by the

Deleted: the

Deleted: the

Deleted: The

Deleted: the

Deleted: Fig. 7

Deleted: ¶

Deleted: In the West European Basin, the MOW was present bu (...)

Deleted: the

Deleted: the

Deleted: with averaged DFe concentrations of

Deleted: (

Deleted: 7)

Deleted: (

Deleted: )

Deleted: The

1 SAIW and IcSPMW ( $0.96 \pm 0.22 \text{ nmol L}^{-1}$ ,  $n=21$  and  $1.0 \pm 0.3 \text{ nmol L}^{-1}$ ,  $n=10$ , respectively, see supplementary material Fig. S3).  
 2  
 3 Finally, in the West European Basin, DFe concentrations in ENACW were the lowest of the whole section with an average  
 4 value of  $0.30 \pm 0.16 \text{ nmol L}^{-1}$  ( $n=64$ ). MOW was present deeper in the water column but was not characterized by particularly  
 5 high or low DFe concentrations relative to the surrounding Atlantic waters (see supplementary material Fig. S3). The median  
 6 DFe value in MOW was very similar to the median value when considering all water masses ( $0.77 \text{ nmol L}^{-1}$ , Fig. 3 and  
 7 supplementary material S3). LSW and IcSPMW displayed slightly elevated DFe concentrations compared to the overall  
 8 median with mean values of  $0.82 \pm 0.08$  ( $n=28$ ) and  $0.80 \pm 0.04$  ( $n=8$ )  $\text{nmol L}^{-1}$ , respectively. The DFe concentrations in  
 9 NEADW were relatively similar to the DFe median value of the GEOVIDE voyage (median DFe =  $0.75 \text{ nmol L}^{-1}$ , Fig. 3 and  
 10 supplementary material Fig. S3) with an average value of  $0.74 \pm 0.16 \text{ nmol L}^{-1}$  ( $n=18$ ) and presented relatively low median  
 11 DFe concentrations (median DFe =  $0.71 \text{ nmol L}^{-1}$ ) compared to other deep water masses.

## 12 4 Discussion

13 In the following sections, we will first discuss the high DFe concentrations observed throughout the water column of stations  
 14 1 and 17 located in the West European Basin (Section 4.1), then, the relationship between water masses and the DFe  
 15 concentrations (Section 4.2) in intermediate (Section 4.2.2 and 4.2.3) and deep (Section 4.2.4 and 4.2.5) waters. We will also  
 16 discuss the role of wind (Section 4.2.1), rivers (Section 4.3.1), meteoric water and sea-ice processes (Section 4.3.2),  
 17 atmospheric deposition (Section 4.3.3) and sediments (Section 4.4) in delivering DFe. Finally, we will discuss the potential Fe  
 18 limitation using DFe:NO<sub>3</sub><sup>-</sup> ratios (Section 4.5).

### 19 4.1 High DFe concentrations at station 1 and 17

20 Considering the entire section, two stations (stations 1 and 17) showed irregularly high DFe concentrations ( $> 1 \text{ nmol L}^{-1}$ )  
 21 throughout the water column, thus suggesting analytical issues. However, these two stations were analysed twice and provided  
 22 similar results, therefore discarding any analytical issues. This means that these high values originated either from genuine  
 23 processes or from contamination issues. If there had been contamination issues, one would expect a more random distribution  
 24 of DFe concentrations and less consistence throughout the water column. It thus appears that contamination issues were  
 25 unlikely to happen. Similarly, the influence of water masses to explain these distributions was discarded as the observed high  
 26 homogenized DFe concentrations were restricted to these two stations. Station 1, located at the continental shelf-break of the  
 27 Iberian Margin, also showed enhanced PFe concentrations, from lithogenic origin suggesting a margin source (Gourain et al.,  
 28 2018). Conversely, no relationship was observed between DFe and PFe nor transmissometry for station 17. However, Ferron  
 29 et al. (2016) reported a strong dissipation rate at the Azores-Biscay Rise (station 17) due to internal waves. The associated  
 30 vertical energy fluxes could explain the homogenized profile of DFe at station 17, although such waves are not clearly  
 31 evidenced in the velocity profiles. Consequently, the elevated DFe concentrations observed at station 17 remain unsolved.

**Deleted:** LSW exhibited higher DFe concentrations with an average value of  $0.96 \pm 0.22 \text{ nmol L}^{-1}$  ( $n=21$ ). The ISOW had an averaged DFe concentration of  $1.0 \pm 0.3 \text{ nmol L}^{-1}$  ( $n=10$ ) (Fig. 7).

**Moved up [4]:** In the Irminger Sea, surface waters were characterized by the SAIW ( $0.56 \pm 0.24 \text{ nmol L}^{-1}$ ,  $n=4$ ) and the IrSPMW ( $0.72 \pm 0.32 \text{ nmol L}^{-1}$ ,  $n=34$ ). The highest open-ocean DFe concentrations (up to  $2.5 \pm 0.3 \text{ nmol L}^{-1}$ , station 44, 2600 m depth) were measured within this basin. In the upper intermediate water the LSW was identified only at stations 40 to 44, and had the highest DFe values with an average of  $1.2 \pm 0.3 \text{ nmol L}^{-1}$  ( $n=14$ ). The ISOW showed higher DFe concentrations than in the Iceland Basin ( $1.3 \pm 0.2 \text{ nmol L}^{-1}$ ,  $n=4$ ). At the bottom, the DSOW was mainly located at stations 42 and 44 and presented the highest average DFe values ( $1.4 \pm 0.4 \text{ nmol L}^{-1}$ ,  $n=5$ ) as well as the highest variability from all the water masses presented in this section (Fig. 7). ¶

**Deleted:** in the Labrador Sea, the IrSPMW exhibited an average DFe concentration of  $0.61 \pm 0.21 \text{ nmol L}^{-1}$  ( $n=14$ ). DFe concentrations in the LSW were the lowest in this basin compared to the other ones, with an average value of  $0.71 \pm 0.27 \text{ nmol L}^{-1}$  ( $n=53$ ) (Fig. 7). Deeper, the ISOW displayed slightly higher DFe concentrations ( $0.82 \pm 0.05 \text{ nmol L}^{-1}$ ,  $n=2$ ). Finally, the DSOW had one of the lowest DFe values for intermediate and deep waters ( $0.68 \pm 0.06 \text{ nmol L}^{-1}$ ,  $n=3$ , Fig. 7).

**Deleted:** 1

**Deleted:** 1

**Deleted:** 1

**Deleted:** 1

**Deleted:** 1

**Deleted:** 1

**Deleted:** 2

**Deleted:** 2

**Deleted:** 2

**Deleted:** 3

**Deleted:** 4

**Formatted:** Heading 2

**Deleted:** only

**Deleted:** . T

**Deleted:** more likely to be impacted by vertical processes

**Deleted:** . Another explanation which cannot be discarded would be a contamination issue, especially for station 1 as it was the first station sampled. With this in mind, one would expect a more random distribution of DFe concentrations and less consistence throughout the water column if there had been a problem with contamination.

**Moved (insertion) [6]**

**Deleted:** potentially

**Moved up [6]:** Another explanation which cannot be discarded would be a contamination issue, especially for station 1 as it was the first station sampled. With this in mind, one would expect a more random distribution of DFe concentrations and less consistence

## 4.2 DFe and hydrology keypoints

### 4.2.1 How do Air-sea interactions affect DFe concentration in the Irminger Sea?

Among the four distinct basins described in this paper, the Irminger Sea exhibited the highest DFe concentrations within the surface waters (from 0 to 250 m depth) with values ranging from 0.23 to 1.3 nmol L<sup>-1</sup> for open-ocean stations. Conversely, low DFe concentrations were previously reported in the central Irminger Sea by Rijkenberg et al. (2014) (April-May, 2010) and Achterberg et al. (2018) (April-May and July-August, 2010) with DFe concentrations ranging from 0.11 to 0.15 and from ~0 to 0.14 nmol L<sup>-1</sup>, respectively (see supplementary material Fig. S4 and Table S2). Differences might be due to the phytoplankton bloom advancement, the high remineralization rate (Lemaître et al., 2017) observed within the LSW in the Irminger Sea (see Section 4.1.3) and a deeper winter convection in early 2014. Indeed, enhanced surface DFe concentrations measured during GEOVIDE in the Irminger Sea could be due to intense wind forcing events that would deepen the winter Z<sub>ed</sub> down to the core of the Fe-rich LSW.

In the North Atlantic Ocean, the warm and salty water masses of the upper limb of the MOC are progressively cooled and become denser, and subduct into the abyssal ocean. In some areas of the SubPolar North Atlantic, deep convective winter mixing provides a rare connection between surface and deep waters of the MOC thus constituting an important mechanism in supplying nutrients to the surface ocean (de Jong et al., 2012; Louanchi and Najjar, 2001). Deep convective winter mixing is triggered by the effect of wind and a pre-conditioning of the ocean in such a way that the inherent stability of the ocean is minimal. Pickart et al. (2003) demonstrated that these conditions are satisfied in the Irminger Sea with the presence of weakly stratified surface water, a close cyclonic circulation, which leads to the shoaling of the thermocline and intense winter air-sea buoyancy fluxes (Marshall and Schott, 1999). Moore (2003) and Piron et al. (2016) described low-level westerly jets centred northeast of Cape Farewell, over the Irminger Sea, known as jet events. These events occur when wind is split around the orographic features of Cape Farewell, and are strong enough to induce deep convective mixing (Bacon et al., 2003; Pickart et al., 2003). It has also been shown that during winters with a positive North Atlantic Oscillation (NAO) index, the occurrence of such events is favoured (Moore, 2003; Pickart et al., 2003), which was the case in the winter 2013-2014, preceding the GEOVIDE voyage as opposed to previous studies (Lherminier, pers. comm.). The winter mixed layer depth prior to the cruise reached up to 1200 m depth in the Irminger Sea (Zunino et al., 2017), which was most likely attributed to a final deepening due to wind forcing events (centred at station 44). Such winter entrainment was likely the process involved in the vertical supply of DFe within surface waters fuelling the spring phytoplankton bloom with DFe values close to those found in LSW.

### 4.2.2 Why don't we see a DFe signature in the Mediterranean Overflow Water (MOW)?

On its northern shores, the Mediterranean Sea is bordered by industrialized European countries, which act as a continuous source of anthropogenic derived constituents into the atmosphere, and on the southern shores by the arid and desert regions of north African and Arabian Desert belts, which act as sources of crustal material in the form of dust pulses (Chester et al., 1993; Guerzoni et al., 1999; Martin et al., 1989). During the summer, when thermal stratification occurs, DFe concentrations in the

Deleted: 1

Deleted: 1

Deleted: ranging from 0.23 to 1.3 nmol L<sup>-1</sup> in open-ocean stations and ...rom 0 to 250 m depth) with values ranging from 0.23 to 1.3 nmol L<sup>-1</sup> for open-ocean stations. Conversely, low Enhanced surface D...Fe concentrations in the Irminger Sea ...ere previously reported in the central Irminger Sea by Rijkenberg et al. (2014) (April-May, 2010) and Achterberg et al. (2018) (April-May and July- ...ugust, 2010) with DFe concentrations ranging from 0.11 to 0.15 and from ~0 to 0.ranging from

Formatted: Superscript

Deleted: However, DFe concentrations measured during our study (May-June, 2014) in the Irminger Sea were higher than those reported before (Table 3). ...ifferences might be due to the phytoplankton bloom advancement, the high remineralization rate observed

Formatted: Subscript

Deleted: In the ...ubPolar North Atlantic, deep convective winter convective ...ixing provides a rare connection between surface and deep waters of the MOC thus constituting an important mechanism in supplying nutrients to the surface ocean represents the dominant nutrient supply process

Deleted: effect

Deleted: .... ADDIN EN.CITE <EndNote><Cite AuthorYear="1"><Author>Pickart</Author><Year>2003</Year><RecNum>1951</RecNum><DisplayText>Pickart et al. (2003)</DisplayText><record-><rec-number>1951</rec-number><foreign-keys><key app="EN" db-id="vzp0d0af8wwwepas0vexzytrws2fxffdp" timestamp="1508047470">1951</key><key app="ENWeb" db-id="">0</key></foreign-keys><ref-type name="Journal Article">17</ref-type><contributors><authors><author>Pickart, R. S.</author><author>Straneo, F.</author><author>Moore, G. W. K.</author></authors></contributors><titles><title>Is Labrador Sea Water formed in the Irminger basin?</title><secondary-title>Deep Sea Research Part I:</secondary-title></titles></periodical><full-title>Deep Sea Research Part I:</full-title></periodical><pages>23-52</pages><volume>50</volume><dates><year>2003</year></date><urls></urls></record-></Cite></EndNote>Pickart et al. (2003) demonstrated that these conditions necessary for the development of deep convection ...re satisfied in the Irminger Sea by ...ith the presence of weakly stratified surface water, a close cyclonic

Deleted: ..., whose ...these events occur when wind is split around the structure depends upon the splitting occurring as the flow encounter the ...rographic features from...f Cape Farewell, and th

Deleted: that are characterized by westerly flow over the Irminger Sea, centred northeast of Cape Farewell. ...re strong enough to induce deep convective mixing (Bacon et al., 2003; Pickart et al.,

Deleted: Therefore, the elevated DFe concentrations observed below 100 m depth from the central Irminger Sea were likely due

Deleted: 1

Deleted: Lack of

Deleted: T...he Mediterranean Sea on its northern shores

Deleted: the ...thermal stratification occurs period

1 SML can increase over the whole Mediterranean Sea by 1.6-5.3 nmol L<sup>-1</sup> in response to the accumulation of atmospheric Fe  
2 from both anthropogenic and natural origins (Bonnet and Guieu, 2004; Guieu et al., 2010; Sarthou and Jeandel, 2001). After  
3 atmospheric deposition, the fate of Fe will depend on the nature of aerosols, vertical mixing, biological uptake and scavenging  
4 processes (Bonnet and Guieu, 2006; Wuttig et al., 2013). During GEOVIDE, MOW was observed from stations 1 to 29  
5 between 1000 and 1200 m depth and associated with high dissolved aluminium (DAL, Menzel Barraqueta et al., 2018)  
6 concentrations (up to 38.7 nmol L<sup>-1</sup>), confirming the high atmospheric deposition in the Mediterranean region. In contrast to  
7 Al, no DFe signature was associated with MOW (Figs. 2 and 3). This feature was also reported in some studies (Hatta et al.,  
8 2015; Thuróczy et al., 2010), while others measured higher DFe concentrations in MOW (Gerringa et al., 2017; Sarthou et al.,  
9 2007). However, MOW coincides with the maximum Apparent Oxygen Utilization (AOU) and it is not possible to distinguish  
10 the MOW signal from the remineralisation one (Sarthou et al., 2007). On the other hand, differences between studies are likely  
11 originating from the intensity of atmospheric deposition and the nature of aerosols. Indeed, Wagener et al. (2010) highlighted  
12 that large dust deposition events can accelerate the export of Fe from the water column through scavenging. As a result, in  
13 seawater with high DFe concentrations and where high dust deposition occurs, a strong individual dust deposition event could  
14 act as a sink for DFe. It thus becomes less evident to observe a systematic high DFe signature in MOW despite dust inputs. ▾

#### 15 4.2.3 Fe enrichment in Labrador Sea Water (LSW)

16 As described in Section 3.1, the LSW exhibited increasing DFe concentrations from its source area, the Labrador Sea, toward  
17 the other basins with the highest DFe concentrations observed within the Irminger Sea, suggesting that the water mass was  
18 enriched in DFe either locally in each basin or during its flow path (see supplementary material Fig. S3). These DFe sources  
19 could originate from a combination of high export of PFe and its remineralisation in the mesopelagic area and/or the dissolution  
20 of sediment.

21 The Irminger and Labrador Seas exhibited the highest averaged integrated TChl-a concentrations (98 ± 32 mg m<sup>-2</sup> and 59 ± 42  
22 mg m<sup>-2</sup>) compared to the West European and Iceland Basins (39 ± 10 mg m<sup>-2</sup> and 53 ± 16 mg m<sup>-2</sup>), when the influence of  
23 margins was discarded. Stations located in the Irminger (stations 40-56) and Labrador (stations 63-77) Seas, were largely  
24 dominated by diatoms (>50% of phytoplankton abundances) and displayed the highest chlorophyllid-a concentrations, a tracer  
25 of senescent diatom cells, likely reflecting post-bloom condition (Tonnard et al., in prep.). This is in line with the highest POC  
26 export data reported by Lemaitre et al. (2018) in these two oceanic basins. This likely suggests that biogenic PFe export was  
27 also higher in the Labrador and Irminger Seas than in the West European and Iceland Basins. In addition, Gourain et al. (2018)  
28 highlighted a higher biogenic contribution for particles located in the Irminger and Labrador Seas with relatively high PFe:PAI  
29 ratios (0.44 ± 0.12 mol:mol and 0.38 ± 0.10 mol:mol, respectively) compared to particles from the West European and Iceland  
30 Basins (0.22 ± 0.10 and 0.38 ± 0.14 mol:mol, respectively, see Fig. 6 in Gourain et al., 2018). However, they reported no  
31 difference in PFe concentrations between the four oceanic basins (see Fig. 12A in Gourain et al., 2018) when the influence of  
32 margins was discarded, which likely highlighted the remineralisation of PFe within the Irminger and Labrador Seas. Indeed,  
33 Lemaitre et al. (2017) reported higher remineralisation rates within the Labrador (up to 13 mmol C m<sup>-2</sup> d<sup>-1</sup>) and Irminger Seas

#### Moved (insertion) [2]

**Moved up [2]:** During our study the MOW signal was clearly observed on dissolved aluminium (DAL, Menzel Barraqueta et al., 2018) with the highest DAL values from the section (up to 38.7 nmol L<sup>-1</sup>), suggesting intense dust deposition inputs to the Mediterranean Sea.

#### Deleted: ¶

Despite these high atmospheric depositions into the Mediterranean Sea providing Fe enrichment of Mediterranean waters and the high Apparent Oxygen Utilization (AOU), during the GEOVIDE voyage, no particular DFe signature was associated with the MOW (Figs. 2 and 4), Gourain et al., submitted Gourain et al. (submitted)

**Deleted:** which was also the case in other studies in the same area (Hatta et al., 2015; Thuróczy et al., 2010). During our study the MOW signal was clearly observed on dissolved aluminium (DAL, Menzel Barraqueta et al., 2018) with the highest DAL values from the section (up to 38.7 nmol L<sup>-1</sup>), suggesting intense dust deposition inputs to the Mediterranean Sea. Conversely, Gerringa et al. (2017) and Sarthou et al. (2007) observed higher DFe concentrations in the MOW. During our study the MOW signal was clearly observed on dissolved aluminium (DAL, Menzel Barraqueta et al., 2018) with the highest DAL values from the section (up to 38.7 nmol L<sup>-1</sup>), suggesting intense dust deposition inputs to the Mediterranean Sea. A concurring phenomenon, suggested by Wagener et al. (2010), is likely to explain this absence of MOW DFe signature. They pointed to the fact that large dust deposition events can accelerate the export of Fe from the water column through scavenging. As a result, in seawater with high DFe and where high dust deposition occurs, a strong individual dust deposition event could act as a sink for DFe.

#### Deleted: the

**Deleted:** The same explanation was reported by Gerringa et al. (2017) to account for the decrease in DFe concentrations between surface and deep waters from the Western Mediterranean Basin.

#### Deleted: 1

#### Deleted: Fe enrichment

**Deleted:** local sources of DFe

**Deleted:** may occur along

**Deleted:** Fig. 7

**Formatted:** Superscript

**Formatted:** Superscript

**Deleted:** Gourain et al. (subm.)

1 (up to 10 mmol C m<sup>-2</sup> d<sup>-1</sup>) using the excess barium proxy (Dehairs et al., 1997), compared to the West European and Iceland  
2 Basins (ranging from 4 to 6 mmol C m<sup>-2</sup> d<sup>-1</sup>). Therefore, the intense remineralisation rates measured in the Irminger and  
3 Labrador Seas likely resulted in enhanced DFe concentrations within LSW.  
4 Higher DFe concentrations were, however, measured in the Irminger Sea compared to the Labrador Sea and coincided with  
5 lower transmissometry values (i.e. 98.0-98.5% vs. >99%), thus suggesting a particle load of the LSW. This could be explained  
6 by the reductive dissolution of Newfoundland Margin sediments. Indeed, Lambelet et al. (2016) reported high dissolved  
7 neodymium (Nd) concentrations (up to 18.5 pmol.kg<sup>-1</sup>) within the LSW at the edge of the Newfoundland Margin (45.73°W,  
8 51.82°N) as well as slightly lower Nd isotopic ratio values relative to those observed in the Irminger Sea. They suggested that  
9 this water mass had been in contact with sediments approximately within the last 30 years (Charette et al., 2015). Similarly,  
10 during GA03, Hatta et al. (2015) attributed the high DFe concentrations in the LSW to continental margin sediments.  
11 Consequently, it is also possible that the elevated DFe concentrations from the three LSW branches which entered the West  
12 European and Iceland Basins and Irminger Sea was supplied through sediment dissolution (Measures et al., 2013) along the  
13 LSW pathway.  
14 The enhanced DFe concentrations measured in the Irminger Sea and within the LSW were thus likely attributed to the  
15 combination of higher productivity, POC export and remineralisation as well as a DFe supply from reductive dissolution of  
16 Newfoundland sediments to the LSW along its flow path.

#### 17 4.2.4 Enhanced DFe concentrations in the Irminger Sea bottom water.

18 Bottom waters from the Irminger Sea exhibited the highest DFe concentrations from the whole section, excluding the stations  
19 at the margins. Such a feature could be due to i) vertical diffusion from local sediment, ii) lateral advection of water mass(es)  
20 displaying enhanced DFe concentrations, and iii) local dissolution of Fe from particles. Hereafter, we discuss the plausibility  
21 of these three hypotheses to occur.

22 The GEOTRACES GA02 voyage (leg 1, 64PE319) which occurred in April-May 2010 from Iceland to Bermuda sampled two  
23 stations north and south of our station 44 (~ 38.95°W, 59.62°N); station 5 (~ 37.91°W, 60.43°N) and 6 (~ 39.71°W, 58.60°N),  
24 respectively. High DFe concentrations in samples collected close to the bottom were also observed and attributed to sediment  
25 inputs highlighting boundary exchange between seawater and surface sediment (Lambelet et al., 2016; Rijkenberg et al., 2014).  
26 However, because a decrease in DFe concentrations was observed at our station 44 from 2500 m depth down to the bottom  
27 (Fig. 3, see supplementary material Fig. S4 and Table S2), it appeared to be unlikely that these high DFe concentrations will  
28 be the result of sediment inputs, as no DFe gradient from the deepest samples to those above was observed.

29 Looking at salinity versus depth for these three stations, one can observe the intrusion of Polar Intermediate Water (PIW) at  
30 station 44 from GEOVIDE, which was not observed during the GA02 voyage and which contributed to about 14% of the water  
31 mass composition (García-Ibáñez et al., this issue) and might therefore be responsible for the high DFe concentrations (see  
32 supplementary material Fig. S5A). On the other hand, the PIW was also observed at station 49 (from 390 to 1240 m depth),  
33 60 (from 440 to 1290 m depth), 63 (from 20 to 1540 m depth), 68 (3340 m depth), 69 (from 3200 to 3440 m depth), 71 (from

Deleted: data

Deleted: Boyd and Ellwood (2010)Boyd et al., 2010Boyd and Ellwood, 2010

Deleted: Fonseca-Batista et al., subm.¶  
Lambelet et al. (2016) reported high dissolved neodymium (Nd) concentrations (up to 18.5 pmol.kg<sup>-1</sup>) within the LSW at the edge of the Newfoundland Margin (45.73°W, 51.82°N) as well as slightly lower Nd isotopic ratio values relative to the one observed in the Irminger Sea. They suggested that this water mass had been in contact with sediments approximately within the last 30 years (Charette et al., 2015). Similarly, during GA03, Hatta et al. (2015) attributed the high DFe concentrations in the LSW to continental margin sediments. Consequently, it is also possible that the elevated DFe concentrations from the three LSW branches which entered the West European and Iceland Basins and Irminger Sea was supplied through sediment dissolution (Measures et al., 2013) along the LSW pathway.¶

Lemaître et al. (2017) reported highest remineralization rates within the Labrador and Irminger Seas Dehairs et al., 1997 where high carbon production rates were observed earlier in the season and were attributed to diatoms (>50% of phytoplankton abundances, Tonnard et al., in prep.). In the Labrador Sea, Lemaître et al. (2017) hypothesized that the important convection of the LSW enabled the deepening of the mesopelagic layer allowing these intense remineralization rates coinciding with the LSW in both basins. Gourain et al. (subm.) measured relatively high PFe:PAI ratios (0.39 ± 0.08 mol mol<sup>-1</sup>) in the LSW from the Irminger and Labrador Seas which could point to a more biogenic PFe contribution. ¶  
Remineralization occurred in both the Labrador and Irminger Seas with slightly higher rates in the former (Lemaître et al., 2017). Conspicuous DFe concentrations were, however, observed in the Irminger Sea. This could be explained by the reductive dissolution of Newfoundland Margin sediments. Nevertheless, remineralization of organic matter likely plays an additional role in the observed high DFe concentrations from the Irminger Sea through bacteria-mediated ligand production (Boyd and Ellwood, 2010) helping the DFe supply from reductive dissolution of Newfoundland sediments to the LSW to remain in solution. ¶

Deleted: 1

Deleted: Bottom Water

Deleted: DFe concentrations

Deleted: above

Deleted: inputs

Deleted: intrusion

Deleted: of an Fe-rich

Deleted:

Deleted: above the seafloor

Deleted: 4

Deleted: 3

Deleted: the above ones

Deleted: the

Deleted: GA01

Deleted: 8

1 2950 to 3440 m depth) and 77 (60 and 2500 m depth) with similar or higher contributions of the PIW without such high DFe  
2 concentrations (maximum DFe =  $1.3 \pm 0.1$  nmol L<sup>-1</sup>, 1240 m depth at station 49). However, considering the short residence  
3 time of DFe and the circulation of water masses in the Irminger Sea, it is possible that instead of being attributed to one specific  
4 water mass, these enhanced DFe concentrations resulted from lateral advection of the deep waters. Figure S5B) shows the  
5 concentrations of both DFe and PFe for the mixing line between DSOW/PIW and ISOW at station 44 and considering 100%  
6 contribution of ISOW for the shallowest sample (2218 m depth) and of DSOW/PIW for the deepest (2915 m depth), as these  
7 were the main water masses. This figure shows increasing DFe concentrations as DSOW/PIW mixed with ISOW. In addition,  
8 Le Roy et al. (2018) reported for the GEOVIDE voyage at station 44 a deviation from the conservative behaviour of <sup>226</sup>Ra  
9 reflecting an input of this tracer centred at 2500 m depth, likely highlighting diffusion from deep-sea sediments and coinciding  
10 with the highest DFe concentrations measured at this station. Although the transmissometry data were lower at the sediment  
11 interface than at 2500 m depth. Deng et al. (2018) reported a stronger scavenged component of the <sup>230</sup>Th at the same depth  
12 range, likely suggesting that the mixture of water masses were in contact with highly reactive particles. If there is evidence  
13 that the enhanced DFe concentrations observed at station 44 coincided with lateral advection of water masses that were in  
14 contact with particles, the difference of behaviour between DFe and <sup>230</sup>Th remains unsolved. The only parameter that would  
15 explain without any ambiguity such differences of behaviour between DFe and <sup>230</sup>Th would be the amount of Fe-binding  
16 organic ligands for these samples. Indeed, although PFe concentrations decreased from the seafloor to the above seawater, this  
17 trend would likely be explained by a strong vertical diffusion alone and not necessarily by the dissolution of particles that were  
18 laterally advected.

19 Therefore, the high DFe concentrations observed might be inferred from local processes as ISOW mixes with both PIW and  
20 DSOW with a substantial load of Fe-rich particles that might have dissolved in solution due to Fe-binding organic ligands.

#### 21 4.2.5 Reykjanes Ridge: Hydrothermal inputs or Fe-rich seawater?

22 Hydrothermal activity was assessed over the Mid Atlantic Ridge, namely the Reykjanes Ridge, from stations 36 to 40. Indeed,  
23 within the interridge database (<http://www.interridge.org>), the Reykjanes Ridge is reported to have active hydrothermal sites.  
24 The sites were either confirmed (Baker and German, 2004a; German et al., 1994; Olafsson et al., 1991; Palmer et al., 1995)  
25 close to Iceland or inferred (e.g. Chen, 2003; Crane et al., 1997; German et al., 1994; Sinha et al., 1997; Smallwood and White,  
26 1998) closer to the GEOVIDE section as no plume was detected but a high backscatter was reported potentially corresponding  
27 to a lava flow. Therefore, hydrothermal activity at the sampling sites remains unclear with no elevated DFe concentrations nor  
28 temperature anomaly above the ridge (station 38). However, enhanced DFe concentrations (up to  $1.5 \pm 0.22$  nmol L<sup>-1</sup>, station  
29 36, 2200 m depth) were measured east of the Reykjanes Ridge (Fig. 3). This could be due to hydrothermal activity and  
30 resuspension of sunken particles at sites located North of the section and transported through the ISOW towards the section  
31 (see supplementary material Fig. S3). Indeed, Achterberg et al. (2018) highlighted at ~60°N and over the Reykjanes Ridge a  
32 southward lateral transport of an Fe plume of up to 250-300 km. In agreement with these observations, previous studies (e.g.  
33 Fagel et al., 1996; Fagel et al., 2001; Lackschewitz et al., 1996; Parra et al., 1985) reported marine sediment mineral clays in

Formatted: Superscript

Formatted: Superscript

Deleted: s

Deleted: Le Roy et al., 2018

Deleted: ¶

Figure 8B) also shows the concentrations of both DFe and PFe for the mixing line between DSOW/PIW and ISOW at station 44 and considering 100% of contribution from these seawater at the deepest (2915 m depth) and the shallowest (2218 m depth) samples, respectively, as these were the main water masses. This figure shows an exponential decrease of PFe concentrations as the DSOW/PIW mixed with the ISOW (Gourain et al., subm.). Concomitantly, DFe concentrations followed a polynomial distribution with a theoretical DFe maxima of 2.6 nmol L<sup>-1</sup> at 51.5% contribution of the ISOW (48.5% of the DSOW/PIW) and corresponding to a theoretical PFe concentration of ~7.0 nmol L<sup>-1</sup>. It is possible that as the ISOW mixed with the Fe-rich particles from the DSOW/PIW, DFe concentrations increased until PFe concentrations reached 7.0 nmol L<sup>-1</sup> after which the amounts of particles tended to scavenge Fe.

Deleted: dissolvable

Deleted: which

Deleted: might be sustained

Deleted: by

Deleted: 1

Deleted: High DFe concentrations (up to  $1.5 \pm 0.22$  nmol L<sup>-1</sup>, station 36, 2200 m depth) were measured east of the Reykjanes Ridge (Fig. 4)

Deleted: W

Deleted: , based on a literature review on existing vent-field databases, and on unpublished sources, ~280 sites of active hydrothermal venting on spreading ridges, volcanic arcs and intraplate volcanoes were reported

Deleted: . In this database

Deleted: inferred

Deleted: that

Deleted: Several studies on hydrothermal activity at Reykjanes Ridge have been conducted (e.g. Chen, 2003; German et al., 1994; Sinha et al., 1997; Smallwood and White, 1998) but it

Deleted: ed

Deleted: , as

Deleted: high

Deleted: were observed

Deleted: According to the water mass circulation, if there was an active hydrothermal vent located on the Reykjanes Ridge, the only possibility to observe a signal would occur from a southward transfer of this signal through the ISOW in the Iceland Basin. Interestingly

1 the Iceland Basin largely dominated by smectite (> 60%), a tracer of hydrothermal alteration of basaltic volcanic materials  
 2 (Fagel et al., 2001; Tréguer and De La Rocha, 2013). Hence, the high DFe concentrations measured east of the Reykjanes  
 3 Ridge could be due to a hydrothermal source and/or the resuspension of particles and their subsequent dissolution,  
 4 West of the Reykjanes Ridge, a DFe enrichment was also observed in ISOW within the Irminger Sea (Figs. 4 and 7). The low  
 5 transmissometer values within ISOW in the Irminger Sea compared to the Iceland Basin suggest a particle load. These particles  
 6 could come from the Charlie Gibbs Fracture Zone (CGFZ, 52.67°N and 34.61°W) and potentially Bight Fracture Zone (BFZ,  
 7 56.91°N and 32.74°W) (Fig. 1) (Lackschewitz et al., 1996; Zou et al., 2017). Indeed, hydrographic sections of the northern  
 8 valley of the CGFZ showed that below 2000 m depth the passage through the Mid-Atlantic Ridge was mainly filled with the  
 9 ISOW (Kissel et al., 2009; Shor et al., 1980). Shor et al. (1980) highlighted a total westward transport across the sill, below  
 10 2000 m depth of about  $2.4 \times 10^6 \text{ m}^3 \text{ s}^{-1}$  with ISOW carrying a significant load of suspended sediment ( $25 \mu\text{g L}^{-1}$ ), including a  
 11 100-m-thick benthic nepheloid layer. It thus appears that the increase in DFe within ISOW likely came from sediment  
 12 resuspension and dissolution as the ISOW flows across CGFZ and BFZ.

#### 13 4.3. What are the main sources of DFe in surface waters?

14 During GEOVIDE, enhanced DFe surface concentrations were observed at several stations (stations 1-4, 53, 61, 78)  
 15 highlighting an external source of Fe to surface waters. The main sources able to deliver DFe to surface waters are riverine  
 16 inputs, glacial inputs and atmospheric deposition. In the following sections, these potential sources of DFe in surface waters  
 17 will be discussed.

##### 18 4.3.1 Tagus riverine inputs

19 Enhanced DFe surface concentrations (up to  $1.07 \pm 0.12 \text{ nmol L}^{-1}$ ) were measured over the Iberian Margin (stations 1-4) and  
 20 coincided with salinity minima ( $\sim <35$ ) and enhanced DAI concentrations (up to  $31.8 \text{ nmol L}^{-1}$ , Menzel Barraqueta et al.,  
 21 2018). DFe and DAI concentrations were both significantly negatively correlated with salinity ( $R^2 = -1$  and 0.94, respectively)  
 22 from stations 1 to 13 (Fig. 5). Salinity profiles from station 1 to 4 showed evidence of a freshwater source with surface salinity  
 23 ranging from 34.95 (station 1) to 35.03 (station 4). Within this area, only two freshwater sources were possible: 1) wet  
 24 atmospheric deposition (4 rain events, Shelley, pers. comm.) and 2) the Tagus River, since the ship SADC data revealed a  
 25 northward circulation (P. Lherminier and P. Zunino, Ifremer Brest, pers. comm.). Our SML DFe inventories were about three  
 26 times higher at station 1 ( $\sim 1 \text{ nmol L}^{-1}$ ) than those calculated during the GA03 voyage ( $\sim 0.3 \text{ nmol L}^{-1}$ , station 1) during which  
 27 atmospheric deposition were about one order of magnitude higher (Shelley et al., 2018; Shelley et al., 2015). the atmospheric  
 28 source seemed to be minor. Consequently, the Tagus River appears as the most likely source responsible for these enhanced  
 29 DFe concentrations, either as direct input of DFe or indirectly through Fe-rich sediment carried by the Tagus River and their  
 30 subsequent dissolution. The Tagus estuary is the largest in the western European coast and very industrialized (Canário et al.,  
 31 2003; de Barros, 1986; Figueres et al., 1985; Gaudencio et al., 1991; Mil-Homens et al., 2009), extends through an area of 320  
 32 km<sup>2</sup> and is characterized by a large water flow of  $15.5 \times 10^9 \text{ m}^3 \text{ y}^{-1}$  (Fiuza, 1984). Many types of industry (e.g. heavy metallurgy,

- Deleted: Lackschewitz et al., 1996.
- Deleted: as previously suggested by Achterberg et al. (2018) w(
- Deleted: While hydrothermalism may explain the enrichment ca
- Deleted:
- Deleted: th
- Deleted: e
- Deleted:
- Moved up [3]: Moreover, higher transmissometer values within
- Moved (insertion) [3]
- Deleted: may come from other sources. An intriguing phenome
- Deleted: 2
- Deleted: M
- Deleted: A01
- Deleted: the
- Deleted: 2
- Deleted: low
- Deleted: ies
- Deleted: .3
- Deleted: 9
- Deleted: ier
- Deleted: et al.,
- Deleted:
- Formatted
- Formatted
- Field Code Changed
- Formatted
- Deleted: However, DFe:DAI ratios were very low ( $0.036 \pm 0.00$
- Formatted
- Formatted
- Formatted
- Deleted: which were indicative of a minor
- Formatted
- Formatted
- Formatted
- Formatted
- Deleted: for those stations
- Formatted
- Formatted
- Deleted: T
- Formatted



1 ore processing, chemical industry) release metals including Fe, which therefore result in high levels recorded in surface  
2 sediments, suspended particulate matter, water and organisms in the lower estuary (Santos-Echeandia et al., 2010).

### 3 4.3.2 High latitude, meteoric water and sea-ice processes

4 Potential sources of Fe at stations 53, 61 and 78 include meteoric water (MW, referring to precipitation, runoff and continental  
5 glacial melt), sea-ice melt (SIM), seawater interaction with shallow sediments and advection of water transported from the  
6 Arctic sourced by the Fe-rich TransPolar Drift (TPD, Klunder et al. (2012); see supplementary material Fig. S4 and Table S2).  
7 The vertical profiles of both potential temperature and salinity in the Greenland and Newfoundland Margins (station 53, 61  
8 and 78, Fig. 4D, E) and F)) highlighted the influence of fresh waters originating from the Arctic Ocean to separate surface  
9 and deeper samples at ~ 60 m (station 53) and ~ 40 m (stations 61 and 78) depth. The presence of this freshwater lens suggests  
10 that sediment derived enrichment to these surface waters was unlikely. The most plausible sources would be freshwater induced  
11 by meteoric water and sea-ice melt. Deeper in the water column, net brine release were observed at stations 53 (below 40 m  
12 depth, Fig. 4D) 61 (in the whole water column, Fig. 4E) and 78 (below 30 m depth, Fig. 4F). The release of brines could  
13 originate from two different processes: the sea-ice formation or the early melting of multiyear sea ice due to gravitational  
14 drainage and subsequent brine release (Petrich and Eicken, 2010; Wadhams, 2000). Indeed, during the winter preceding the  
15 GEOVIDE voyage, multiyear sea ice extended 200 km far from our Greenland stations (<http://nsidc.org/arcticseaicenews/>). In  
16 the following sections, we discuss the potential for meteoric water supply, sea-ice formation and sea-ice melting to affect DFe  
17 distribution.

#### 18 4.3.2.1 The Greenland shelf

19 Considering the sampling period at stations 53 (16 June 2014) and 61 (19 June 2014), sea-ice formation is unlikely to happen  
20 as this period coincides with summer melting in both the Central Arctic and East Greenland (Markus et al., 2009). However,  
21 it is possible that the brines observed in our study could originate from sea-ice formation, which occurred during the previous  
22 winter(s) at 66°N (and/or higher latitudes). The residence time can vary from days (von Appen et al., 2014) to 6-9 months  
23 (Sutherland et al., 2009). Due to our observed strong brine signal at station 61 we suggest that the residence time was potentially  
24 longer than average. Given that the brine signal was higher at station 61 than at station 53 (which was located upstream in the  
25 EGC), we suggest that station 53 was exhibiting a freshening as a result of the transition between the freezing period toward  
26 the melting period. This would result in a dilution of the brine signal at the upstream station. Consequently, the salinity of this  
27 brine signal may reflect sea ice formation versus melting which may have an effect on the trace metal concentration within  
28 this water (Hunke et al., 2011). The associated brine water at station 61 (100 m depth) was slightly depleted in both DFe and  
29 PFe<sub>2</sub>, which may be attributed to sea ice formation processes. Indeed, Janssens et al. (2016) highlighted that as soon as sea ice  
30 forms, sea salts are efficiently flushed out of the ice while PFe is trapped within the crystal matrix and DFe accumulates,  
31 leading to an enrichment factor of these two Fe fractions compared to underlying seawater. Conversely, the brine signal  
32 observed at station 53 (100 m depth) showed slight enrichment in DFe, which may be attributed to brine release during early  
33

#### Formatted

**Deleted:** Many types of industry (e.g. heavy metallurgy, ore processing, chemical industry, petroleum refinery, shipbuilding, chlor-alkali industry, a smelter and a pyrite roasting plant) release heavy metals such as lead (Pb, Carvalho, 1995), mercury (Hg, Canario, 2000; Ferreira, 1997; Figueres et al., 1985), arsenic (As, Andreae et al., 1983), or other trace metals (Cd, Cu, Ni, Zn, Cotté-Krief et al., 2000) into the river which therefore result in high levels of these elements recorded in surface sediments, suspended particulate matter, water and organisms in the lower estuary. Santos-Echeandia et al. (2010) reported that sediments, pore water and belowground biomass colonised by salt marsh plants from the Tagus estuary contained high concentrations of Fe, Mn, Zn, Cu, Pb and Cd which were exported to the water column as a result of tidal inundation. Similar discharge processes releasing large amount of DFe from creeks draining coastal wetland to the ocean have also been reported by Sanders et al. (2015). Consequently, the enhanced DFe concentrations observed above the Iberian Margin likely originated from the Tagus River, wet atmospheric deposition playing a minor additional source

#### Formatted

#### Field Code Changed

**Deleted:** 2

**Deleted:** s

**Deleted:** 3...2). The vertical profiles of both potential temperature and salinity in the Greenland and Newfoundland Margins (station 53, 61 and 78, Fig. 45...D, E) and F)) highlighted the influence of fresh and cold...waters originating from the Arctic Ocean to separate and deeper samples at ~ 60 m (station 53) and ~ 40 m (stations 61 and 78) depth. The presence of this front...freshwater lens suggests that sediment derived enrichment to these surface waters was unlikely. The most plausible sources would be freshwater induced by meteoric water and sea-ice melt. Deeper in the water column, net brine release were observed at stations 53 (below 40 m depth, Fig. 4D) 61 (in the whole water column, Fig. 4E) and 78 (below 30 m depth, Fig. 4F). The release of brines could originate from two different processes: the sea-ice formation or the early melting of multiyear sea ice due to gravitational drainage and subsequent brine release (Petrich and Eicken, 2010; Wadhams, 2000). Indeed, during the winter preceding the GEOVIDE voyage, multiyear sea ice extended glacial sources with multi-year sea-ice (which extended...as close as ...00 km far from our Greenland stations)

**Formatted:** Not Highlight

**Deleted:** and land ice sheet.

**Formatted:** Highlight

**Deleted:** SIM and MW contributions were determined for stations 53, 61 and 78, with mass balance calculations based on the end-members presented in Benetti et al. (2016). For stations over the

**Moved (insertion) [5]**

**Moved up [5]:** In Figure 5 D, E) and F), negative sea-ice fractions indicated a net brine release while positive sea-ice fractions indicated a net sea-ice melting.

**Deleted:** In Figure 5 D, E) and F), negative sea-ice fractions indicated a net brine release while positive sea-ice fractions indicated a net sea-ice melting. It appears that the highest brine

1 sea ice melting and the associated release of DFe into the underlying water column as the brine sinks until reaching neutral  
2 buoyancy due to higher density.

3 Surface waters (from 0 to ~100 m depth) from station 53 and 61 were characterized by high MW fractions (ranging from 8.3  
4 to 7.4% and from 7.7 to 7.3%, respectively, from surface to ~100 m depth, Figs. 5D and E). These high MW fractions were  
5 both enriched in PFe and DFe (except station 53 for which no data was available close to the surface) compared to seawater  
6 located below 50 m depth, thus suggesting a MW source. These results are in line with previous observations, which  
7 highlighted strong inputs of DFe from a meteoric water melting source in Antarctica (Annett et al., 2015). Although the ability  
8 of MW from Greenland Ice Sheet and runoffs to deliver DFe and PFe to surrounding waters has previously been demonstrated  
9 (Bhatia et al., 2013; Hawkings et al., 2014; Schroth et al., 2014; Statham et al., 2008), both Fe fractions were lower at the  
10 sample closest to the surface, then reached a maximum at ~50 m depth and decreased at ~70 m depth, for station 61 (Fig.  
11 4D). The surface DFe depletion was likely explained by phytoplankton uptake, as indicated by the high TChl-*a* concentrations  
12 (up to 6.6 mg m<sup>-3</sup>) measured from surface to about 40 m depth, drastically decreasing at ~50 m depth to 3.9 mg m<sup>-3</sup> (Fig. 4D).  
13 Hence, it seemed that meteoric water inputs from the Greenland Margin likely fertilized surface waters with DFe, enabling the  
14 phytoplankton bloom to subsist. The profile of PFe can be explained by two opposite plausible hypotheses: 1) MW inputs did  
15 not release PFe, as if it was the case, one should expect higher PFe concentrations at the surface (~25 m depth) than the one  
16 measured at 50 m depth due to both the release from MW and the assimilation of DFe by phytoplankton 2) MW inputs can  
17 release PFe in a form that is directly accessible to phytoplankton with subsequent export of PFe as phytoplankton died. The  
18 latter solution explains the PFe maximum measured at ~50 m depth and is thus the most plausible.

#### 19 4.3.2.2 The Newfoundland shelf

20 Newfoundland shelf waters (station 78) were characterized by high MW fractions (up to 7%), decreasing from surface to 200  
21 m depth (~2%). These waters were associated with a net sea-ice melting signal from the near surface to ~10 m depth followed  
22 by a brine release signal down to 200 m depth with the maximum contribution measured at ~30 m depth. Within the surface  
23 waters (above 20 m depth), no elevation in DFe, DA1 nor PFe was noticed despite the low measured TChl-*a* concentrations  
24 (TChl-*a* ~ 0.20 mg m<sup>-3</sup>). This suggests that none of these inputs (sea-ice melting and meteoric water) were able to deliver DFe  
25 or that these inputs were minor compared to sediment inputs from the Newfoundland Margin. Surprisingly, the highest TChl-*a*  
26 biomass (TChl-*a* > 9 mg m<sup>-3</sup>) from the whole section was measured at 30 m depth corresponding to the strongest brine release  
27 signal. This either suggests that the brine likely contained important amounts of Fe (dissolved and/or particulate Fe) that were  
28 readily available for phytoplankton and consumed at the sampling period by potentially sea-ice algae themselves (Riebesell et  
29 al., 1991) or that another nutrient was triggering the phytoplankton bloom.

#### 30 4.3.3 Atmospheric deposition

31 On a regional scale, the North Atlantic basin receives the largest amount of atmospheric inputs due to its proximity to the  
32 Saharan Desert (Jickells et al., 2005), yet even in this region of high atmospheric deposition, inputs are not evenly distributed.

Deleted: sea

Deleted: .

Deleted: 5

Deleted: 4

Deleted: 5

Deleted: with sea-ice melting contribution (1.5%, 4 m depth) for station 53 and low contribution (0.6%) from brine release at the surface, linearly increasing with depth (1.3% at 50 m depth and 2.2 % at 100 m depth).

Deleted: Station 53, exhibited enhanced PFe concentrations (19 nmol L<sup>-1</sup>, 25 m depth) at the surface. The corresponding DFe sample was lost and therefore no information was available. Conversely,

Deleted: .

Deleted: t

Deleted: These results are in agreement with the capacity of MW from Greenland Ice Sheet and runoffs to deliver DFe and PFe to surrounding waters (Bhatia et al., 2013; Hawkings et al., 2014; Schroth et al., 2014; Statham et al., 2008).

Deleted: These results are also in line with previous observations which highlighted strong inputs of DFe from a meteoric water melting source in Antarctica (Annett et al., 2015, with DFe:DA1 ratios up to 1.6 mol mol<sup>-1</sup>; Hawkings et al., 2014), noting that our DFe:DA1 ratios from a MW source were 3 to 5 times lower than the one observed by Annett et al. (2015). These differences were likely explained by the sampling period and the stage of phytoplankton bloom development in our study. ¶

Deleted:

Deleted: Tonnard et al., in prep. Sarthou et al., 2018; Tonnard et al., in prep.. If such was the case, then a PFe maximum should be noticed at the same depth. However, it should be noted that TChl-*a* and δ<sup>18</sup>O samples were collected about four hours prior to sampling for DFe and PFe. Therefore, it is more likely that by the time DFe and PFe samples were collected, the PFe was exported deeper in the water column. Indeed, Krembs et al. (2002) highlighted the presence of exopolymeric substances (EPS) in sea ice. Such compounds were reported to undergo fast aggregation (minutes to hours) from the colloidal to the particulate phase (i.e. Transparent Exopolymer Particles, TEP) (e.g. Baalousha et al., 2006; Verdugo et al., 2004) taking in-depth other particulate material as they sank.

Deleted: 2

1 Indeed, aerosol Fe loading measured during GEOVIDE (Shelley et al., 2017) were much lower (up to four orders of magnitude)  
2 than those measured during studies from lower latitudes in the North Atlantic (e.g. Baker et al., 2013; Buck et al., 2010; and  
3 for GA03, Shelley et al., 2015), but atmospheric inputs could still be an important source of Fe to surface waters in areas far  
4 from land.

5 In an attempt to estimate whether there was enough atmospheric input to sustain the SML DFe concentrations, we calculated  
6 Turnover Times relative to Atmospheric Deposition (TTADs, Guieu et al., 2014). To do so, we made the following  
7 assumptions: 1) the aerosol concentrations are a snapshot in time but are representative of the study region, 2) the aerosol  
8 solubility estimates based on two sequential leaches are an upper limit of the aerosol Fe in seawater and 3) the water column  
9 stratified just before the deposition of atmospheric inputs, so MLD DFe will reflect inputs from above. Thus, the TTADs were  
10 defined as the integrated DFe concentrations in the SML for each station divided by the contribution of soluble Fe contained  
11 in aerosols averaged per basin to the water volume of the SML. Although, TTADs were lower in the West European and  
12 Iceland Basins with an average of  $9 \pm 3$  months compared to other basins ( $7 \pm 2$  years and  $5 \pm 2$  years for the Irminger and  
13 Labrador Seas, respectively) (Fig. 6) they were about three times higher than those reported for areas impacted by Saharan  
14 dust inputs ( $\sim 3$  months, Guieu et al., 2014). Therefore, the high TTADs measured in the Irminger and Labrador Seas and  
15 ranging from 2 to 15 years provided further evidence that atmospheric deposition were unlikely to supply Fe in sufficient  
16 quantity to be the main source of DFe (see Sections 4.2.1 and 4.3.2) while in the West European and Iceland Basins they  
17 played an additional source, perhaps the main source of Fe especially at station 36 which displayed TTAD of 3 months.

#### 18 4.4 Sediment input

##### 19 4.4.1 Margins:

20 DFe concentration profiles from all coastal stations (stations 2, 4, 53, 56, 61 and 78) are reported in Figure 4. To avoid surface  
21 processes, only depths below 100 m depth will be considered in the following discussion. DFe and PFe followed a similar  
22 pattern at stations 2, 53, 56, and 78 with increasing concentrations towards the sediment, suggesting that either the sources of  
23 Fe supplied both Fe fractions (dissolved and particulate) or that PFe dissolution from sediments supplied DFe. Among the  
24 different margins, the Newfoundland Margin exhibited the highest deep-water DFe concentrations. Conversely, stations 4 and  
25 61 exhibited a decrease in DFe concentrations at the closest samples to the seafloor whereas PFe increased. DFe:PFe ratios  
26 ranged from 0.01 (station 2, bottom sample) to 0.27 (station 4,  $\sim 400$  m depth)  $\text{mol} \cdot \text{mol}^{-1}$  with an average value of  $0.11 \pm 0.07$   
27  $\text{mol} \cdot \text{mol}^{-1}$  ( $n = 23$ , Table 3), highlighting a different behaviour of Fe among margins. This could be explained by the different  
28 nature of the sediments and/or different sediment conditions (e.g. redox, organic content). Based on particulate and dissolved  
29 Fe and dissolved Al data (Gourain et al., 2018; Menzel Barraqueta et al., 2018, Table 3), three main different types of margins  
30 were reported (Gourain et al., 2018) with the highest lithogenic contribution observed at the Iberian Margin (stations 2 and 4)  
31 and the highest biogenic contribution at the Newfoundland Margin (station 78). These observations are consistent with higher  
32 TChl-*a* concentrations measured at the Newfoundland Margin and to a lesser extent at the Greenland Margin and the  
33 predominance of diatoms relative to other functional phytoplankton classes at both margins (Tonnard et al., in prep.). To sum

**Deleted:** in the North Atlantic, two areas can be separated: from  $\sim 5$  to  $30^\circ\text{N}$  which receives the vast majority of mineral dust from the Saharan outflow, and north of  $\sim 30^\circ\text{N}$ , which is frequently (but not always) outside of the influence of the atmospheric transport of dust from North African dust source regions and where atmospheric inputs are more likely to contain a higher proportion of anthropogenic aerosols (from Europe and North America) and high latitude sources in Iceland and Greenland, and occasionally volcanic sources (Achterberg et al., 2013; Bullard et al., 2016; Jickells and Moore, 2015). This division in atmospheric inputs was reflected in the aerosol Fe loading observed during GA01 (Shelley et al., 2017b) which were much lower (up to four orders of magnitude) than those measured during studies from lower latitudes in the North Atlantic (e.g. Baker et al., 2013; Buck et al., 2010; and for GA03, Shelley et al., 2015), but atmospheric inputs could still be an important source of Fe in areas far from land. During GA01, 18 aerosol samples were collected roughly every 48 h (Shelley et al., 2017a; 2017b). Shelley et al. (2017a; 2017b) used a combination of air mass back trajectories (five-day simulation period), aerosol trace element concentrations, elemental ratios and multivariate statistics to broadly group the aerosol samples by their dominant, but not mutually-exclusive, source(s). Using this approach, the GA01 transect can be split into four sections. Shelley et al. (2017b) These are those predominantly influenced by: (1) atmospheric inputs from sources in Iceland and Greenland which likely include proglacial till (stations 11-29), (2) (...)

**Formatted:** Font: 12 pt

**Deleted:** compare the integrated SML DFe concentrations for ea (...)

**Deleted:** To do so, we made the following assumptions: 1) the (...)

**Deleted:** s

**Deleted:** might be

**Deleted:** 2

**Deleted:** . However, atmospheric deposition could potentially ha (...)

**Deleted:** 3

**Deleted:** o

**Deleted:** 5

**Deleted:** Stations where

**Deleted:** followed a similar pattern are s

**Deleted:**

**Deleted:** <sup>-1</sup>

**Deleted:**

**Deleted:** <sup>-1</sup>

**Deleted:** between DFe

**Deleted:** and

**Deleted:** PFe and suggesting

**Deleted:** different composition of sediments between different (...)

**Deleted:** 4

**Deleted:** .

**Deleted:** The East (stations 53 and 56) and West (station 61) (...)

**Deleted:** the

1 up, the most biogenic sediments (Newfoundland Margin) were able to mobilise more Fe in the dissolved phase than the most  
2 lithogenic sediments (Iberian Margin), in agreement with Boyd et al. (2010) who reported greater remineralization of PFe from  
3 biogenic PFe than from lithogenic PFe based on field experiment and modelling simulations.

#### 5 4.4.2 Nepheloid layers:

6 Samples associated with high levels of particles (transmissometer < 99%) and below 500 m depth displayed a huge variability  
7 in DFe concentrations. From the entire dataset, 63 samples (~13% of the entire dataset) followed this criterion with 14 samples  
8 from the West European Basin (station 1), 4 samples from the Iceland Basin (stations 29, 32, 36 and 38), 43 samples from the  
9 Irminger Sea (stations 40, 42, 44, 49 and 60) and 2 samples from the Labrador Sea (station 69). To determine which parameter  
10 was susceptible to explain the variation in DFe concentrations in these nepheloid layers, a Principal Component Analysis  
11 (PCA) on these samples. The input variables of the PCA were the particulate Fe, Al, and particulate manganese (PMn) (Gourain  
12 et al., 2018), the DAI (Menzel Barraqueta et al., 2018) and the Apparent Oxygen Utilization (AOU) and were all correlated to  
13 DFe concentrations explaining all together 93% of the subset variance (see supplementary material Fig. S6). The first  
14 dimension of the PCA was represented by the PAI, PFe and PMn concentrations and explained 59.5% of the variance, while  
15 the second dimension was represented by the DAI and the AOU parameters, explaining 33.2% of the variance. The two sets  
16 of variables were nearly at right angle from each other, indicating no correlation between them.

17 The variations in DFe concentrations measured in bottom samples from stations 32, 36 (Iceland Basin), 42 and 44 (Irminger  
18 Sea) and 69 (Labrador Sea) were mainly explained by the first dimension of the PCA (see supplementary material Fig. S6).  
19 Therefore, samples characterized by the lowest DFe concentrations (stations 32 and 69) were driven by particulate Al and Mn  
20 concentrations and resulted in an enrichment of Fe within particles. These results are in agreement with previous studies  
21 showing that the presence of Mn within particles can induce the formation of Fe-Mn oxides, contributing to the removal of Fe  
22 and Mn from the water column (Kan et al., 2012; Teng et al., 2001).

23 Low DFe concentrations (bottom samples from stations 42 and 1) were linked to DAI inputs and associated with lower AOU  
24 values. The release of Al has previously been observed from Fe and Mn oxide coatings on resuspended sediments under mildly  
25 reducing conditions (Van Beusekom, 1988). Conversely, higher DFe concentrations were observed for stations 44 and 49 and  
26 to a lesser extent station 60 coinciding with low DAI inputs and higher oxygen levels. This observation challenges the  
27 traditional view of Fe oxidation with oxygen, either abiotically or microbially induced. Indeed, remineralisation can decrease  
28 sediment oxygen concentrations, promoting reductive dissolution of PFe oxyhydroxides to DFe that can then diffuse across  
29 the sediment water interface as DFe(II) colloids (Homoky et al., 2011). Such processes will inevitably lead to rapid Fe removal  
30 through precipitation of nanoparticulate or colloidal Fe (oxyhydr)oxides, followed by aggregation or scavenging by larger  
31 particles (Boyd and Ellwood, 2010; Lohan and Bruland, 2008) unless complexation with Fe-binding organic ligands occurs  
32 (Batchelli et al., 2010; Gerringa et al., 2008). There exist, however, another process that is favoured in oxic benthic boundary  
33 layers (BBL) with low organic matter degradation and/or low Fe oxides, which implies the dissolution of particles after  
34 resuspension, namely the non-reductive dissolution of sediment (Homoky et al., 2013; Radic et al., 2011). In addition, these

**Deleted:** was performed on samples which exhibited a transmissometry lower than 99% and below 500 m depth to avoid surface processes.

**Deleted:** From the entire dataset, 66 samples (~13% of the entire dataset) respected this criterion with 3 samples from the Iberian Margin (station 4), 14 samples from the West European Basin (station 1), 4 samples from the Iceland Basin (stations 29, 32, 36 and 38), 43 samples from the Irminger Sea (stations 40, 42, 44, 49 and 60) and 2 samples from the Labrador Sea (station 69). T

**Deleted:** oxides

**Deleted:** O<sub>2</sub>

**Deleted:** were the input variables of the PCA and explained ~93% of the subset

**Deleted:** Fig. 11

**Deleted:** O<sub>2</sub>

**Deleted:** concentrations

**Deleted:** Fig. 11

**Deleted:** O<sub>2</sub>

**Deleted:** oxide

**Deleted:** accelerates

**Deleted:** O<sub>2</sub>

**Deleted:** concentrations

**Deleted:**

**Deleted:** which will inevitably leads to rapid Fe removal through precipitation of nanoparticulate or colloidal Fe (oxyhydr)oxides, followed by aggregation or scavenging by larger particles (Boyd and Ellwood, 2010; Lohan and Bruland, 2008). Liu and Millero, 2002 It is only when sufficient organic matter and more specifically organic ligands are present in solution, that these sediment-derived DFe can remain in solution in excess of its solubility through complexation (Kondo and Moffett, 2015; Noble et al., 2012) or in suspension as colloids or nanoparticles (Raiswell and Canfield, 2012). T

1 higher oxygenated samples were located within DSO<sub>W</sub>, which mainly originate (75% of the overflow) from the Nordic Seas  
2 and the Arctic Ocean (Tanhua et al., 2005), in which the ultimate source of Fe was reported by Klunder et al. (2012) to come  
3 from Eurasian river waters. The major Arctic rivers were highlighted by Slagter et al. (2017) to be a source of Fe-binding  
4 organic ligands that are then further transported via the TPD across the Denmark Strait. Hence, the enhanced DFe  
5 concentrations measured within DSO<sub>W</sub> might result from Fe-binding organic ligand complexation that were transported to the  
6 deep ocean as DSO<sub>W</sub> formed rather than the non-reductive dissolution of sediment.

#### 7 4.5. How does biological activity modify DFe distribution?

8 Overall, almost all the stations from the GEOVIDE voyage displayed DFe minima in surface water associated with some  
9 maxima of TChl-*a* (see supplementary material Fig. S1). In the following section, we specifically address the question of  
10 whether DFe concentrations potentially limit phytoplankton growth. Note that macronutrients and DFe limitations relative to  
11 phytoplankton functional classes are dealt in Tonnard et al. (in prep.).

12 A key determinant for assessing the significance of a DFe source is the magnitude of the DFe:macronutrient ratio supplied,  
13 since this term determines to which extent DFe will be utilised. The DFe:NO<sub>3</sub><sup>-</sup> ratios in surface waters varied from 0.02 (station  
14 36) to 38.6 (station 61) mmol:mol<sup>-1</sup> with an average of 5 ± 10 mmol:mol (see supplementary material Fig. S7). Values were  
15 typically equal or lower than 0.28 mmol mol<sup>-1</sup> in all basins except at the margins and at stations 11, 13, 68, 69 and 77. The low  
16 nitrate concentrations observed at the eastern and western Greenland and Newfoundland Margins reflected a strong  
17 phytoplankton bloom which had reduced the concentrations as highlighted by the elevated integrated TChl-*a* concentrations  
18 ranging from 129.6 (station 78) to 398.3 (station 61) mg m<sup>-2</sup>. At the Iberian Margin, they likely reflected the influence of the  
19 N-limited Tagus River (stations 1, 2 and 4) with its low TChl-*a* integrated concentrations that ranged from 31.2 (station 1) to  
20 46.4 (station 4) mg m<sup>-2</sup>. The high DFe:NO<sub>3</sub><sup>-</sup> ratios determined at those stations, which varied from 13.4 (station 78) to 38.6  
21 (station 61) mmol:mol, suggested that waters from these areas, despite having the lowest NO<sub>3</sub><sup>-</sup> concentrations, were relatively  
22 enriched in DFe compared to waters from Iceland Basin and Irminger Sea.

23 In our study, DFe:NO<sub>3</sub><sup>-</sup> ratios displayed a gradient from the West European Basin to Greenland (supplementary material S7  
24 and S8). This trend only reverses when the influence of Greenland was encountered, as also observed by Painter et al. (2014).  
25 The remineralisation of organic matter is a major source of macro and micronutrients in subsurface waters (from 50 to 250 m  
26 depth). Remineralisation is associated with the consumption of oxygen and therefore, Apparent Oxygen Utilization (AOU)  
27 can provide a quantitative estimate of the amount of material that has been remineralised. While no relationship was observed  
28 below 50 m depth for NO<sub>3</sub><sup>-</sup> or DFe and AOU considering all the stations, a significant correlation was found in the Subpolar  
29 gyre when removing the influence of margins (stations 29-49, 56, 60, 63-77) (AOU = 3.88 NO<sub>3</sub><sup>-</sup> - 39.32, R<sup>2</sup>=0.79, n=69, p-  
30 value < 0.001). This correlation indicates that remineralisation of Particulate Organic Nitrogen (PON) greatly translates into  
31 Dissolved Inorganic Nitrogen (DIN) and that NO<sub>3</sub><sup>-</sup> can be used as a good tracer for remineralisation in the studied area. Within  
32 these Subpolar gyre waters, there was a significant correlation between DFe and AOU (AOU = 22.6 DFe, R<sup>2</sup>=0.34, n=53, p-  
33 value < 0.001). The open-ocean stations from Subpolar gyre also exhibited a good linear correlation between DFe and NO<sub>3</sub><sup>-</sup>

Deleted: the

Deleted: has been reported by Tanhua et al. (2005) to mainly originate (75% of the overflow) from the Nordic Seas and the Arctic Ocean. Klunder et al. (2012) noticed that the ultimate source of Fe to the Arctic Ocean is coming from Eurasian river waters and

Deleted: reported that the

Deleted: and therefore the Arctic major rivers are a source of Fe-binding organic ligands. Consequently, these

Deleted: s

Deleted: are likely

Deleted: the

Deleted: enabling higher DFe concentrations in seawater.

Deleted: In summary, the occurrence of particulate MnO<sub>2</sub> and the amount of organic matter are the main drivers explaining the DFe distributions within the benthic nepheloid layers. ¶

Deleted: 4

Deleted:

Deleted: and biological activity

Deleted: GA01

Deleted: Fig. 3

Deleted: Consideration of the relationship between DFe and biological uptake are

Deleted: discussed in Tonnard et al. (in prep.), while following discussion specifically

Deleted: es

Deleted: "Did

Deleted: ?"

Deleted: ¶

Deleted: ¶

Deleted: 7

Deleted: 68

Deleted:

Deleted: l<sup>1</sup>

Deleted: 7

Deleted: The

Formatted: Superscript

Deleted: at

Formatted: Superscript

Deleted: , East Greenland, West Greenland and Newfoundland Margins reflected both a strong phytoplankton bloom which had ...

Formatted: Highlight

Formatted: Normal, Indent: Before: 0 cm

Deleted: Phytoplankton cellular Fe:N ratios have been found to ...

1 ( $R^2=0.42$ ,  $n=51$ ,  $p$ -value  $< 0.05$ ). The slope of the relationship, representing the typical remineralisation ratio, was  $R_{Fe:N} = 0.07$   
2  $\pm 0.01$  mmol mol<sup>-1</sup>. The intercept of the regression line was  $-0.4 \pm 0.2$  nmol L<sup>-1</sup>, reflecting possible excess of preformed NO<sub>3</sub><sup>-</sup>  
3 compare to DFe in these water masses. These significant correlations allow us to use the Fe\* tracer to assess where DFe  
4 concentrations potentially limit phytoplankton growth by subtracting the contribution of organic matter remineralisation from  
5 the dissolved Fe pool, as defined by Rijkenberg et al. (2014) and Parekh et al. (2005) for PO<sub>4</sub><sup>3-</sup>, and modified here for NO<sub>3</sub><sup>-</sup> as  
6 follow:

$$Fe^* = [DFe] - R_{Fe:N} \times [NO_3^-] \quad (\text{eq. 4})$$

7 where  $R_{Fe:N}$  refers to the average biological uptake ratio Fe over nitrogen, and [NO<sub>3</sub><sup>-</sup>] refers to nitrate concentrations in  
8 seawater. Although, we imposed a fixed biological  $R_{Fe:N}$  of 0.05 mmol mol<sup>-1</sup>, it is important to note that the biological uptake  
9 ratio of DFe:NO<sub>3</sub><sup>-</sup> is not likely to be constant. Indeed, this ratio has been found to range from 0.05 to 0.9 mmol mol<sup>-1</sup> depending  
10 on species (Ho et al., 2003; Sunda and Huntsman, 1995; Twining et al., 2004). The ratio we choose is thus less drastic to assess  
11 potential Fe limitation and more representative of the average biological uptake of DFe over NO<sub>3</sub><sup>-</sup> calculated for this study (i.e.  
12  $R_{Fe:N} = 0.07 \pm 0.01$  mmol mol<sup>-1</sup>, for Subpolar waters). Negative values of Fe\* indicate the removal of DFe that is faster than  
13 the input through remineralisation or external sources and positive values suggest input of DFe from external sources (Fig. 7).

14 Consequently, figure 7 shows that phytoplankton communities with very high Fe requirements relative to NO<sub>3</sub><sup>-</sup> ( $R_{Fe:N} = 0.9$ )  
15 will only be able to grow above continental shelves where there is a high supply of DFe as previously reported by Nielsdóttir  
16 et al. (2009) and Painter et al. (2014). All these results are corroborating the importance of the Tagus River (Iberian Margin,  
17 see section 4.2.1), glacial inputs in the Greenland and Newfoundland Margins (see section 4.2.2) and to a lesser extent  
18 atmospheric inputs (see section 4.2.3) in supplying Fe with Fe:N ratios higher than the average biological uptake/demand ratio.  
19 Figure 7 (see also supplementary material S7, S8, S9 and S10) also highlights the Fe limitation for the low-Fe requirement  
20 phytoplankton class ( $R_{Fe:N} = 0.05$ ) within the Iceland Basin, Irminger and Labrador Seas. The Fe deficiency observed in surface  
21 waters (> 50 m depth) from the Irminger and Labrador Seas might be explained by low atmospheric deposition for the ICSPMW  
22 and the LSW (Shelley et al., 2017). Low atmospheric Fe supply and sub-optimal Fe:N ratios in winter overturned deep water  
23 could favour the formation of the High-Nutrient, Low-Chlorophyll (HNLC) conditions. The West European Basin, despite  
24 exhibiting some of the highest DFe:NO<sub>3</sub><sup>-</sup> ratios within surface waters (see supplementary material Fig. S8), displayed the  
25 strongest Fe-depletion from 50 m depth down to the bottom, suggesting that the main source of Fe was coming from dust  
26 deposition and/or riverine inputs.

27 Similarly as for the West European Basin, the pattern displayed in the surface map of DFe:NO<sub>3</sub><sup>-</sup> ratios (supplementary material  
28 S8) extended to about 50 m depth, after which the trend reversed (Fig. 7 and supplementary material Fig. S7). Below 50 m  
29 depth, the Fe\* tracer (Fig. 7) was positive in the Irminger Sea and overall negative in the other basins. In the Irminger Sea  
30 positive Fe\* values were likely the result of the winter entrainment of Fe-rich LSW (see section 4.2.1) coinciding with high  
31 remineralised carbon fluxes in this area (station 44; Lemaître et al., 2017) (see section 4.2.2). The largest drawdown in  
32 DFe:NO<sub>3</sub><sup>-</sup> ratios was observed between stations 34 and 38 and was likely due to the intrusion of the ICSPMW, this water mass  
33 exhibiting low DFe and high in NO<sub>3</sub><sup>-</sup> (from 7 to 8 μmol L<sup>-1</sup>) concentrations. Similarly, the SAIW exhibited high NO<sub>3</sub><sup>-</sup>  
34

Formatted: Normal, Centered, Indent: Before: 0 cm

Deleted: To assess where DFe concentrations potentially limit phytoplankton growth we subtracted the contribution of organic matter remineralization to the dissolved Fe pool using the tracer Fe\*, as defined by Rijkenberg et al. (2014) and Parekh et al. (2005) for PO<sub>4</sub><sup>3-</sup>, and modified here for NO<sub>3</sub><sup>-</sup> as follow:  
 $Fe^* = [DFe] - R_{Fe:N} \times [NO_3^-]$  (eq. 1)

Deleted: In the following, we use the two end-member ratios  $R_{Fe:N}$  ratios which represented the lowest and highest Fe:N uptake found in literature ( $R_{Fe:N} = 0.05$  and  $0.9$  mmol mol<sup>-1</sup>, respectively).

Deleted: a deficit in DFe concentrations whereas positive values are pointing out to a source of DFe relative to the uptake of NO<sub>3</sub><sup>-</sup>

Deleted: 13

Moved (insertion) [9]

Deleted: 13

Deleted: Fonseca-Batista et al., subm.

Formatted: Font: Not Bold, Font color: Auto, Complex Script  
Font: Times New Roman, Not Bold

Deleted: ¶

Moved (insertion) [10]

Deleted: z

Deleted: .

1 concentrations. Both the I<sub>c</sub>SPMW and the SAIW sourced from the NAC. The NAC as it flows along the coast of North  
2 America receives atmospheric depositions from anthropogenic sources (Shelley et al., 2017; 2015) which deliver high N  
3 relative to Fe (Jickells and Moore, 2015) and might be responsible for the observed ranges.

#### 4 **5 Conclusion**

5 The DFe concentrations measured during this study were in good agreement with previous studies that spanned the West  
6 European Basin. However, within the Irminger Basin the DFe concentrations measured during this study were up to 3 times  
7 higher than those measured by Rijkenberg et al. (2014) in deep waters (> 1000 m depth). This is likely explained by the  
8 different water masses encountered (i.e. the Polar Intermediate Water, ~ 2800 m depth) and by a stronger signal of the Iceland  
9 Scotland Overflow Water (ISOW) from 1200 to 2300 m depth. This corresponded to the most striking feature of the whole  
10 section with DFe concentrations reaching up to 2.5 nmol L<sup>-1</sup> within the ISOW, Denmark Strait Overflow Water (DSOW) and  
11 Labrador Sea Water (LSW), three water masses that are part of the Deep Western Boundary Current and was likely the result  
12 of a lateral advection of particles in the Irminger. However, as these water masses reached the Labrador Sea, lower DFe levels  
13 were measured. These differences could be explained by different processes occurring within the benthic nepheloid layers,  
14 where DFe was sometimes trapped onto particles due to Mn-sediment within the Labrador Sea (Gourain et al., 2018) and  
15 sometimes released from the sediment potentially as a result of interactions with dissolved organic matter. Such Fe-binding  
16 organic ligands could have also been produced locally due to the intense remineralisation rate reported by Lemaître et al.  
17 (2017) of biogenic particles (Boyd et al., 2010; Gourain et al., 2018). The LSW exhibited increasing DFe concentrations along  
18 its flow path, likely resulting from sediment inputs at the Newfoundland Margin. Although DFe inputs through hydrothermal  
19 activity were expected at the slow spreading Reykjanes Ridge (Baker and German, 2004b; German et al., 1994), our data did  
20 not provide evidence of this specific source as previously suggested by Achterberg et al. (2018) at ~60°N.

21 In surface waters several sources of DFe were highlighted especially close to land, with riverine inputs from the Tagus River  
22 at the Iberian margin (Menzel Barraqueta et al., 2018) and meteoric inputs (including coastal runoff and glacial meltwater) at  
23 the Newfoundland and Greenland margins (Benetti et al., 2016). Substantial sediment input was observed at all margins but  
24 with varying intensity. The highest DFe sediment input was located at the Newfoundland margin, while the lowest was  
25 observed at the eastern Greenland margin. These differences could be explained by the different nature of particles with the  
26 most lithogenic located at the Iberian margin and the most biogenic, at the Newfoundland margin (Gourain et al., 2018).  
27 Although previous studies (e.g. Jickells et al., 2005; Shelley et al., 2015) reported that atmospheric inputs substantially  
28 fertilized surface waters from the West European Basin, in our study, only stations located in the West European and Iceland  
29 Basins exhibited enhanced SML DFe inventories with lower TTADs. However, these TTADs were about three times higher  
30 than those reported for Saharan dust inputs and thus atmospheric deposition appeared to be a minor source of Fe during the  
31 sampling period. Finally, there was evidence of convective inputs of the LSW to surface seawater caused by long tip jet event

**Moved up [9]:** Consequently, figure 13 shows that phytoplankton communities with very high Fe requirements relative to NO<sub>3</sub> (R<sub>Fe:N</sub> = 0.9) will only be able to grow above continental shelves where there is a high supply of DFe. All these results are corroborating the importance of the Tagus River (Iberian Margin, see section 4.2.1), glacial inputs in the Greenland and Newfoundland Margins (see section 4.2.2) and to a lesser extent atmospheric inputs (see section 4.2.3) in supplying Fe with Fe:N ratios higher than the average biological uptake/demand ratio. ¶

**Moved up [10]:** coinciding with high remineralized carbon fluxes in this area (station 44; Lemaître et al., 2017).

**Deleted: ¶**  
Figures 12 and 14 also highlight the Fe limitation for the low-Fe requirement phytoplankton class (R<sub>Fe:N</sub> = 0.05, Fig. 13) within the Iceland Basin, Irminger and Labrador Seas. The Fe deficiency from the Iceland Basin and Labrador Sea might be explained by low atmospheric Fe supply and sub-optimal Fe:N ratios in winter overturned deep water could facilitate the formation of the High-Nutrient, Low-Chlorophyll (HNLC) conditions, representing the inefficiency of the biological carbon pump as little or no carbon is transferred below 1000 m depth (Lemaître et al., 2017; Nielsdóttir et al., 2009). Consequently, the low DFe:NO<sub>3</sub> ratios observed above 100 m depth were probably due to the phytoplankton bloom advancement, coinciding with high remineralized carbon fluxes in this area (station 44; Lemaître et al., 2017). The West European Basin, despite exhibiting some of the highest DFe:NO<sub>3</sub> ratios within surface waters (Fig. 12), displayed the strongest Fe-depletion from 50 m depth down to the bottom, suggesting that the main source of Fe was coming from dust deposition. In our study, Shelley et al. (2017b) reported low aerosol Fe loading compared to other studies in the ...

**Formatted:** Indent: First line: 0 cm

**Deleted:** the ones

**Deleted:** that was

**Deleted:**

**Formatted:** English (Australia)

**Formatted:** English (Australia)

**Formatted:** English (Australia)

**Formatted:** English (Australia)

**Deleted:** pointed

**Deleted:** further north

**Deleted:** (-

**Deleted:** ) from our section

**Formatted:** Normal

**Deleted:** s

**Deleted:** s

**Deleted:** ere

**Deleted:** different

**Deleted:** t

**Deleted:** at

1 (Piron et al., 2016) that deepened the winter mixed layer down to ~ 1200 m depth (Zunino et al., 2017), in which Fe was in  
2 excess of nitrate and therefore, Fe was not limiting.

### 3 Acknowledgements

4 We are greatly indebted to the master, Gilles Ferrand, the officers and crew from the N/O *Pourquoi Pas?* for their logistic  
5 support during the GEOVIDE voyage. We would like to give a special thanks to Pierre Branellec, Michel Hamon, Catherine  
6 Kermabon, Philippe Le Bot, Stéphane Leizour, Olivier Ménage (Laboratoire d'Océanographie Physique et Spatiale), Fabien  
7 Pérault and Emmanuel de Saint Léger (Division Technique de l'INSU, Plouzané, France) for their technical expertise during  
8 clean CTD deployments as well as Emilie Grosteffan and Manon Le Goff for the analysis of nutrients. We also wanted to  
9 thank the Pôle Spectrométrie Océan (PSO, Plouzané, France) for letting us use the Element XR HR-ICP-MS. Greg Cutter is  
10 also strongly acknowledged for his help in setting up the new French clean sampling system. Catherine Schmechtig is thanked  
11 for the LEFE-CYBER database management. This work was funded by the French National Research Agency ANR  
12 GEOVIDE (ANR-13-BS06-0014) and RPD0C BITMAP (ANR-12-PDOC-0025-01), the French National Center for  
13 Scientific Research (CNRS-LEFE-CYBER), the LabexMER (ANR-10-LABX-19) and Ifremer and was supported for the  
14 logistic by DT-INSU and GENAVIR. Manon Tonnard was supported by a cotutelle joint PhD scholarship from the Université  
15 de Bretagne Occidentale (UBO-IUEM) and the University of Tasmania (UTAS-IMAS).

16  
17 All dissolved iron (DFe) data are available in the supplementary material S1.

### 19 References

20 Achterberg, E. P., Steigenberger, S., Marsay, C. M., LeMoigne, F. A., Painter, S. C., Baker, A. R., Connelly, D. P.,  
21 Moore, C. M., Tagliabue, A., and Tanhua, T.: Iron Biogeochemistry in the High Latitude North Atlantic Ocean, Scientific  
22 reports, 8, 1-15, 10.1038/s41598-018-19472-1, 2018.

23 Aminot, A., and Kerouel, R.: Dosage automatique des nutriments dans les eaux marines, Quae ed., 2007.

24 Annett, A. L., Skiba, M., Henley, S. F., Venables, H. J., Meredith, M. P., Statham, P. J., and Ganeshram, R. S.:  
25 Comparative roles of upwelling and glacial iron sources in Ryder Bay, coastal western Antarctica Peninsula, Marine  
26 Chemistry, 176, 21-33, 10.1016/j.marchem.2015.06.017, 2015.

27 Bacon, S., Gould, W. J., and Jia, Y.: Open-ocean convection in the Irminger Sea, Geophysical Research Letters, 30,  
28 1246, doi:10.1029/2002GL016271, 2003.

29 Baker, A. R., Adams, C., Bell, T. G., Jickells, T. D., and Ganzeveld, L.: Estimation of atmospheric nutrient inputs  
30 to the Atlantic Ocean from 50°N to 50°S based on large-scale field sampling: Iron and other dust-associated elements,  
31 Global Biogeochemical Cycles, 27, 755-767, 10.1002/gbc.20062, 2013.

Deleted: where thus

Deleted: at the sampling period.

Formatted: Font: (Default) +Headings CS (Times New Roman), Complex Script Font: +Headings CS (Times New Roman)

Deleted: The objectives of the present paper were to describe and discuss the DFe distributions over the whole water column along the 5000 km long transect in the North Atlantic Ocean and the Labrador Sea. ¶

The most striking feature observed during the GEOVIDE voyage was the increasing DFe concentrations inherent to the LSW along its flow path which were likely explained by two processes: i) dissolution of Newfoundland sediments, and ii) potential bacteria-mediated Fe-binding organic ligand production as indicated by intense remineralization rates in the Irminger Sea. This observation has a broader implication in terms of primary production. Indeed, the intense wind-forcing of deep convection occurring in the Irminger Sea enables the LSW with its enhanced DFe concentrations to reach surface waters, thus initially sustaining intense phytoplankton growth during spring, but which will potentially limit the biological activity later on in the season due to its relative depletion in NO<sub>3</sub> as indicated by Fe\*. ¶

The distribution of DFe along the section also revealed the influence of external sources such as meteoric water melting in the subpolar gyre close to margins and the input of DFe from the Tagus river above the Iberian Margin. The latter source appears to have less impact as DFe is scavenged onto particles which will inevitably remove it from the mixed layer and entrained it to deep ocean. Dust deposition appears to have been only a minor source of DFe into surface waters, except in the subtropical gyre closer to the African continent. ¶

If the partition between dissolved and particulate forms of Fe is still not well understood in deep ocean, it is clear that it is mainly dependant of the nature of the sediments and not a direct function of the hydrographic characteristics. Indeed, different processes occurring within the DSOW in the Irminger and Labrador Seas result in DFe sometimes being scavenged onto particles due to Mn-oxide-sediment composition, yet at other times being released from the sediment. We have no clear explanation regarding the unusually high DFe concentrations (for a non-hydrothermal source) measured between 2000 and 3000 m depth in the Irminger Sea, except from dissolution of Fe-rich particles within DSOW and PIW as they mixed with ISOW. ¶



1 Baker, A. T., and German, C. R.: On the Global Distribution of Hydrothermal vent Fields, in: Mid-Ocean Ridges,  
2 edited by: German, C. R., Lin, J., and Parson, L. M., 2004a.

3 Baker, E. T., and German, C. R.: Hydrothermal Interactions Between the Lithosphere and Oceans, in: Mid-Ocean  
4 Ridges, edited by: German, C. R., Lin, J., and Parson, L. M., Geophysical Monograph Series, AGU, 245-266, 2004b.

5 Barton, A. D., Greene, C. H., Monger, B. C., and Pershing, A. J.: The Continuous Plankton Recorder survey and the  
6 North Atlantic Oscillation: Interannual- to Multidecadal-scale patterns of phytoplankton variability in the North Atlantic  
7 Ocean, *Progress in Oceanography*, 58, 337-358, 10.1016/j.pocean.2003.08.012, 2003.

8 Batchelli, S., Muller, F. L. L., Chang, K. C., and Lee, C. L.: Evidence for Strong but Dynamic Iron-Humic  
9 Colloidal Associations in Humic-Rich Coastal Waters., *Environmental Science & Technology*, 44, 8485-8490, 2010.

10 Benetti, M., Reverdin, G., Pierre, C., Khatiwala, S., Tournadre, B., Olafsdottir, S., and Naamar, A.: Variability of  
11 sea ice melt and meteoric water input in the surface Labrador Current off Newfoundland, *Journal of Geophysical Research*  
12 *Oceans*, 121, 2841-2855, doi:10.1002/2015JC011302., 2016.

13 Benetti, M., Reverdin, G., Lique, C., Yashayaev, I., Holliday, N. P., Tynan, E., Torres-Valdes, S., Lherminier, P.,  
14 Tréguer, P., and Sarthou, G.: Composition of freshwater in the spring of 2014 on the southern Labrador shelf and slope,  
15 *Journal of Geophysical Research: Oceans*, 122, 1102-1121, 10.1002/2016jc012244, 2017.

16 Bersch, M., Yashayaev, I., and Koltermann, K. P.: Recent changes of the thermohaline circulation in the subpolar  
17 North Atlantic, *Ocean Dynamics*, 57, 223-235, 10.1007/s10236-007-0104-7, 2007.

18 Bhatia, M. P., Kujawinski, E. B., Das, S. B., Breier, C. F., Henderson, P. B., and Charette, M. A.: Greenland  
19 meltwater as a significant and potentially bioavailable source of iron to the ocean, *Nature Geoscience*, 2013, 274-278,  
20 10.1038/ngeo1746, 2013.

21 Bonnet, S., and Guieu, C.: Dissolution of atmospheric iron in seawater, *Geophysical Research Letters*, 31,  
22 10.1029/2003gl018423, 2004.

23 Bonnet, S., and Guieu, C.: Atmospheric forcing on the annual iron cycle in the western Mediterranean Sea: A 1-  
24 year survey, *Journal of Geophysical Research*, 111, 10.1029/2005jc003213, 2006.

25 Boyd, P. W., Watson, A. J., Law, C. S., Abraham, E. R., Trull, T., Murdoch, R., Bakker, D. C. E., Bowie, A. R.,  
26 Buesseler, K. O., Chang, H., Charette, M., Croot, P., Downing, K., Frew, R., Gall, M., Hadfield, M., Hall, J., Harvey, M.,  
27 Jameson, G., LaRoche, J., Liddicoat, M., Ling, R., Maldonado, M. T., McKay, R. M., Nodder, S., Pickmere, S., Pridmore,  
28 R., Rintoul, S., Safi, K., Sutton, P., Strzepek, R., Tanneberger, K., Turner, S., Waite, A., and Zeldis, J.: A mesoscale  
29 phytoplankton bloom in the polar Southern Ocean stimulated by iron fertilization, *Nature*, 407, 695-702, 2000.

30 Boyd, P. W., and Ellwood, M. J.: The biogeochemical cycle of iron in the ocean, *Nature Geoscience*, 3, 675-682,  
31 10.1038/ngeo964, 2010.

32 Boyd, P. W., Ibsanmi, E., Sander, S. G., Hunter, K. A., and Jackson, G. A.: Remineralization of upper ocean  
33 particles: Implications for iron biogeochemistry, *Limnology and Oceanography*, 55, 1271-1288, 10.4319/lo.2010.55.3.1271,  
34 2010.

35 Buck, C. S., Landing, W. M., Resing, J. A., and Measures, C. I.: The solubility and deposition of aerosol Fe and  
36 other trace elements in the North Atlantic Ocean: Observations from the A16N CLIVAR/CO2 repeat hydrography section,  
37 *Marine Chemistry*, 120, 57-70, 10.1016/j.marchem.2008.08.003, 2010.

1 Canário, J., Vale, C., Caetano, M., and Madureira, M. J.: Mercury in contaminated sediments and pore waters  
2 enriched in sulphate (Tagus Estuary, Portugal), *Environmental Pollution*, 126, 425-433, 10.1016/S0269-7491(03)00234-3,  
3 2003.

4 Charette, M. A., Morris, P. J., Henderson, P. B., and Moore, W. S.: Radium isotope distributions during the US  
5 GEOTRACES North Atlantic cruises, *Marine Chemistry*, 177, 184-195, 10.1016/j.marchem.2015.01.001, 2015.

6 Chen, Y. J.: Influence of the Iceland mantle plume on crustal accretion at the inflated Reykjanes Ridge: Magma lens  
7 and low hydrothermal activity, *Journal of Geophysical Research*, 108, 2524, 2003.

8 Chester, R., Murphy, K. J. T., Lin, F. J., Berry, A. S., Bradshaw, G. A., and Corcoran, P. A.: Factors controlling the  
9 solubilities of trace-metals from nonremote aerosols deposited to the sea-surface by the dry deposition mode, *Marine*  
10 *Chemistry*, 42, 107-126, 10.1016/0304-4203(93)90241-f, 1993.

11 Conway, T. M., and John, S. G.: Quantification of dissolved iron sources to the North Atlantic Ocean, *Nature*, 511,  
12 212-215, 10.1038/nature13482, 2014.

13 Cooper, L. W., Whitlege, T. E., Grebmeier, J. M., and Weingartner, T.: The nutrient, salinity, and stable oxygen  
14 isotope composition of Bering and Chukchi Seas waters in and near the Bering Strait, *Journal of Geophysical Research*, 102,  
15 12,563-512,573, 1997.

16 Cooper, L. W., McClelland, J. W., Holmes, R. M., Raymond, P. A., Gibson, J. J., Guay, C. K., and Peterson, B. J.:  
17 Flow-weighted values of runoff tracers ( $\delta^{18}\text{O}$ , DOC, Ba, alkalinity) from the six largest Arctic rivers, *Geophysical Research*  
18 *Letters*, 35, 1-5, 10.1029/2008GL035007, 2008.

19 Crane, K., Johnson, L., Appelgate, B., Nishimura, C., Buck, R., Jones, C., Vogt, P., and Kos'yan, R.: Volcanic and  
20 Seismic Swarm Events on the Reykjanes Ridge and Their Similarities to Events on Iceland: Results of a Rapid Response  
21 Mission, *Marine Geophysical Researches*, 19, 319-338, 1997.

22 Cutter, G., Casciotti, K., Croot, P., Geibert, W., Heimbürger, L. E., Lohan, M., Planquette, H., and van de Fliedert,  
23 T.: Sampling and the Sample-handling Protocols for GEOTRACES Cruises, 2017.

24 Daniault, N., Mercier, H., Lherminier, P., Sarafanov, A., Falina, A., Zunino, P., Pérez, F. F., Ríos, A. F., Ferron, B.,  
25 Huck, T., Thierry, V., and Gladyshev, S.: The northern North Atlantic Ocean mean circulation in the early 21st century,  
26 *Progress in Oceanography*, 146, 142-158, 10.1016/j.pocean.2016.06.007, 2016.

27 de Barros, M. C.: A case study of waste inputs in the Tagus estuary, in: *The role of the Oceans as a Waste Disposal*  
28 *Option*, edited by: Kullenberg, G., NATO ASI Series; Series C: Mathematical and Physical Sciences, 172, Springer  
29 Netherlands, 307-324, 1986.

30 de Jong, M. F., van Aken, H. M., Våge, K., and Pickart, R. S.: Convective mixing in the central Irminger Sea:  
31 2002–2010, *Deep Sea Research Part I: Oceanographic Research Papers*, 63, 36-51, 10.1016/j.dsr.2012.01.003, 2012.

32 Dehairs, F., Shopova, D., Ober, S., Veth, C., and Goeyens, L.: Particulate barium stocks and oxygen consumption  
33 in the Southern Ocean mesopelagic water column during spring and early summer: Relationship with export production,  
34 *Deep Sea Research II*, 44, 497-516, 10.1016/S0967-0645(96)00072-0, 1997.

35 Deng, F., Henderson, G. M., Castrillejo, M., and Perez, F. F.: Evolution of  $^{231}\text{Pa}$  and  $^{230}\text{Th}$  in overflow waters of  
36 the North Atlantic, *Biogeosciences*, 1-24, 10.5194/bg-2018-191, 2018.

1 Fagel, N., Robert, C., and Hilaire-Marcel, C.: Clay mineral signature of the NW Atlantic Boundary Undercurrent,  
2 *Marine Geology*, 130, 19-28, 1996.

3 Fagel, N., Robert, C., Preda, M., and Thorez, J.: Smectite composition as a tracer of deep circulation: the case of the  
4 Northern North Atlantic, *Marine Geology*, 172, 309-330, 2001.

5 Ferron, B., Kokoszka, F., Mercier, H., Lherminier, P., Huck, T., Ríos, A., and Thierry, V.: Variability of the  
6 Turbulent Kinetic Energy Dissipation along the A25 Greenland–Portugal Transect Repeated from 2002 to 2012, *Journal of*  
7 *Physical Oceanography*, 46, 1989-2003, 10.1175/jpo-d-15-0186.1, 2016.

8 Figueres, G., Martin, J. M., Meybeck, M., and Seyler, P.: A comparative study of mercury contamination in the  
9 Tagus estuary (Portugal) and major French estuaries (Gironde, Loire, Rhone), *Estuarine, Coastal and Shelf Science*, 20, 183-  
10 203, 1985.

11 Fiuza, A.: *Hidrologia e dinamica das aguas costeiras de Portugal*, Ph. D., Universidade de Lisboa, Lisboa, Portugal,  
12 unpublished, 1984.

13 Follows, M., and Dutkiewicz, S.: Meteorological modulation of the North Atlantic Spring Bloom, *Deep Sea*  
14 *Research Part II: Topical Studies in Oceanography*, 49, 321-344, 2001.

15 García-Ibáñez, M. I., Pardo, P. C., Carracedo, L. I., Mercier, H., Lherminier, P., Ríos, A. F., and Pérez, F. F.:  
16 Structure, transports and transformations of the water masses in the Atlantic Subpolar Gyre, *Progress in Oceanography*, 135,  
17 18-36, 10.1016/j.pocean.2015.03.009, 2015.

18 García-Ibáñez, M. I., Pérez, F. F., Lherminier, P., Zunino, P., Mercier, H., and Tréguer, P.: Water mass distributions  
19 and transports for the 2014 GEOVIDE cruise in the North Atlantic, *Biogeosciences*, 15, 2075-2090, 10.5194/bg-15-2075-  
20 2018, 2018.

21 García-Ibáñez, M. I., Pérez, F. F., Lherminier, P., Zunino, P., and Tréguer, P.: Water mass distributions and  
22 transports for the 2014 GEOVIDE cruise in the North Atlantic, *Biogeosciences*, this issue.

23 Gaudencio, M. J., Guerra, M. T., and Glemarec, M.: Recherches biosédimentaires sur la zone maritime de l'estuaire  
24 du Tage, Portugal: données sédimentaires préliminaires. , in: *Estuaries and Coasts: Spatial and Temporal Intercomparisons*,  
25 edited by: Elliot, M., and Ducrottoy, J. C., Olsen and Olsen, Fredensborg, 11-16, 1991.

26 German, C. R., Briem, J., Chin, C. S., Danielsen, M., Holland, S., James, R. H., Jonsdottir, A., Ludford, E., Moser,  
27 C., Olafsson, J., Palmer, M. R., and Rudnicki, M. D.: Hydrothermal activity on the Reykjanes Ridge: the Steinahóll vent-  
28 field at 63°06'N, *Earth and Planetary Science Letters*, 121, 647-654, 1994.

29 Gerringa, L. J. A., Blain, S., Laan, P., Sarthou, G., Veldhuis, M. J. W., Brussaard, C. P. D., Viollier, E., and  
30 Timmermans, K. R.: Fe-binding dissolved organic ligands near the Kerguelen Archipelago in the Southern Ocean (Indian  
31 sector), *Deep Sea Research Part II: Topical Studies in Oceanography*, 55, 606-621, 10.1016/j.dsr2.2007.12.007, 2008.

32 Gerringa, L. J. A., Slagter, H. A., Bown, J., van Haren, H., Laan, P., de Baar, H. J. W., and Rijkenberg, M. J. A.:  
33 Dissolved Fe and Fe-binding organic ligands in the Mediterranean Sea – GEOTRACES G04, *Marine Chemistry*, 194, 100-  
34 113, 10.1016/j.marchem.2017.05.012, 2017.

35 Gourain, A., Planquette, H., Cheize, M., Menzel-Barraqueta, J. L., Boutorh, J., Shelley, R. U., Pereira-Contreira, L.,  
36 Lemaitre, N., Lacan, F., Lherminier, P., and Sarthou, G.: particulate trace metals along the GEOVIDE section,  
37 *Biogeosciences*, 2018.

1 Guerzoni, S., Chester, R., Dulac, F., Herut, B., Loye-Pilot, M.-D., Measures, C., Migon, C., Molinaroli, E., Moulin,  
2 C., Rossini, P., Saydam, C., Soudine, A., and Ziveri, P.: The role of atmospheric deposition in the biogeochemistry of the  
3 Mediterranean Sea, *Progress in Oceanography*, 44, 147-190, 1999.

4 Guieu, C., Loye-Pilot, M. D., Benyahya, L., and Dufour, A.: Spatial variability of atmospheric fluxes of metals (Al,  
5 Fe, Cd, Zn and Pb) and phosphorus over the whole Mediterranean from a one-year monitoring experiment: Biogeochemical  
6 implications, *Marine Chemistry*, 120, 164-178, 10.1016/j.marchem.2009.02.004, 2010.

7 Guieu, C., Aumont, O., Paytan, A., Bopp, L., Law, C. S., Mahowald, N., Achterberg, E. P., Marañón, E., Salihoglu,  
8 B., Crise, A., Wagener, T., Herut, B., Desboeufs, K., Kanakidou, M., Olgun, N., Peters, F., Pulido-Villena, E., Tovar-  
9 Sanchez, A., and Völker, C.: The significance of the episodic nature of atmospheric deposition to Low Nutrient Low  
10 Chlorophyll regions, *Global Biogeochemical Cycles*, 28, 1179-1198, 10.1002/2014gb004852, 2014.

11 Harrison, W. G., Yngve Børshiem, K., Li, W. K. W., Maillet, G. L., Pepin, P., Sakshaug, E., Skogen, M. D., and  
12 Yeats, P. A.: Phytoplankton production and growth regulation in the Subarctic North Atlantic: A comparative study of the  
13 Labrador Sea-Labrador/Newfoundland shelves and Barents/Norwegian/Greenland seas and shelves, *Progress in*  
14 *Oceanography*, 114, 26-45, 10.1016/j.pcean.2013.05.003, 2013.

15 Hatta, M., Measures, C. I., Wu, J., Roshan, S., Fitzsimmons, J. N., Sedwick, P., and Morton, P.: An overview of  
16 dissolved Fe and Mn distributions during the 2010-2011 US GEOTRACES north Atlantic cruises: GEOTRACES GA03,  
17 *Deep-Sea Research Part II-Topical Studies in Oceanography*, 116, 117-129, 10.1016/j.dsr2.2014.07.005, 2015.

18 Hawkings, J. R., Wadham, J. L., Tranter, M., Raiswell, R., Benning, L. G., Statham, P. J., Tedstone, A., Nienow, P.,  
19 Lee, K., and Telling, J.: Ice sheets as a significant source of highly reactive nanoparticulate iron to the oceans, *Nature*  
20 *communications*, 5, 1-8, 10.1038/ncomms4929, 2014.

21 Henson, S. A., Dunne, J. P., and Sarmiento, J. L.: Decadal variability in North Atlantic phytoplankton blooms,  
22 *Journal of Geophysical Research*, 114, 10.1029/2008jc005139, 2009.

23 Ho, T.-Y., Quigg, A., Finkel, Z. V., Milligan, A. J., Wyman, K., Falkowski, P. G., and Morel, F. M. M.: The  
24 elemental composition of some marine phytoplankton, *Journal of Phycology*, 39, 1145-1159, 2003.

25 Homoky, W. B., Hembury, D. J., Hepburn, L. E., Mills, R. A., Statham, P. J., Fones, G. R., and Palmer, M. R.: Iron  
26 and manganese diagenesis in deep sea volcanogenic sediments and the origins of pore water colloids, *Geochimica Et*  
27 *Cosmochimica Acta*, 75, 5032-5048, 10.1016/j.gca.2011.06.019, 2011.

28 Homoky, W. B., John, S. G., Conway, T. M., and Mills, R. A.: Distinct iron isotopic signatures and supply from  
29 marine sediment dissolution, *Nature Communications*, 4, 10.1038/ncomms3143, 2013.

30 Humphreys, M. P., Griffiths, A. M., Achterberg, E. P., Holliday, N. P., Rérolle, V., Menzel Barraqueta, J. L.,  
31 Couldrey, M. P., Oliver, K. I., Hartman, S. E., and Esposito, M.: Multidecadal accumulation of anthropogenic and  
32 remineralized dissolved inorganic carbon along the Extended Ellett Line in the northeast Atlantic Ocean, *Global*  
33 *Biogeochemical Cycles*, 30, 293-310, doi: 10.1002/2015GB005246, 2016.

34 Hunke, E. C., Notz, D., Turner, A. K., and Vancoppenolle, M.: The multiphase physics of sea ice: a review for  
35 model developers, *The Cryosphere*, 5, 989-1009, 10.5194/tc-5-989-2011, 2011.

36 Janssens, J., Meiners, K. M., Tison, J.-L., Dieckmann, G., Delille, B., and Lannuzel, D.: Incorporation of iron and  
37 organic matter into young Antarctic sea ice during its initial growth stages, *Elementa: Science of the Anthropocene*, 4,  
38 000123, 10.12952/journal.elementa.000123, 2016.

1 Jickells, T., and Moore, C. M.: The importance of atmospheric deposition for ocean productivity, *Annual Review of*  
2 *Ecology, Evolution, and Systematics*, 46, 481-501, 10.1146/annurev-ecolsys-112414-054118, 2015.

3 Jickells, T. D., An, Z. C., Andersen, K. K., Baker, A. R., Bergametti, G., Brooks, N., Cao, J. J., Boyd, P. W., Duce,  
4 R. A., Hunter, K. A., Kawahata, H., Kubilay, N., laRoche, J., Liss, P. S., Mahowald, N., Prospero, J. M., Ridgwell, A. J.,  
5 Tegen, I., and Torres, R.: Global iron connections between desert dust, ocean biogeochemistry, and climate, *Science*, 308,  
6 67-71, 2005.

7 Jones, E. P., Anderson, L. G., and Swift, J. H.: Distribution of Atlantic and Pacific waters in the upper Arctic  
8 Ocean: Implications for circulation, *Geophysical Research Letters*, 25, 765-768, 1998.

9 Kan, C. C., Chen, W. H., Wan, M. W., Phatai, P., Wittayakun, J., and Li, K. F.: The preliminary study of iron and  
10 manganese removal from groundwater by NaOCl oxidation and MF filtration, *Sustain. Environ. Res.*, 22, 25-30, 2012.

11 Kara, A. B., Rochford, P. A., and Hurlburt, H. E.: An optimal definition for ocean mixed layer depth, *Journal of*  
12 *Geophysical Research*, 105, 16,803-816,821, 10.1029/2000JC900072, 2000.

13 Kissel, C., Laj, C., Mulder, T., Wandres, C., and Cremer, M.: The magnetic fraction: A tracer of deep water  
14 circulation in the North Atlantic, *Earth and Planetary Science Letters*, 288, 444-454, 10.1016/j.epsl.2009.10.005, 2009.

15 Klunder, M. B., Bauch, D., Laan, P., de Baar, H. J. W., van Heuven, S. M. A. C., and Ober, S.: Dissolved iron in  
16 the Arctic shelf seas and surface waters of the Central Arctic Ocean: impact of Arctic river water and ice-melt, *Journal of*  
17 *Geophysical Research*, 117, 1-18, 2012.

18 Lackschewitz, K. S., Endler, R., Gehrke, B., Wallrabe-Adams, H.-J., and Thiede, J.: Evidence for topography- and  
19 current-controlled deposition on the Reykjanes Ridge between 59°N and 60°N, *Deep-Sea Research I*, 43, 1683-1711, 1996.

20 Laes, A., Blain, S., Laan, P., Achterberg, E. P., Sarthou, G., and de Baar, H. J. W.: Deep dissolved iron profiles in  
21 the eastern North Atlantic in relation to water masses, *Geophysical Research Letters*, 30, 10.1029/2003gl017902, 2003.

22 Lagerström, M. E., Field, M. P., Seguret, M., Fischer, L., Hann, S., and Sherrell, R. M.: Automated on-line flow-  
23 injection ICP-MS determination of trace metals (Mn, Fe, Co, Ni, Cu and Zn) in open ocean seawater: Application to the  
24 GEOTRACES program, *Marine Chemistry*, 155, 71-80, 10.1016/j.marchem.2013.06.001, 2013.

25 Lambelet, M., van de Fliedert, T., Crocket, K., Rehkamper, M., Katharina, K., Coles, B., Rijkenberg, M. J. A.,  
26 Gerringa, L. J. A., de Baar, H. J. W., and Steinfeldt, R.: Neodymium isotopic composition and concentration in the western  
27 North Atlantic Ocean: Results from the GEOTRACES GA02 section, *Geochimica Et Cosmochimica Acta*, 177, 1-29, 2016.

28 Le Roy, E., Sanial, V., Charette, M. A., van Beek, P., Lacan, F., Jacquet, S. H. M., Henderson, P. B., Souhaut, M.,  
29 García-Ibáñez, M. I., Jeandel, C., Pérez, F. F., and Sarthou, G.: The 226Ra–Ba relationship in the North Atlantic during  
30 GEOTRACES-GA01, *Biogeosciences*, 15, 3027-3048, 10.5194/bg-15-3027-2018, 2018.

31 Lemaître, N., Planchon, F., Planquette, H., Dehairs, F., Fonseca-Batista, D., Roukaerts, A., Deman, F., Tang, Y.,  
32 Mariez, C., and Sarthou, G.: High variability of export fluxes along the North Atlantic GEOTRACES section GA01:  
33 Particulate organic carbon export deduced from the 234Th method *Biogeosciences*, 1-38, 10.5194/bg-2018-190, 2018.

34 Lemaître, N., planquette, H., Planchon, F., Sarthou, G., Jacquet, S., Garcia-Ibanez, M. I., Gourain, A., Cheize, M.,  
35 Monin, L., Andre, L., Laha, P., Terryn, H., and Dehairs, F.: Particulate barium tracing significant mesopelagic carbon  
36 remineralisation in the North Atlantic *Biogeosciences Discussions*, 2017.

1 Lohan, M. C., and Bruland, K. W.: Elevated Fe(II) and Dissolved Fe in Hypoxic Shelf Waters off Oregon and  
2 Washington: An Enhanced Source of Iron to Coastal Upwelling Regimes, *Environmental Science & Technology*, 42, 6462-  
3 6468, 10.1021/es800144j, 2008.

4 Longhurst, A. R.: *Ecological geography of the Sea*, Second Edition ed., Elsevier Academic Press publications,  
5 Burlington, 542 pp., 2007.

6 Louanchi, F., and Najjar, R. G.: Annual cycles of nutrients and oxygen in the upper layers of the North Atlantic  
7 Ocean, *Deep Sea Research Part II: Topical Studies in Oceanography*, 48, 2155-2171, 2001.

8 Markus, T., Stroeve, J. C., and Miller, J.: Recent changes in Arctic sea ice melt onset, freezeup, and melt season  
9 length, *Journal of Geophysical Research*, 114, 10.1029/2009jc005436, 2009.

10 Marshall, J., and Schott, F.: Open-ocean convection: observations, theory, and models, *Reviews of Geophysics*, 37,  
11 1-64, doi: 10.1029/98RG02739, 1999.

12 Martin, J.-M., Elbaz-Poulichet, F., Guieu, C., Loÿe-Pilot, M.-D., and Han, G.: River versus atmospheric input of  
13 material to the Mediterranean Sea: an overview\*, *Marine Chemistry*, 28, 159-182, 1989.

14 Martin, J. D., and Fitzwater, S. E.: Iron deficiency limits phytoplankton growth in the north-east Pacific subarctic,  
15 *Nature*, 331, 341-343, 1988.

16 Martin, J. H., Fitzwater, S. E., and Gordon, R. M.: Iron deficiencies limits phytoplankton growth in Antarctic  
17 waters, *Global Biogeochemical Cycles*, 4, 5-12, 1990.

18 Martin, J. H., Coale, K. H., Johnson, K. S., Fitzwater, S. E., Gordon, R. M., Tanner, S. J., Hunter, C. N., Elrod, V.  
19 A., Nowicki, J. L., Coley, T. L., Barber, R. T., Lindley, S., Watson, A. J., Van Scoy, K., Law, C. S., Liddicoat, M. I., Ling,  
20 R., Stanton, T., Stockel, J., Collins, C., Anderson, A., Bidigare, R., Ondrusek, M., Latasa, M., Millero, F. J., Lee, K., Yao,  
21 W., Zhang, J. Z., Friederich, G., Sakamoto, C., Chavez, F., Buck, K., Kolber, Z., Greene, R., Falkowski, P., Chisholm, S.  
22 W., Hoge, F., Swift, R., Yungel, J., Turner, S., Nightingale, P., Hatton, A., Liss, P., and Tindale, N. W.: Testing the Iron  
23 Hypothesis in Ecosystems of the Equatorial Pacific Ocean, *Nature*, 371, 123-129, 10.1038/371123a0, 1994.

24 Measures, C. I., Brown, M. T., Selph, K. E., Apprill, A., Zhou, M., Hatta, M., and Hiscock, W. T.: The influence of  
25 shelf processes in delivering dissolved iron to the HNLC waters of the Drake Passage, Antarctica, *Deep Sea Research Part*  
26 *II: Topical Studies in Oceanography*, 90, 77-88, 10.1016/j.dsr2.2012.11.004, 2013.

27 Melling, H., and Moore, R. M.: Modification of halocline source waters during freezing on the Beaufort Sea shelf:  
28 Evidence from oxygen isotopes and dissolved nutrients, *Continental Shelf Research*, 15, 89-113, 1995.

29 Menzel Barraqueta, J. L., Schlosser, C., Planquette, H., Gourain, A., Cheize, M., Boutorh, J., Shelley, R. U., Pereira  
30 Contreira, L., Gledhill, M., Hopwood, M. J., Lherminier, P., Sarthou, G., and Achterberg, E. P.: Aluminium in the North  
31 Atlantic Ocean and the Labrador Sea (GEOTRACES GA01 section): roles of continental inputs and biogenic particle  
32 removal, *Biogeosciences Discussions*, 1-28, 10.5194/bg-2018-39, 2018.

33 Mercier, H., Lherminier, P., Sarafanov, A., Gaillard, F., Daniault, N., Desbruyères, D., Falina, A., Ferron, B.,  
34 Gourcuff, C., Huck, T., and Thierry, V.: Variability of the meridional overturning circulation at the Greenland-Portugal  
35 OVIDE section from 1993 to 2010, *Progress in Oceanography*, 132, 250-261, 10.1016/j.pcean.2013.11.001, 2015.

1 Mil-Homens, M., Branco, V., Lopes, C., Vale, C., Abrantes, F., Boer, W., and Vicente, M.: Using factor analysis to  
2 characterise historical trends of trace metal contamination in a sediment core from the Tagus Prodelta, Portugal, *Water, Air,  
3 and Soil Pollution*, 197, 277-287, 2009.

4 Moore, C. M., Mills, M. M., Langlois, R., Milne, A., Achterberg, E. P., La Roche, J., and Geider, R. J.: Relative  
5 influence of nitrogen and phosphorus availability on phytoplankton physiology and productivity in the oligotrophic sub-  
6 tropical North Atlantic Ocean, *Limnology and Oceanography*, 53, 291-205, 2008.

7 Moore, C. M., Mills, M. M., Arrigo, K. R., Berman-Frank, I., Bopp, L., Boyd, P. W., Galbraith, E. D., Geider, R. J.,  
8 Guieu, C., Jaccard, S. L., Jickells, T. D., La Roche, J., Lenton, T. M., Mahowald, N. M., Marañón, E., Marinov, I., Moore, J.  
9 K., Nakatsuka, T., Oschlies, A., Saito, M. A., Thingstad, T. F., Tsuda, A., and Ulloa, O.: Processes and patterns of oceanic  
10 nutrient limitation, *Nature Geoscience*, 6, 701-710, 10.1038/ngeo1765, 2013.

11 Moore, G. W. K.: Gale force winds over the Irminger Sea to the east of Cape Farewell, Greenland, *Geophysical  
12 Research Letters*, 30, n/a-n/a, 10.1029/2003gl018012, 2003.

13 Nielsdóttir, M. C., Moore, C. M., Sanders, R., Hinz, D. J., and Achterberg, E. P.: Iron limitation of the postbloom  
14 phytoplankton communities in the Iceland Basin, *Global Biogeochemical Cycles*, 23, n/a-n/a, 10.1029/2008gb003410, 2009.

15 Olafsson, J., Thors, K., and Cann, J. R.: A sudden cruise off Iceland, *RIDGE Events*, 2, 35-28, 1991.

16 Oschlies, A.: Nutrient supply to the surface waters of the North Atlantic: A model study, *Journal of Geophysical  
17 Research*, 107, 10.1029/2000jc000275, 2002.

18 Painter, S. C., Henson, S. A., Forryan, A., Steigenberger, S., Klar, J., Stinchcombe, M. C., Rogan, N., Baker, A. R.,  
19 Achterberg, E. P., and Moore, C. M.: An assessment of the vertical diffusive flux of iron and other nutrients to the surface  
20 waters of the subpolar North Atlantic Ocean, *Biogeosciences*, 11, 2113-2130, 10.5194/bg-11-2113-2014, 2014.

21 Palmer, M. R., Ludford, E. M., German, C. R., and Lilley, M. D.: Dissolved methane and hydrogen in the  
22 Steinahóll hydrothermal plume, 63°N, Reykjanes Ridge, in: *Hydrothermal Vents and Processes*, edited by: Parson, L. M.,  
23 Walker, C. L., and Dixon, D. R., Special Publications, Geological Society, London, 111-120, 1995.

24 Parekh, P., Follows, M. J., and Boyle, E. A.: Decoupling of iron and phosphate in the global ocean, *Global  
25 Biogeochemical Cycle*, 19, 2005.

26 Parra, M., Delmont, P., Ferragne, A., Latouche, C., Pons, J. C., and Puechmaille, C.: Origin and evolution of  
27 smectites in recent marine sediments of the NE Atlantic, *Clay Minerals*, 20, 335-346, 1985.

28 Pérez, F. F., Mercier, H., Vázquez-Rodríguez, M., Lherminier, P., Velo, A., Pardo, P. C., Rosón, G., and Ríos, A.  
29 F.: Atlantic Ocean CO<sub>2</sub> uptake reduced by weakening of the meridional overturning circulation, *Nature Geoscience*, 6, 146-  
30 152, 10.1038/ngeo1680, 2013.

31 Pérez, F. F., Treguer, P., Branellec, P., García-Ibáñez, M. I., Lherminier, P., and Sarthou, G.: The 2014 Greenland-  
32 Portugal GEOVIDE bottle data (GO-SHIP A25 and GEOTRACES GA01). SEANOE (Ed.), 2018.

33 Petrich, C., and Eicken, H.: Growth, structure and properties of sea ice, in: *Sea Ice*. 2nd ed., edited by: Thomas, D.  
34 N., and Dieckmann, G. S., Wiley-Blackwell, Oxford, U.K., 23-77, 2010.

35 Pickart, R. S., Straneo, F., and Moore, G. W. K.: Is Labrador Sea Water formed in the Irminger basin?, *Deep Sea  
36 Research Part I*, 50, 23-52, 2003.

1 Piron, A., Thierry, V., Mercier, H., and Caniaux, G.: Argo float observations of basin-scale deep convection in the  
2 Irminger sea during winter 2011–2012, *Deep Sea Research Part I: Oceanographic Research Papers*, 109, 76-90,  
3 10.1016/j.dsr.2015.12.012, 2016.

4 Radic, A., Lacan, F., and Murray, J. W.: Iron isotopes in the seawater of the equatorial Pacific Ocean: New  
5 constraints for the oceanic iron cycle, *Earth and Planetary Science Letters*, 306, 1-10, 10.1016/j.epsl.2011.03.015, 2011.

6 Ras, J., Claustre, H., and Uitz, J.: Spatial variability of phytoplankton pigment distribution in the Subtropical South  
7 Pacific Ocean: comparison between *in situ* and predicted data, *Biogeosciences*, 5, 353-369, 2008.

8 Riebesell, U., Schloss, I., and Smetacek, V.: Aggregation of algae released from melting sea ice: implications for  
9 seeding and sedimentation, *Polar Biology*, 11, 239-248, 1991.

10 Rijkenberg, M. J., Middag, R., Laan, P., Gerringa, L. J., van Aken, H. M., Schoemann, V., de Jong, J. T., and de  
11 Baar, H. J.: The distribution of dissolved iron in the West Atlantic Ocean, *PLoS One*, 9, e101323,  
12 10.1371/journal.pone.0101323, 2014.

13 Sabine, C. L., Feely, R. A., Gruber, N., Key, R. M., Lee, K., Bullister, J. L., Wanninkhof, R., Wong, C. S., Wallace,  
14 D. W. R., Tilbrook, B., Millero, F. J., Peng, T.-H., Kozyr, A., Ono, T., and Rios, A. F.: The Oceanic sink for anthropogenic  
15 CO<sub>2</sub>, *Science*, 305, 367-371, 2004.

16 Sanders, R., Brown, L., Henson, S., and Lucas, M.: New production in the Irminger Basin during 2002, *Journal of*  
17 *Marine Systems*, 55, 291-310, [http:// dx.doi.org/10.1016/j.jmarsys.2004.09.002](http://dx.doi.org/10.1016/j.jmarsys.2004.09.002), 2005.

18 Santos-Echeandia, J., Vale, C., Caetano, M., Pereira, P., and Prego, R.: Effect of tidal flooding on metal distribution  
19 in pore waters of marsh sediments and its transport to water column (Tagus estuary, Portugal), *Mar Environ Res*, 70, 358-  
20 367, 10.1016/j.marenvres.2010.07.003, 2010.

21 Sarthou, G., and Jeandel, C.: Seasonal variations of iron concentrations in the Ligurian Sea and iron budget in the  
22 Western Mediterranean Sea, *Marine Chemistry*, 74, 115-129, 10.1016/s0304-4203(00)00119-5, 2001.

23 Sarthou, G., Baker, A. R., Kramer, J., Laan, P., Laës, A., Ussher, S., Achterberg, E. P., de Baar, H. J. W.,  
24 Timmermans, K. R., and Blain, S.: Influence of atmospheric inputs on the iron distribution in the subtropical North-East  
25 Atlantic Ocean, *Marine Chemistry*, 104, 186-202, 10.1016/j.marchem.2006.11.004, 2007.

26 Sarthou, G., Vincent, D., Christaki, U., Obermosterer, I., Timmermans, K. R., and Brussaard, C. P. D.: The fate of  
27 biogenic iron during a phytoplankton bloom induced by natural fertilisation: Impact of copepod grazing, *Deep Sea Research*  
28 *Part II: Topical Studies in Oceanography*, 55, 734-751, 10.1016/j.dsr2.2007.12.033, 2008.

29 Sarthou, G., Lherminier, P., Achterberg, E. P., Alonso-Pérez, F., Bucciarelli, E., Boutorh, J., Bouvier, V., Boyle, E.  
30 A., Branellec, P., Carracedo, L. I., Casacuberta, N., Castrillejo, M., Cheize, M., Contreira Pereira, L., Cossa, D., Danialt,  
31 N., De Saint-Léger, E., Dehairs, F., Deng, F., Desprez de Gésincourt, F., Devesa, J., Foliot, L., Fonseca-Batista, D.,  
32 Gallinari, M., García-Ibáñez, M. I., Gourain, A., Grossteffan, E., Hamon, M., Heimbürger, L. E., Henderson, G. M., Jeandel,  
33 C., Kermabon, C., Lacan, F., Le Bot, P., Le Goff, M., Le Roy, E., Lefèbvre, A., Leizour, S., Lemaitre, N., Masqué, P.,  
34 Ménage, O., Menzel Barraqueta, J.-L., Mercier, H., Perault, F., Pérez, F. F., Planquette, H. F., Planchon, F., Roukaerts, A.,  
35 Sanial, V., Sauzède, R., Shelley, R. U., Stewart, G., Sutton, J. N., Tang, Y., Tisnérat-Laborde, N., Tonnard, M., Tréguer, P.,  
36 van Beek, P., Zurbrick, C. M., and Zunino, P.: Introduction to the French GEOTRACES North Atlantic Transect (GA01):  
37 GEOVIDE cruise, *Biogeosciences Discussions*, 1-24, 10.5194/bg-2018-312, 2018.

38 Ocean Data View, <https://odv.awi.de> ODV4, version 4.7.6 (23 March 2016), access: 6 April, 2016.



1 Schroth, A. W., Crusius, J., Hoyer, I., and Campbell, R.: Estuarine removal of glacial iron and implications for iron  
2 fluxes to the ocean, *Geophysical Research Letters*, 41, 3951-3958, 10.1002/2014GL060199, 2014.

3 Shelley, R. U., Morton, P. L., and Landing, W. M.: Elemental ratios and enrichment factors in aerosols from the  
4 US-GEOTRACES North Atlantic transects, *Deep Sea Research*, 116, 262-272, 2015.

5 Shelley, R. U., Roca-Martí, M., Castrillejo, M., Sanial, V., Masqué, P., Landing, W. M., van Beek, P., Planquette,  
6 H., and Sarthou, G.: Quantification of trace element atmospheric deposition fluxes to the Atlantic Ocean (>40°N;  
7 GEOVIDE, GEOTRACES GA01) during spring 2014, *Deep Sea Research Part I: Oceanographic Research Papers*, 119, 34-  
8 49, 10.1016/j.dsr.2016.11.010, 2017.

9 Shelley, R. U., Landing, W. M., Ussher, S. J., Planquette, H., and Sarthou, G.: Characterisation of aerosol  
10 provenance from the fractional solubility of Fe (Al, Ti, Mn, Co, Ni, Cu, Zn, Cd and Pb) in North Atlantic aerosols  
11 (GEOTRACES cruises GA01 and GA03) using a two stage leach, *Biogeosciences*, 2018.

12 Shor, A., Lonsdale, P., Hollister, D., and Spencer, D.: Charlie-Gibbs fracture zone: bottom-water transport and its  
13 geological effects, *Deep Sea Research*, 27A, 325-345, 1980.

14 Sinha, M. C., Navin, D. A., MacGregor, L. M., Constable, S., Peirce, C., White, A., Heinson, G., and Inglis, M. A.:  
15 Evidence for accumulated melt beneath the slow-spreading Mid-Atlantic Ridge, *Philosophical Transactions of the Royal  
16 Society A*, 355, 233-253, 1997.

17 Slagter, H. A., Reader, H. E., Rijkenberg, M. J. A., Rutgers van der Loeff, M., de Baar, H. J. W., and Gerringa, L. J.  
18 A.: Organic Fe speciation in the Eurasian Basins of the Arctic Ocean and its relation to terrestrial DOM, *Marine Chemistry*,  
19 197, 11-25, 10.1016/j.marchem.2017.10.005, 2017.

20 Smallwood, J. R., and White, R. S.: Crustal accretion at the Reykjanes Ridge, 61°-62°N, *Journal of Geophysical  
21 Research: Solid Earth*, 103, 5185-5201, 10.1029/97jb03387, 1998.

22 Statham, P. J., Skidmore, M., and Tranter, M.: Inputs of glacially derived dissolved and colloidal iron to the coastal  
23 ocean and implications for primary productivity, *Global Biogeochemical Cycles*, 22, 1-11, 10.1029/2007GB003106, 2008.

24 Sunda, W. G., and Huntsman, S. A.: Iron uptake and growth limitation in oceanic and coastal phytoplankton,  
25 *Marine Chemistry*, 50, 189-206, 10.1016/0304-4203(95)00035-p, 1995.

26 Sutherland, D. A., Pickart, R. S., Peter Jones, E., Azetsu-Scott, K., Jane Eert, A., and Ólafsson, J.: Freshwater  
27 composition of the waters off southeast Greenland and their link to the Arctic Ocean, *Journal of Geophysical Research*, 114,  
28 10.1029/2008jc004808, 2009.

29 Tanhua, T., Olsson, K. A., and Jeansson, E.: Formation of Denmark Strait overflow water and its hydro-chemical  
30 composition, *Journal of Marine Systems*, 57, 264-288, 10.1016/j.jmarsys.2005.05.003, 2005.

31 Teng, Z., Huang, J. Y., Fujito, K., and Takizawa, S.: Manganese removal by hollow fiber micro-filter.Membrane  
32 separation for drinking water, *European Conference on Desalination and the Environment*, Amsterdam, 28 May, 2001.

33 Thuróczy, C. E., Gerringa, L. J. A., Klunder, M. B., Middag, R., Laan, P., Timmermans, K. R., and de Baar, H. J.  
34 W.: Speciation of Fe in the Eastern North Atlantic Ocean, *Deep Sea Research Part I: Oceanographic Research Papers*, 57,  
35 1444-1453, 10.1016/j.dsr.2010.08.004, 2010.

1 Tonnard, M., Donval, A., Lampert, L., Tréguer, P., Bowie, A. R., van der Merwe, P., planquette, H., Claustre, H.,  
2 Dimier, C., Ras, J., and Sarthou, G.: Phytoplankton assemblages in the North Atlantic Ocean and in the Labrador Sea along  
3 the GEOVIDE section (GEOTRACES section GA01) determined by CHEMTAX analysis from HPLC pigment data,  
4 *Biogeosciences*, in prep.

5 Tovar-Sanchez, A., Duarte, C. M., Alonso, J. C., Lacorte, S., Tauler, R., and Galban-Malagon, C.: Impacts of  
6 metals and nutrients released from melting multiyear Arctic sea ice, *Journal of Geophysical Research-Oceans*, 115,  
7 10.1029/2009jc005685, 2010.

8 Tréguer, P. J., and De La Rocha, C. L.: The world ocean silica cycle, *Ann Rev Mar Sci*, 5, 477-501,  
9 10.1146/annurev-marine-121211-172346, 2013.

10 Twining, B. S., Baines, S. B., Fisher, N. S., and Landry, M. R.: Cellular iron contents of plankton during the  
11 Southern Ocean Iron Experiment (SOFeX), *Deep Sea Research Part I: Oceanographic Research Papers*, 51, 1827-1850,  
12 10.1016/j.dsr.2004.08.007, 2004.

13 Van Beusekom, J. E. E.: Distribution of aluminium in surface waters of the North Sea: influence of suspended  
14 matter., in: *Biogeochemistry and Distribution of Suspended Matter in the North Sea and Implications to fisheries Biology*,  
15 edited by: Kempe, S., *Mitteilungen aus dem Geologisch-Paläontologischen Institut der Universität Hamburg*,  
16 SCOPE/UNEP Sonderband, 117-136, 1988.

17 von Appen, W.-J., Koszalka, I. M., Pickart, R. S., Haine, T. W. N., Mastropole, D., Magaldi, M. G., Valdimarsson,  
18 H., Giron, J., Jochumsen, K., and Krahnemann, G.: The East Greenland Spill Jet as an important component of the Atlantic  
19 Meridional Overturning Circulation, *Deep Sea Research Part I: Oceanographic Research Papers*, 92, 75-84,  
20 10.1016/j.dsr.2014.06.002, 2014.

21 Wadhams, P.: *Ice in the Ocean*, Gordon and Breach Science Publishers, London, UK, 2000.

22 Wagener, T., Guieu, C., and Leblond, N.: Effects of dust deposition on iron cycle in the surface Mediterranean Sea:  
23 results from a mesocosm seeding experiment, *Biogeosciences Discussions*, 7, 2799-2830, 2010.

24 Woodgate, R. A., and Aagaard, K.: Revising the Bering Strait freshwater flux into the Arctic Ocean, *Geophysical*  
25 *Research Letters*, 32, 10.1029/2004GL021747., 2005.

26 Wuttig, K., Wagener, T., Bressac, M., Dammshäuser, A., Streu, P., Guieu, C., and Croot, P. L.: Impacts of dust  
27 deposition on dissolved trace metal concentrations (Mn, Al and Fe) during a mesocosm experiment, *Biogeosciences*, 10,  
28 2583-2600, 10.5194/bg-10-2583-2013, 2013.

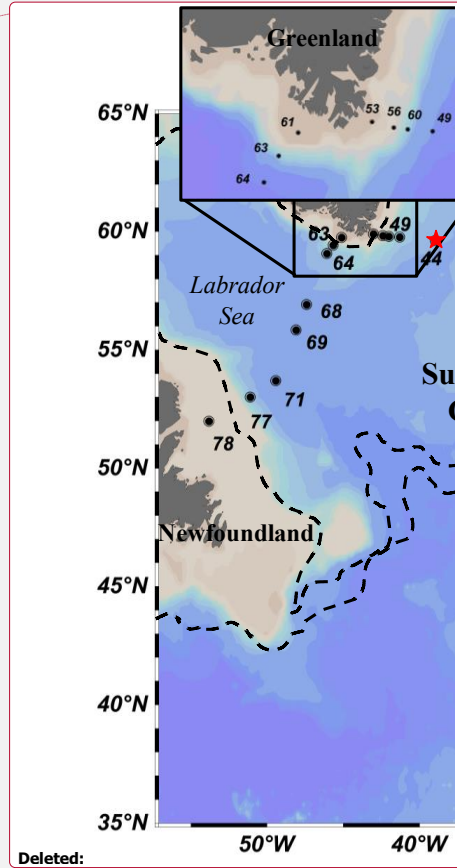
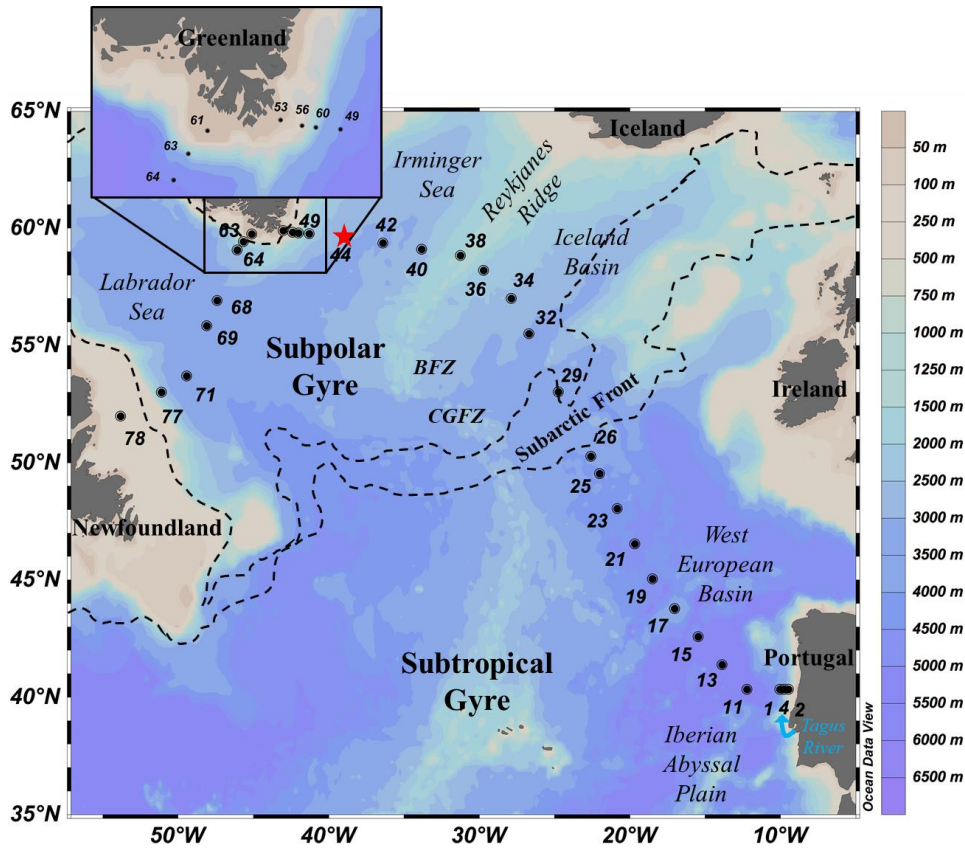
29 Zou, S., Lozier, S., Zenk, W., Bower, A., and Johns, W.: Observed and modeled pathways of the Iceland Scotland  
30 Overflow Water in the eastern North Atlantic, *Progress in Oceanography*, 159, 211-222, 10.1016/j.pocean.2017.10.003,  
31 2017.

32 Zunino, P., Lherminier, P., Mercier, H., Danialt, N., García-Ibáñez, M. I., and Pérez, F. F.: The GEOVIDE cruise  
33 in may-June 2014 revealed an intense MOC over a cold and fresh subpolar North Atlantic, *Biogeosciences*, 2017.

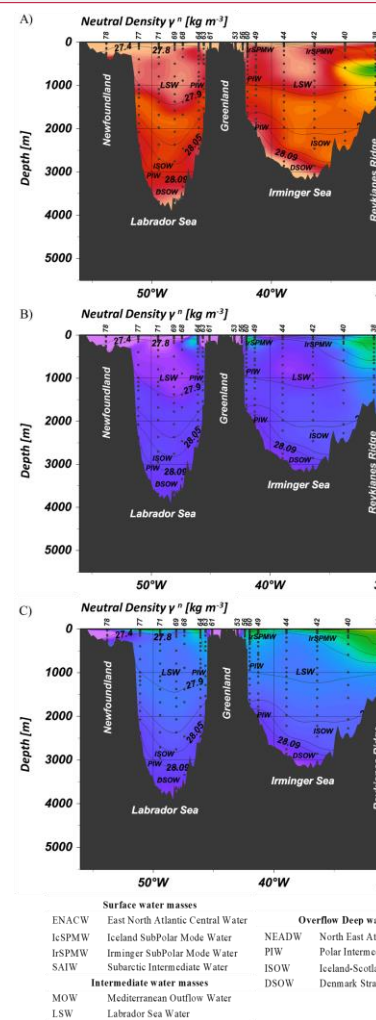
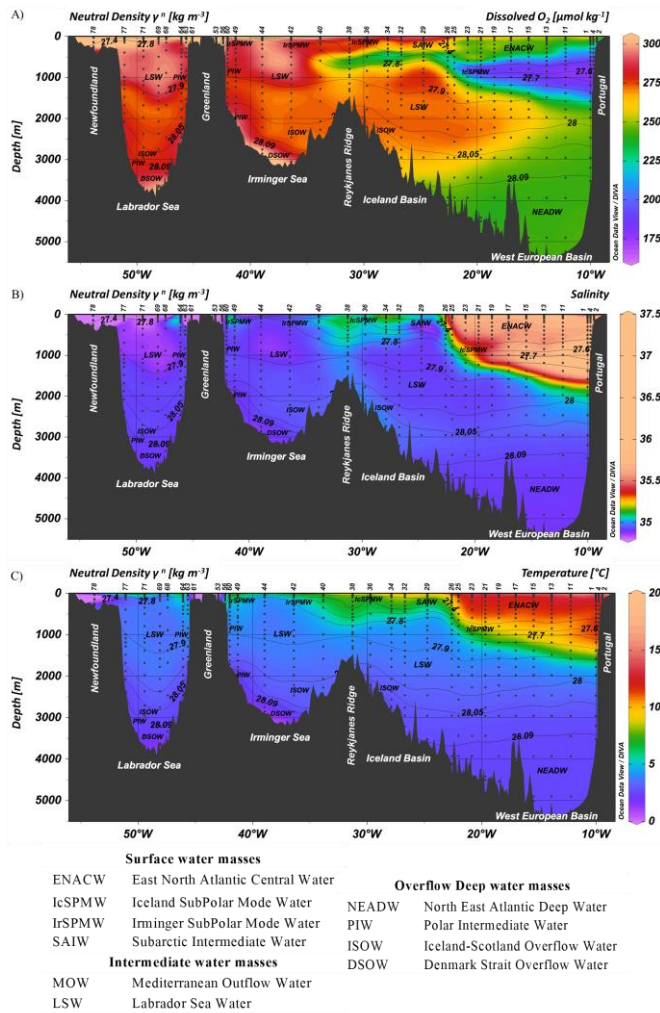
34

35

1 Figure 1: Map of the GEOTRACES GA01 voyage plotted on bathymetry as well as the major topographical features and main  
 2 basins. Crossover station with GEOTRACES voyage (GA03) is shown as a red star. (Ocean Data View (ODV) software, version  
 3 4.7.6, R. Schlitzer, <http://odv.awi.de>, 2016). **BFZ: Bight Fracture Zone**, **CGFZ: Charlie-Gibbs Fracture Zone**.

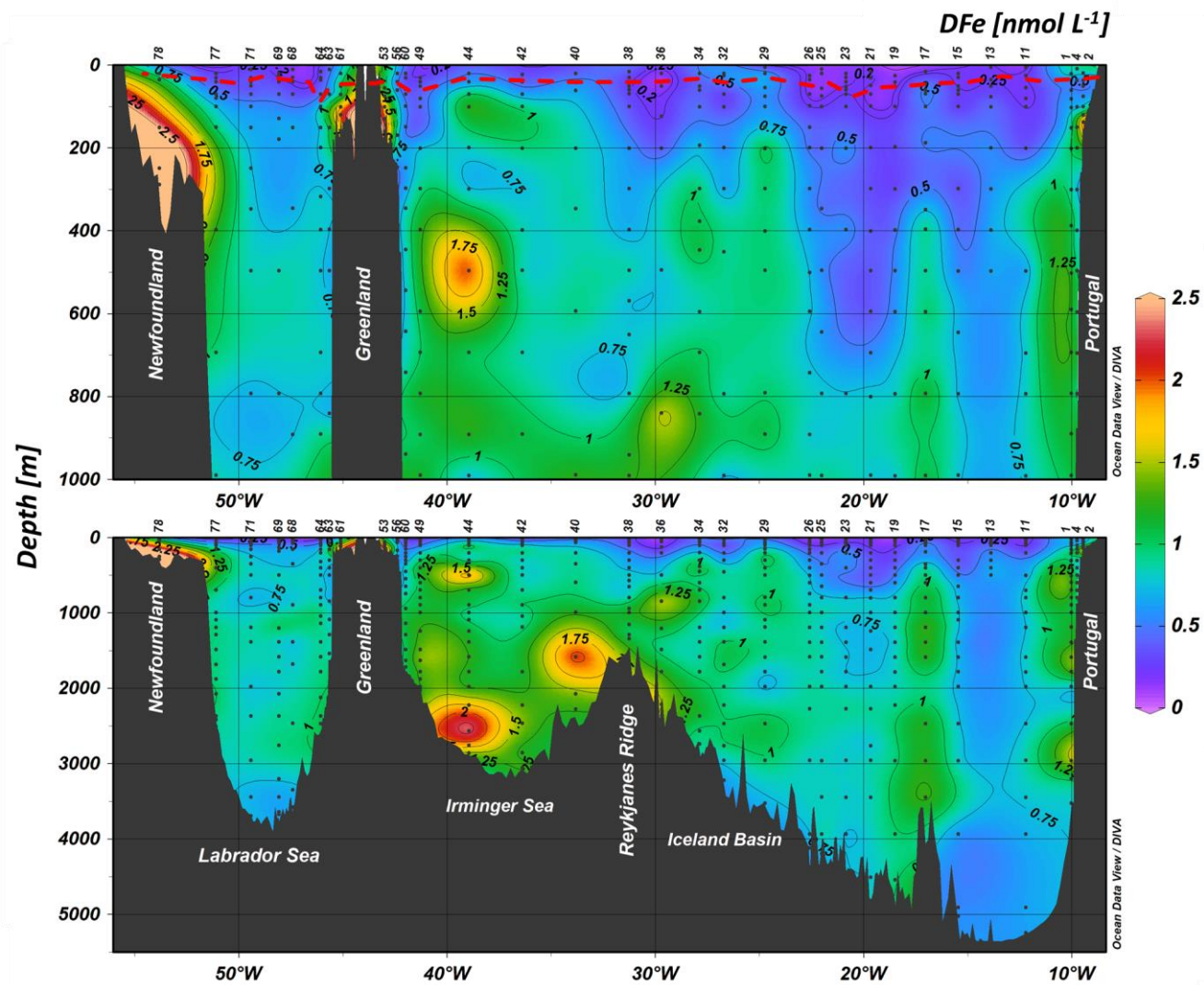


1 Figure 2: Parameters measured from the regular CTD cast represented as a function of depth for GA01 section for (A) Dissolved  
 2 Oxygen ( $O_2$ ,  $\mu\text{mol kg}^{-3}$ ), (B) Salinity and (C) Temperature ( $^{\circ}\text{C}$ ). The contour lines represent isopycnals (neutral density,  $\gamma^n$ , in units  
 3 of  $\text{kg m}^{-3}$ ).



Deleted:

**Figure 3:** Contour plot of the distribution of dissolved iron (DFe) concentrations in  $\text{nmol L}^{-1}$  along the GA01 voyage transect: upper 1000 m (top) and full depth range (bottom). The red dashed line indicates the depth of the Surface Mixed Layer (SML). Small black dots represent collected water samples at each sampling station. (Ocean Data View (ODV) software, version 4.7.6, R. Schlitzer, <http://odv.awi.de>, 2016).



Deleted: Figure 3 shows the distribution of dissolved iron (DFe) concentrations (color scale) along the GA01 voyage transect. The top panel shows the upper 1000 m depth range, and the bottom panel shows the full depth range. The red dashed line indicates the depth of the Surface Mixed Layer (SML). Small black dots represent collected water samples at each sampling station. The plot was generated using Ocean Data View (ODV) software (<http://odv.awi.de>).

Depth [m]

0

50

100

150

200

250

Deleted: 4

Figure 4: Vertical profiles of dissolved iron (DFe, black dots, solid line), particulate iron (PFe, black open dots, dashed line, Gourain et al., in prep.) and dissolved aluminium (DAI, grey dots, Menzel Barraqueta et al., 2018) at Stations 2 (A), and 4 (B) located above the Iberian shelf, Station 56 (C), Stations 53 (D) 53 and Station 61 (E) located above the Greenland shelf and Station 78 (F) located above the Newfoundland shelf. Note that for stations 53, 61 and 78, plots of the percentage of meteoric water (open dots) and sea-ice (black dots and dashed line) (Benetti et al., see text for details), Total Chlorophyll-*a* (TChl-*a*, green), temperature (blue) and salinity (black) are also displayed as a function of depth.

Deleted: 5

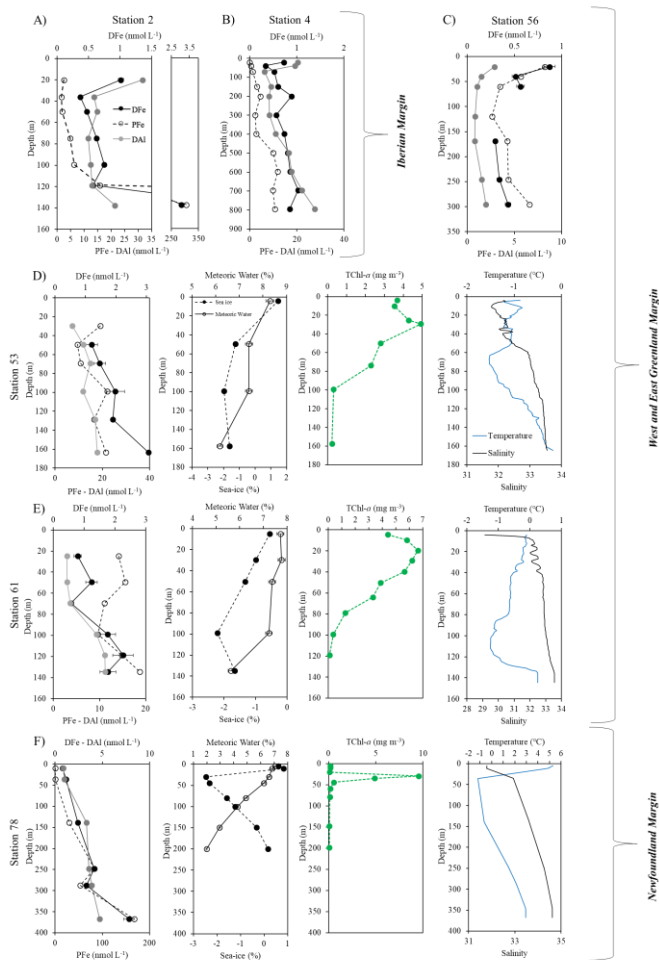
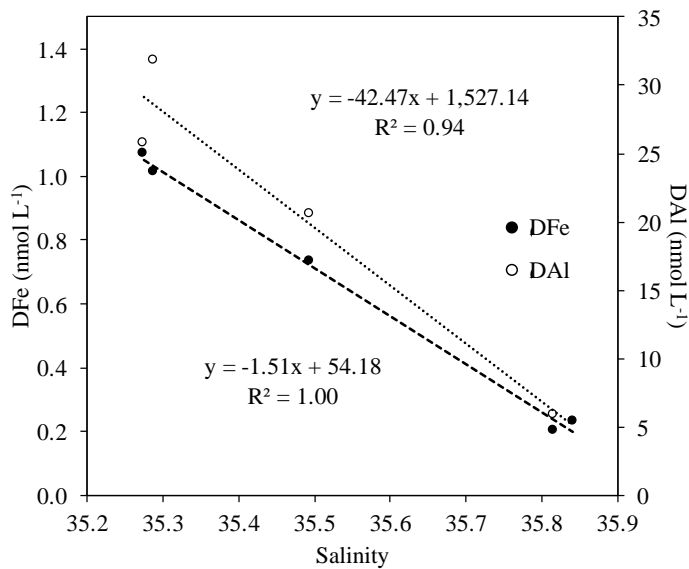
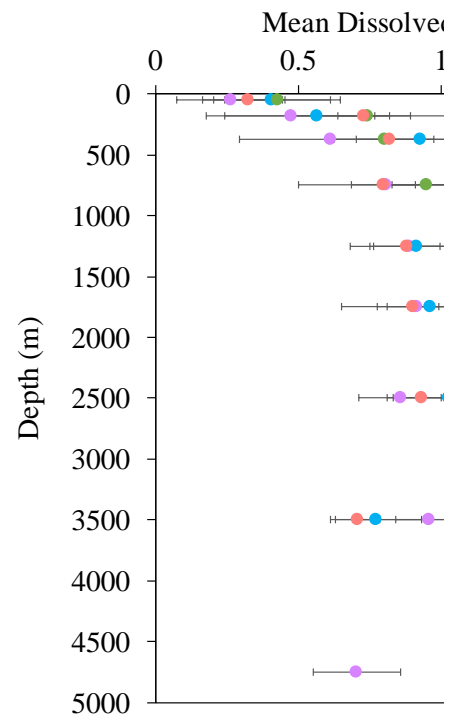


Figure 5: Plot of dissolved iron (DFe, black circles) and dissolved aluminium (DAI, white circles, Menzel Barraqueta et al., 2018) along the salinity gradient between stations 1, 2, 4, 11 and 13 with linear regression equations. Numbers close to sample points representing station numbers.



5

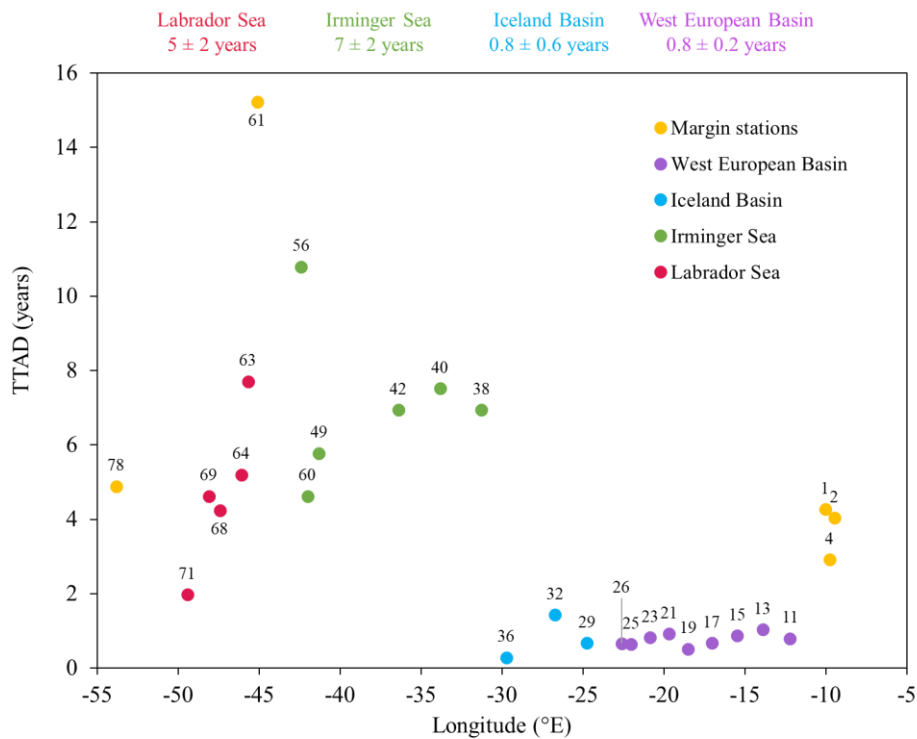
Deleted: Figure 6: Mean profiles of dissolved iron (Fe) along the North Atlantic section in the West European Basin (purple), Iceland Basin (blue), Irminger Sea (green) and Labrador Sea (red) over the depth intervals: 0-100 m, 100-250 m, 250-500 m, 500-1000 m, 1000-1500 m, 1500-2000 m, 2000-3000 m, 3000-4000 m, 4000-5500 m without considering stations located above the continental plateau.¶



Deleted: Figure 7: Box and whisker plot of dissolved iron (DFe) in nmol L<sup>-1</sup> per water mass and basin. Color coding representing from West to East: the Labrador Sea (red), the Irminger Sea (green), the Iceland Basin (blue) and the West European Basin (purple). Note that stations 1 and 17 were not considered in this plot. SAIW: Sub-Arctic Intermediate Water, ENACW: East North Atlantic Central Water, IrSPMW: Irminger Sub-Polar Mode Water, IcSPMW: Iceland Sub-Polar Mode Water, MOW: Mediterranean Overflow Water, LSW: Labrador Sea Water, ISOW: Iceland-Scotland Overflow Water, DSOW: Denmark ...

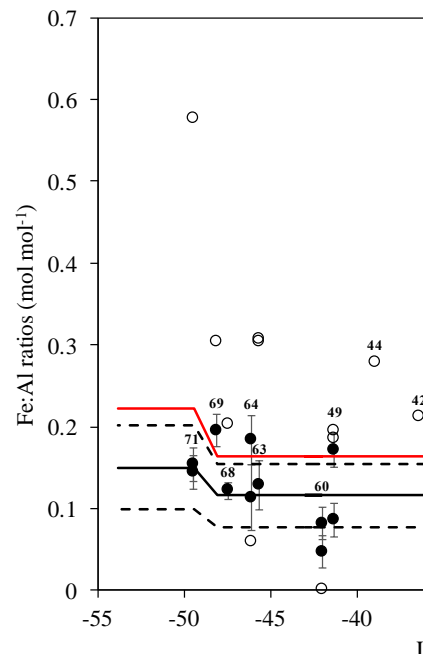
Deleted: 9

**Figure 6:** Plot of dissolved Fe (DFe) Turnover Times relative to Atmospheric Deposition (TTADs) calculated from soluble Fe contained in aerosols estimated from a two-stage sequential leach (UHP water, then 25% HAc, Shelley et al., this issue). Note that numbers on top of points represent station numbers and that the colour coding refers to different region with in yellow, margin stations; in purple, the West European Basin; in blue, the Iceland Basin; in green, the Irminger Sea and in red, the Labrador Sea. The numbers on top of the plot represent TTADs averaged for each oceanic basin and their standard deviation.



Deleted: 10

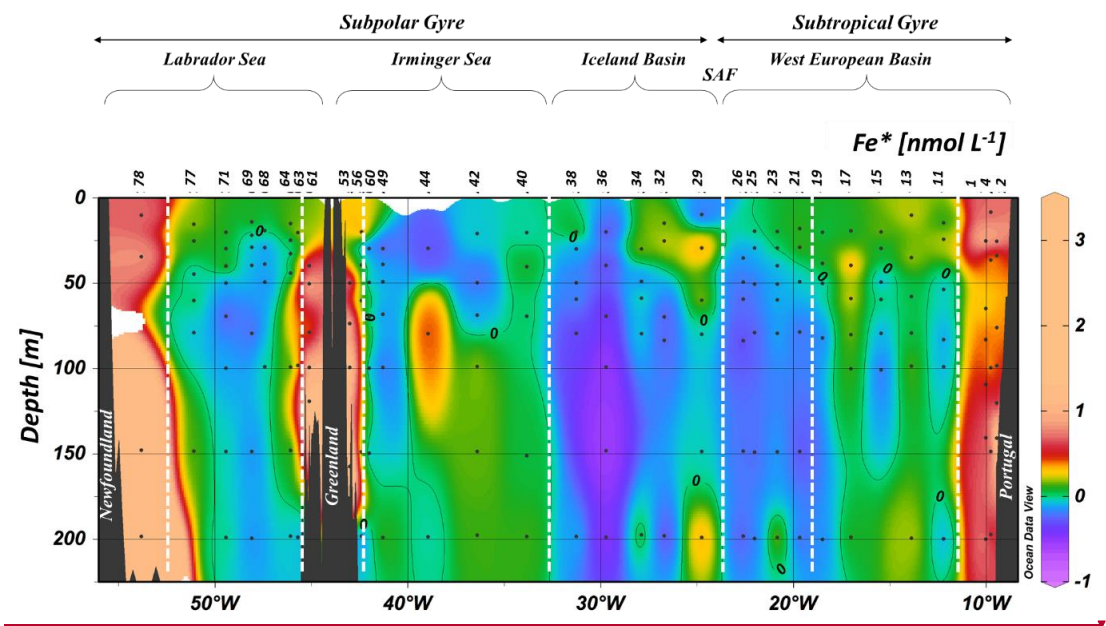
Deleted: Graph of iron:aluminium (Fe:Al) ratios for: dissolved (DFe:DAI, black dots, Menzel Barraqueta et al., 2018), particulate (PFe:PAI, open dots, Gourain et al., in prep.), total aerosol (Fe:Al aerosols total, red continuous line) and soluble aerosol (Fe:Al aerosols soluble, black continuous line and dashed lines as standard deviation) estimated from a two-stage sequential leach (UHP water, then 25% HAc, Shelley et al., this issue). Note that for total and soluble aerosols the Fe:Al ratios are averages per section of transect grouped by aerosol source region (Europe, N. America, High latitude, Marine; Shelley et al., this issue). Note that numbers on top of points represent station numbers. ¶



Page Break



**Figure 7: Section plot of the Fe\* tracer in the North Atlantic Ocean with a remineralization rate ( $R_{Fe:N}$ ) of  $0.05 \text{ mmol mol}^{-1}$  from surface to 225 m depth. A contour line of 0 separates areas of negative Fe\* from areas with positive Fe\*. Positive values of Fe\* imply there is enough iron to support complete consumption of  $\text{NO}_3^-$  when this water is brought to surface, and negative Fe\* values imply a deficit. See text for details.**



Formatted: Ca

**Deleted:** Figure 7: Section plot of the Fe\* tracer in the North Atlantic Ocean with a remineralization rate ( $R_{Fe:N}$ ) of  $0.05 \text{ mmol mol}^{-1}$  from surface to 225 m depth. A contour line of 0 separates areas of negative Fe\* from areas with positive Fe\*. Positive values of Fe\* imply there is enough iron to support complete consumption of  $\text{NO}_3^-$  when this water is brought to surface, and negative Fe\* values imply a deficit. See text for details.

Station	Date sampling DD/MM/YYYY	filtration $\mu\text{m}$	Latitude $^{\circ}\text{N}$	Longitude $^{\circ}\text{E}$	$Z_m$ m	DFe (nmol L <sup>-1</sup> )		
						average	SD	n
1	19/05/2014	0.2	40.33	-10.04	25.8	1.07	± 0.12	1
2	21/05/2014	0.2	40.33	-9.46	22.5	1.01	± 0.04	1
4	21/05/2014	0.2	40.33	-9.77	24.2	0.73	± 0.03	1
11	23/05/2014	0.2	40.33	-12.22	31.3	0.20	± 0.11	2
13	24/05/2014	0.45	41.38	-13.89	18.8	0.23	± 0.02	1
15	28/05/2014	0.2	42.58	-15.46	34.2	0.22	± 0.03	2
17	29/05/2014	0.2	43.78	-17.03	36.2	0.17	± 0.01	1
19*	30/05/2014	0.45	45.05	-18.51	44.0	0.13	± 0.05	2
21	31/05/2014	0.2	46.54	-19.67	47.4	0.23	± 0.08	2
23*	02/06/2014	0.2	48.04	-20.85	69.5	0.21	± 0.05	6
25	03/06/2014	0.2	49.53	-22.02	34.3	0.17	± 0.04	2
26	04/06/2014	0.45	50.28	-22.60	43.8	0.17	± 0.03	2
29	06/06/2014	0.45	53.02	-24.75	23.8	0.17	± 0.02	1
32	07/06/2014	0.2	55.51	-26.71	34.8	0.59	± 0.08	2
34	09/06/2014	0.45	57.00	-27.88	25.6	NA	±	0
36	10/06/2014	0.45	58.21	-29.72	33.0	0.12	± 0.02	1
38	10/06/2014	0.45	58.84	-31.27	34.5	0.36	± 0.16	2
40	12/06/2014	0.45	59.10	-33.83	34.3	0.39	± 0.05	1
42	12/06/2014	0.45	59.36	-36.40	29.6	0.36	± 0.05	1
44	13/06/2014	0.2	59.62	-38.95	25.8	NA	±	0
49	15/06/2014	0.45	59.77	-41.30	60.3	0.30	± 0.05	2
53*	17/06/2014	0.45	59.90	-43.00	36.4	NA	±	0
56*	17/06/2014	0.45	59.82	-42.40	30.0	0.87	± 0.06	1
60*	17/06/2014	0.45	59.80	-42.00	36.6	0.24	± 0.02	2
61*	19/06/2014	0.45	59.75	-45.11	39.8	0.79	± 0.12	1
63*	19/06/2014	0.45	59.43	-45.67	86.7	0.40	± 0.03	1
64	20/06/2014	0.45	59.07	-46.09	33.9	0.27	± 0.06	2
68*	21/06/2014	0.45	56.91	-47.42	26.3	0.22	± 0.01	1
69*	22/06/2014	0.45	55.84	-48.09	17.5	0.24	± 0.02	1
71	24/06/2014	0.45	53.69	-49.43	36.7	0.32	± 0.04	2
77*	26/06/2014	0.45	53.00	-51.10	26.1	NA	±	0
78	27/06/2014	0.45	51.99	-53.82	13.4	0.79	± 0.05	1

Table 1: Station number, date of sampling (in the DD/MM/YYYY format), size pore used for filtration ( $\mu\text{m}$ ), station location, mixed layer depth (m) and associated average dissolved iron (DFe) concentrations, standard deviation and number of samples during the GEOTRACES GA01 transect. Note that the asterisk next to station numbers refers to disturbed temperature and salinity profiles as opposed to uniform profiles.

55

Deleted:

Seawater used for calibration	SeaFAST-pico™ DFe values (nmol L <sup>-1</sup> )			reference or certified DFe values (nmol L <sup>-1</sup> )		
	Average	SD	n	Average	SD	
SAFe S	0.100	± 0.006	2	0.095	± 0.008	
GSP	0.16	± 0.04	15	NA	± NA	
NASS-7	6.7	± 1.7	12	6.3	± 0.5	

60

**Table 2: SAFe S, GSP and NASS-7 dissolved iron concentrations (DFe, nmol L<sup>-1</sup>) determined by the SeaFAST-pico™ and their consensus (SAFe S, GSP; <https://websites.pmc.ucsc.edu/~kbruland/GeotracesSaFe/kwbGeotracesSaFe.html>) and certified (NASS-7; [https://www.nrc-cnrc.gc.ca/eng/solutions/advisory/crm/certificates/nass\\_7.html](https://www.nrc-cnrc.gc.ca/eng/solutions/advisory/crm/certificates/nass_7.html)) DFe concentrations. Note that yet no consensual value is reported for the GSP seawater.**

Deleted: Area ...  
Formatted Table

Margins	Stations #	DFe:DAI (mol:mol)		PFe:PAI (mol:mol)		DFe:PFe (mol:mol)		n
		average	SD	average	SD	average	SD	
<i>Iberian Margin</i>	2 and 4	0.07	± 0.03	0.20	± 0.01	<u>0.13</u>	± <u>0.09</u>	10
<i>East Greenland Margin</i>	56 and 53	0.21	± 0.09	0.30	± 0.01	<u>0.12</u>	± <u>0.03</u>	6
<i>West Greenland Margin</i>	61	0.18	± 0.02	0.32	± 0.01	<u>0.14</u>	± <u>0.04</u>	3
<i>Newfoundland Margin</i>	78	1.1	± 0.41	0.31	± 0.01	<u>0.06</u>	± <u>0.02</u>	4

**Table 3:** Averaged DFe:DAI (Menzel Barraqueta et al., 2018) and PFe:PAI (Gourain et al., in prep.) ratios reported per margins. Note that to avoid phytoplankton uptake, only depth below 100 m depth are considered.

Deleted: Area

Formatted Table

Deleted:

Deleted: <sup>-1</sup>

Deleted:

Formatted Table

Deleted: <sup>-1</sup>

Deleted: 4